



저작자표시-비영리-변경금지 2.0 대한민국

이용자는 아래의 조건을 따르는 경우에 한하여 자유롭게

- 이 저작물을 복제, 배포, 전송, 전시, 공연 및 방송할 수 있습니다.

다음과 같은 조건을 따라야 합니다:



저작자표시. 귀하는 원저작자를 표시하여야 합니다.



비영리. 귀하는 이 저작물을 영리 목적으로 이용할 수 없습니다.



변경금지. 귀하는 이 저작물을 개작, 변형 또는 가공할 수 없습니다.

- 귀하는, 이 저작물의 재이용이나 배포의 경우, 이 저작물에 적용된 이용허락조건을 명확하게 나타내어야 합니다.
- 저작권자로부터 별도의 허가를 받으면 이러한 조건들은 적용되지 않습니다.

저작권법에 따른 이용자의 권리는 위의 내용에 의하여 영향을 받지 않습니다.

이것은 [이용허락규약\(Legal Code\)](#)을 이해하기 쉽게 요약한 것입니다.

[Disclaimer](#)

**Doctor of Philosophy**

**Over 4500 mm<sup>3</sup> Engineered Liver Scaffold  
for Implantable Artificial Liver**

The Graduate School

of the University of Ulsan

Department of Electrical, Electronic

and Computer Engineering

**Chanh-Trung Nguyen**

**Over 4500 mm<sup>3</sup> Engineered Liver Scaffold  
for Implantable Artificial Liver**

**Supervisor: Professor Kyo-in Koo**

A Dissertation

Submitted to

the Graduate School of the University of Ulsan

In partial Fulfillment of the Requirements  
for the Degree of

Doctor of Philosophy

by

**Chanh-Trung Nguyen**

Department of Electrical, Electronic

and Computer Engineering


University of Ulsan, Korea

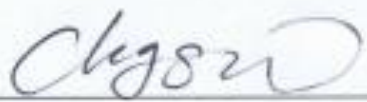
August 2024

## Over 4500 mm<sup>3</sup> Engineered Liver Scaffold for Implantable Artificial Liver

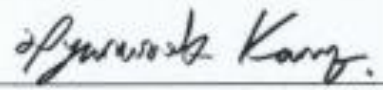
This certifies that the dissertation  
of Chanh-Trung Nguyen is approved

  
\_\_\_\_\_  
Committee Chair: Dr. Sung Hoon Back

  
\_\_\_\_\_  
Committee Member: Dr. Kyo-in Koo

  
\_\_\_\_\_  
Committee Member: Dr. Su Wol Chung

  
\_\_\_\_\_  
Committee Member: Dr. Dong Kim

  
\_\_\_\_\_  
Committee Member: Dr. Huyn-Wook Kang

Department of Electrical, Electronic and Computer Engineering

University of Ulsan, Korea

August 2024



# ACKNOWLEDGMENTS

I would like to take this opportunity to express my deepest gratitude to the individuals and institutions who have been instrumental in the successful completion of my Ph.D. dissertation.

First and foremost, I am profoundly thankful to my academic advisor, **Prof. Kyo-in Koo**, for their unwavering guidance, mentorship, and patience throughout this long and challenging process. Their expertise and dedication have been invaluable to my academic growth. I would also like to thank the members of my dissertation committee, Prof. Sung Hoon Back, Prof. Su Wol Chung, Prof. Dong Kim, and Prof. Hyun-Wook Kang. Their insightful feedback and constructive criticism have significantly enriched the quality of this research.

I sincerely thank my fellow researchers, colleagues, and friends who have offered support, encouragement, and collaborative insights. Your camaraderie has made this academic journey not only manageable but also enjoyable. I am grateful to the University of Ulsan for providing a conducive research environment and access to extensive resources, including the Department of Electrical, Electronic and Computer Engineering, the School of Biological Sciences, and the Department of Chemistry.

My family and friends have been a constant source of encouragement and motivation. I am indebted to them for their unwavering belief in my abilities and support. Last, I want to thank the research funding agencies and grants supporting my research endeavors. I offer my sincere gratitude to all whose names may not be mentioned here but have been a part of this incredible journey.

This dissertation is the culmination of years of hard work, dedication, and collaboration, and I owe its completion to the collective efforts of all those mentioned above. Thank you for being an integral part of my academic journey.

Chanh-Trung Nguyen

Ulsan, South Korea, August 2024.

# ABSTRACT

## Over 4500 mm<sup>3</sup> Engineered Liver Scaffold for Implantable Artificial Liver

by

**Chanh-Trung Nguyen**

*Supervisor: Professor Kyo-in Koo*

*Submitted in Partial Fulfillment of the Requirements for the Degree of*

*Doctor of Philosophy (Electrical Engineering)*

*August 2024*

Liver diseases, encompassing conditions from hepatitis to cirrhosis, present a global health challenge affecting millions and straining healthcare systems. These diseases are often debilitating and life-threatening. Liver transplantation, long an essential life-saving procedure for patients with end-stage liver disease, is hindered by a constant shortage of suitable donor organs and the need for lifelong immunosuppression to prevent graft rejection. A promising solution arises in liver tissue engineering, which aims to create functional liver tissue using methodologies like decellularized extracellular matrix scaffolds and 3D bioprinting. Liver tissue engineering aims to diminish reliance on organ donors by using a patient's own cells to create bio-engineered liver tissue. In doing so, this field promises to substantially reduce the challenges associated with organ shortages and the need for lifelong immunosuppression, effectively minimizing complications from immune-related responses.

Part 1 of this dissertation comprises two pivotal chapters. Chapter 1 provides information on the liver anatomy. We delve into the liver's components, from the diversity of cell types to the complexities of the extracellular matrix. The chapter also dissects the essential role of growth factors in orchestrating the liver's functions. The liver regeneration process, a unique attribute of the liver, is unveiled. It also addresses the sobering reality of liver diseases, explaining various afflictions, their causes, and their profound implications for liver health. Chapter 2 ventures into liver tissue engineering,

introducing the utilization of various cells and biomaterials for creating artificial liver tissues. Here, we explore the techniques and methodologies that underpin this field. Liver tissue engineering presents a promising avenue, blending advanced science and technology, to craft synthetic liver tissues that might approach the functionality of a healthy liver. These two chapters collectively lay the foundation for an in-depth exploration of the liver's intricacies, from its structural anatomy to the exciting prospects of engineering liver tissues.

Part 2 details our artificial liver project, focusing on developing a large-volume functional liver scaffold comprising three distinct models for two different culture conditions. These models are meticulously designed to explore the influence of cell culture conditions, including both static and dynamic flow conditions. Inspired by previous research, we employed 3D extrusion bioprinting with an inverse-gravity technique and a laminar-flow device to generate these large-volume constructs. To address the challenge of nutrient and oxygen diffusion within large scaffolds, we implemented a pumping system that directly delivers cell culture medium through a hollow channel embedded within the scaffold. Additionally, we conducted investigations into the appropriate material matrix for cell maturation, aiming to mimic the biological environment of native liver tissue and sustain long-term culture. A rigorous biological analysis process was employed to evaluate our models. This process included assessment of cell proliferation, cell viability, liver function through albumin and urea secretion, and examination of cell morphology. This chapter marks significant progress in advancing the field of artificial liver research.

# Contents

ACKNOWLEDGMENTS .....	i
ABSTRACT .....	ii
Contents .....	iv
List of Figures.....	viii
List of tables.....	ix
Nomenclature .....	x
Part I .....	1
INTRODUCTION OF LIVER AND LIVER TISSUE ENGINEERING.....	1
Chapter 1 .....	2
Overview of liver function, structure and biology .....	2
1.1. Introduction to Liver Anatomy.....	2
1.2. Cell types in the liver .....	4
1.3. Hepatic extracellular matrix .....	6
1.4. Growth factors.....	7
1.5. Liver regeneration.....	8
1.6. Diseases of the Liver .....	9
Chapter 2 .....	11
Liver tissue engineering.....	11
2.1. Introduction.....	11
2.2. Cell-based approaches for studying the liver .....	13
2.2.1. Primary hepatocytes .....	13
2.2.2. Cell lines .....	14
2.2.3. Embryonic stem cells and induced pluripotent stem cells.....	15
2.2.4. Adult stem cells.....	16
2.2.5. Hepatic progenitor cells .....	16
2.2.6. Human fetal hepatocytes .....	16
2.2.7. Hepatoblasts .....	17
2.2.8. Hepatocyte-like cells .....	17
2.3. Biomaterials in liver Tissue engineering .....	18
2.3.1. Natural hydrogels.....	19
2.3.2. Synthetic hydrogels .....	22
2.3.3. Decellularized liver hydrogel .....	24
2.3.4. Decellularization process .....	24



2.3.5. Characterization of the decellularized tissue.....	26
2.4. Fabrication techniques of liver tissue engineering.....	28
Part II.....	31
Over 4500 mm <sup>3</sup> Engineered Liver Scaffold for Implantable Artificial Livers .....	31
Chapter 1: .....	32
Angiogenesis in Free-Standing Two-Vasculature-Embedded Scaffold Extruded by Two-Core La minar Flow Device .....	32
I. Background.....	32
II. Materials and Methods.....	33
1. Two-core laminar flow device .....	33
2. HUVEC culture .....	34
3. Two-vasculature-embedded scaffold formation .....	34
4. Laboratory made connecting device.....	35
5. Three types of culture condition .....	35
6. Diffusion from the hollow channel.....	36
7. Perfusibility in the two vasculatures.....	36
8. GFs for angiogenic sprouting .....	36
9. Immunofluorescent staining.....	36
10. Statistical analysis .....	37
III. Results .....	37
1. Fabrication of the two-vasculature-embedded scaffold.....	37
2. Perfusability.....	39
3. Cell morphology according to the culture condition.....	41
4. Angiogenic sprouting .....	42
IV. Discussion.....	44
V. Conclusion .....	45
Chapter 2: .....	46
Biinspired Liver dECM Scaffold using Sacrificial Calcium Alginate for Artificial Liver .....	46
I. Background.....	46
II. Materials and Methods.....	48
1. Hydrogel mixture .....	48
1.1. Liver dECM synthesis .....	48
1.2. Bioink preparation (Liver dECM-Alginate).....	48
2. Cell culture.....	48
3. Scaffold generation.....	49
4. Immunofluorescence staining.....	49
5. <i>In vivo</i> experiment.....	49

6.	Histological analysis .....	50
7.	Statistical analysis .....	51
III.	Results .....	51
1.	The formation of vascular networks and hepatocyte cluster .....	51
2.	<i>In vivo</i> implanted experiment.....	52
IV.	Discussion.....	53
V.	Conclusion .....	55
Chapter 3: .....		56
Double-layered blood vessels over 3 mm in diameter extruded by the inverse-gravity technique		5
6		
I.	Background.....	56
II.	Materials and Methods .....	57
1.	Simulation .....	57
2.	Extrusion device .....	57
III.	Results and Discussion.....	58
IV.	Conclusion .....	60
Chapter 4: .....		61
Over 4500 mm <sup>3</sup> Engineered Liver Scaffold for Implantable Artificial Livers .....		61
I.	Background.....	61
II.	Materials and Methods.....	63
1.	Bioink preparation (Liver dECM-Alg) .....	63
2.	Cell culture.....	64
3.	Laminar device .....	64
4.	Large-volume liver engineered scaffold formation .....	65
5.	The formation of vascular networks in large-volume liver scaffold .....	65
6.	Pumping culture system .....	66
7.	Three types of culture condition .....	67
8.	Cell viability.....	67
9.	Cell proliferation .....	68
10.	Liver function .....	68
11.	Immunofluorescence staining.....	68
12.	Statistical analysis .....	68
III.	Results and Discussion.....	69
1.	Fabrication of the two-vasculature-embedded scaffold.....	69
2.	Impact of different culture conditions on cell viability.....	69
3.	Impact of different culture conditions on cell proliferation .....	71
4.	Morphological Analysis of Liver Scaffold Architecture.....	72

5. Evaluating liver synthetic function in liver scaffolds .....	74
IV. Conclusion .....	76
References .....	77
Appendices .....	89

## List of Figures

Figure 1. Illustration of the human liver anatomy.....	3
Figure 2. Organizational units of the liver .....	4
Figure 3. Different approaches toward the liver treatment of a damaged liver from a healthy liver ....	12
Figure 4. Schematic diagram of the two-vasculature-embedded scaffold .....	33
Figure 5. Two-core laminar flow device is presented .....	34
Figure 6. Fabrication process of the connecting device.....	35
Figure 7. Three types of culture conditions .....	35
Figure 8. Fabricated two-vasculature-embedded scaffold .....	38
Figure 9. Time-lapse images of the perfused channel from 5 min to 30 min .....	39
Figure 10. Perfusion assay .....	40
Figure 11. Fluorescence images of the two-vasculature-embedded scaffold.....	41
Figure 12. Morphology characterization in the HUVEC channel on day 2 .....	42
Figure 13. Angiogenic sprouting in all three culture conditions.....	43
Figure 14. Schematic diagram of the liver fiber scaffold.....	47
Figure 15. Immunofluorescence images of the vascular network formation.....	52
Figure 16. Animal experiment .....	53
Figure 17. Geometries used for the simulations are shown .....	57
Figure 18. Schematic sketch and picture of extrusion devices .....	58
Figure 19. Simulating water flow into a main pipe.....	59
Figure 20. Coaxial laminar scaffold formation using alginate and collagen .....	60
Figure 21. Schematic diagram of the large-volume liver engineered scaffold .....	63
Figure 22. Laminar flow device.....	64
Figure 23. 3D-printed reservoir for the connecting device.....	66
Figure 24. Three types of culture conditions .....	67
Figure 25. The fabricated large-volume scaffold .....	69
Figure 26. The fluorescence images of the live-/dead-stained liver scaffold.....	70
Figure 28. Cell viability of the liver scaffold over 14 days.....	71
Figure 28. Cell proliferation in liver scaffolds.....	72
Figure 29. Liver scaffold morphology by immunofluorescence imaging.....	74
Figure 30. Assessment of liver synthetic function in liver scaffolds .....	75

## List of tables

Table 1. Fabrication techniques of liver tissue engineering ..... 29

# Nomenclature

## Notation Description

TCA	Tricarboxylic acid
NPCs	Non-parenchymal cells
SECs	Sinusoidal endothelial cells
ECM	Extracellular matrix
TGF- $\beta$	Transforming growth factor-beta
ET-1	Endothelin-1
HSCs	Hepatic stellate cells
ROS	Reactive oxygen species
MAPKs	Mitogen-activating protein kinases
RGD	Arginine-Glycine-Aspartic acid
GAGs	Glycosaminoglycans
HS	Heparan sulfate
CS	Chondroitin
DS	Dermatan sulfate
KS	Keratan sulfate
FGF	Fibroblast growth factor
VEGF	Vascular endothelial growth factor
PDGF	Platelet-derived growth factor
HGF	Hepatocyte growth factor
EGF	Epidermal growth factor
FGF	Fibroblast growth factor
uPA	Urokinase-type plasminogen activator
MMPs	Matrix metalloproteinases
TNF- $\alpha$	Tumor necrosis factor-alpha
2D	Two-dimensional
3D	Three-dimensional
DMSO	Dimethyl sulfoxide
SV40	Simian virus 40
ES	Embryonic stem
BAL	Bio-artificial liver
iPSCs	Induced pluripotent stem cells
MSCs	Mesenchymal stem cells
IHeps	Hepatocyte-like cells
GelMA	Gelatin Methacrylate
PEG	Poly ethylene glycol
PVA	Poly vinyl alcohol
DNA	Deoxyribonucleic acid
SDS	Sodium dodecyl sulfate
H&E	Hematoxylin and Eosin
SEM	Scanning electron microscopy
dECM	Decellularized extracellular matrix
PEG	Poly ethylene glycol
ICC	Inverted colloidal crystal
DAPI	4',6-diamidino-2-phenylindole
ELAD	Extracorporeal Liver Assist Device
MELS	Modular Extracorporeal Liver Support
AMC-BAL	Amsterdam Medical Centre Bioartificial Liver
BLSS	Bioartificial Liver Support System
DI	Deionized

NaOH	Sodium hydroxide
ID	Internal diameter
PDMS	Polydimethylsiloxane
PFA	Paraformaldehyde

## **Part I**

# **INTRODUCTION OF LIVER AND LIVER TISSUE ENGINEERING**



# Chapter 1

## Overview of liver function, structure and biology

### 1.1. Introduction to Liver Anatomy

The human liver is the largest solid organ and the largest gland in the human body. In females, its weight ranges from 1.2 to 1.4 kg; in males, it spans from 1.5 to 1.7 kg, comprising approximately 2% to 3% of the total body weight. Nestled on the upper right side of the body, the liver finds protection within the shelter of the lower rib cage. A healthy, well-perfused liver displays a reddish-brown hue, characterized by its soft, highly pliable nature that renders it susceptible to laceration. Its exceptional vascularity adds to its distinctive attributes [1]. The liver is a hub of activity, orchestrating a range of pivotal functions, including central metabolism, detoxification, synthesis, digestion, endocrine regulation, immune modulation, and exocrine activities [2]. Remarkably, it takes charge of over 500 life-sustaining processes within the human body.

The superior aspect of the liver forms attachments to the diaphragm and the anterior abdominal wall through a triangular fold of the peritoneum known as the falciform ligament. This ligament's point of attachment demarcates the liver into the right and left lobes. Moreover, the transverse fissure further delineates the liver's division, leading to two additional lobes: the quadrate and caudate. The gallbladder is linked through the cystic duct at the posterior of the liver's quadrate lobe [3].

The liver, recognized as the most abundantly perfused organ within the human body, accommodates approximately 10% to 15% of the total blood volume [4]. Blood supply to the liver originates from two distinct sources: the hepatic artery, responsible for delivering oxygenated blood, and the portal vein, responsible for supplying nutrient-rich blood stemming from the intestines, spleen, pancreas, and gallbladder. Impressively, the portal vein contributes 80% of the liver's blood flow,

underscoring its pivotal role in metabolic processes. To complete the circulatory cycle, the hepatic vein facilitates the drainage of deoxygenated blood from the liver into the inferior vena cava.

The transport of bile from the liver involves the right and left hepatic ducts, which converge with the cystic duct, culminating in the formation of the common bile duct that leads to the intestines. This complex network comprising the hepatic portal vein, the proper hepatic artery, and the common bile duct collectively constitutes the porta hepatis [5].

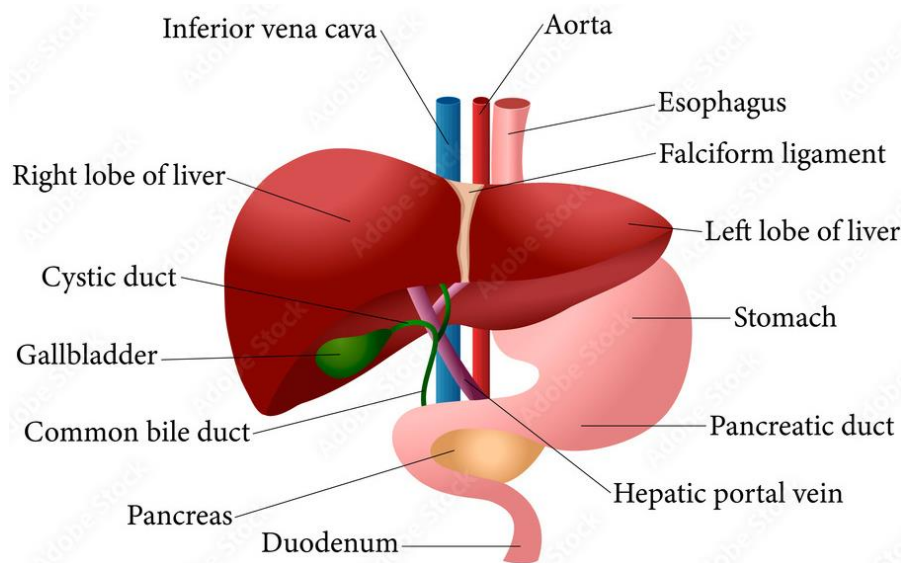


Figure 1. Illustration of the human liver anatomy

These arterial, venous, and ductal components branch out to nourish the liver's smallest histological unit, the lobule. These liver lobules take on a hexagonal configuration reminiscent of honeycombs, with a diameter of approximately 1mm. Fueling these lobules is the intricate capillary network of the liver, termed sinusoids, which represents the most finely divided capillary system [6]. Unlike conventional basement membranes, sinusoids are characterized by their specialized, discontinuous fenestrated endothelium. These sinusoids are intimately situated near the Space of Disse, a region bordering the liver cells, thus facilitating the unhindered diffusion of metabolites and metabolic products to and from these cells.

Each liver lobule is structured into three distinct zones based on their proximity to the portal triad, comprising the hepatic artery, portal vein, and bile ducts [7]. Zone I, situated closest to the portal

triad, enjoys the highest oxygenation, rendering the cells in this zone relatively resilient against ischemic injury. Conversely, zone II lies in immediate proximity to the central vein of the lobule, receiving the lowest oxygen levels, rendering the cells within it particularly vulnerable to ischemic injury [8]. The functionality of cells within the lobule corresponds to its zonal distribution [9]. Crucial metabolic processes, including albumin production, ammonia detoxification, urea synthesis, glutamine synthesis, cytochrome P450 drug metabolism, gluconeogenesis, glycolysis, oxidative phosphorylation, lipogenesis, and the tricarboxylic acid (TCA) cycle, exhibit distinctive functionality that aligns with the specific zones.

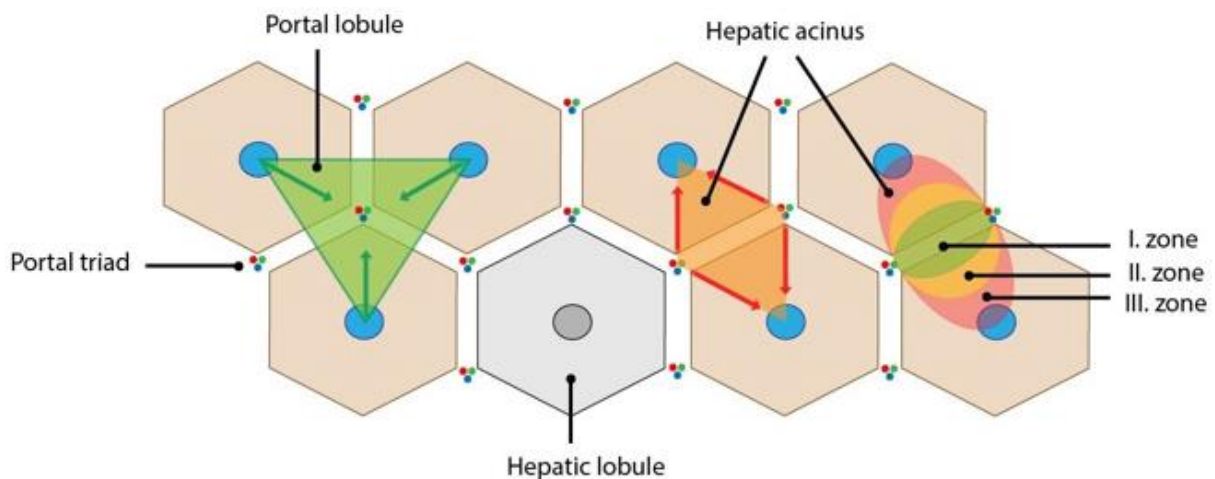


Figure 2. Organizational units of the liver include the hepatic lobule with zonation, portal lobule, and hepatic acinus

## 1.2. Cell types in the liver

The intricate array of liver functions is made possible by the intricate assembly of its highly specialized cell types. Comprising around 35-40% of the liver's cellular composition, non-parenchymal cells (NPCs) encompass diverse components [10, 11]. These include Kupffer cells, liver macrophages, sinusoidal endothelial cells, stellate cells, biliary epithelial cells, and mobile immune cells like leukocytes and lymphocytes [12]. Parenchymal cells, or hepatocytes, constitute the cellular mass's dominant portion (60-80%). The hepatocytes shoulder the lion's share of the liver's metabolic functions. These include synthesizing essential circulating proteins like albumin, protease inhibitors, and coagulation factors. Hepatocytes play a role in pH regulation and ammonia detoxification. Hepatocytes

serve as the linchpin for maintaining the equilibrium of glucose and glycogen levels, cholesterol, bile, and vitamins A and D [13]. They metabolize amino acids, heme, and bilirubin. Functioning in concert with hepatocytes, the NPCs in the liver are meticulously organized both functionally and structurally. They play a vital role in ensuring hepatocyte survival and optimal function.

Sinusoidal endothelial cells (SECs) constitute the lining of the liver lobule's sinusoids, distinguished by the absence of a consistent basal lamina, eliminating a continuous barrier between the blood and hepatocytes. These cells feature substantial pores, measuring 0.1 – 0.3 $\mu$ m, that facilitate the unimpeded movement of molecules to and from hepatocytes. Beyond this, SECs perform a lymphatic function, orchestrating scavenger receptor-mediated clearance of diverse molecules, including endotoxins and bacteria. They play an integral role in the recruitment of leukocytes and regulating inflammatory cascades. Remarkably, they double as antigen-presenting cells to circulating T-cells. SECs contribute to the extracellular matrix (ECM) by generating fibronectin and collagen IV [14]. They activate transforming growth factor beta (TGF- $\beta$ ) into its active form. Autocrine vasoactive compounds, such as endothelin-1 (ET-1), are produced by SECs, influencing blood flow dynamics and uptake from the sinusoidal lumen.

Within the Space of Disse, nestled between SECs and hepatocytes, reside hepatic stellate cells (HSCs) [15]. These cells often likened to 'stem-like' entities, exhibit neuronal and neuroendocrine markers such as nestin and CD133 alongside hemopoietic markers like GATA1. HSCs serve as vitamin A repositories under normal conditions, yet during inflammatory stages, they metamorphose into the source of liver myofibroblasts, pivotal in the progression, regression, and maintenance of hepatic fibrosis. Their role extends to regulating the extracellular matrix through the secretion of matrix metalloproteinases, hepatocyte-influencing growth factors, and ECM molecules [16].

Kupffer cells, also known as liver macrophages, inhabit the microvessels of the sinusoids, strategically poised to intercept pathogens entering the liver [17]. This highlights the liver's central role in acute immune responses; the liver harbors 80% of the body's macrophages, specifically Kupffer cells. In their macrophage capacity, they adhere to the traditional roles of clearing cellular debris and

exogenous particles and driving inflammatory responses by releasing cytokines, chemokines, eicosanoids, proteolytic enzymes, reactive oxygen species (ROS), and nitric oxide [18].

Biliary epithelial cells, or cholangiocytes, trace the biliary tract and directly interact with neighboring hepatocytes [19]. Their primary responsibility involves the secretion and modification of bile, an essential digestive acid. They actively maintain the osmolality of bile secretions and absorb hormones, amino acids, neurotransmitters, and other molecules, thereby contributing to the intricate homeostasis within the liver lobule.

### **1.3. Hepatic extracellular matrix**

The ECM is a non-cellular component within all tissues, delivering indispensable support to the residing cells [20]. This intricate network, a fusion of water, proteins, and polysaccharides, envelops cells within solid tissues. Crucially, the ECM ranks among the paramount regulators of cellular and tissue functions across the body. While functioning as a physical scaffold and structural foundation for cells, the ECM also triggers crucial biochemical and biomechanical signals that underpin tissue homeostasis, differentiation, morphogenesis, and overall physiological equilibrium [20]. Indeed, the ECM exerts control over vital cellular tasks, spanning adhesion, migration, proliferation, and survival [21]. The cellular response and function are inherently interwoven with the niche microenvironment provided by the organ's unique ECM [22]. The production and breakdown of ECM components are often implicated in the onset of pathologies. Every tissue adheres to its distinct ECM "recipe," resulting from an ongoing interplay between various cellular constituents and the tissue's microenvironment. Prominent among these constituents are collagen I, collagen II, elastin, fibronectin, and laminin, which enjoy an almost ubiquitous presence throughout the mammalian body, contributing strength, structure, and flexibility [23]. Furthermore, the ECM displays remarkable plasticity, subject to continuous modification and exhibiting substantial tissue variation.

In the liver, the extracellular matrix presents as an intricately specialized cellular microenvironment, particularly within the Space of Disse. While other human organs feature two basement membranes and a collagen-based ECM bridging endothelial and epithelial cells, liver lobules

deviate with a discontinuous, low-density basement membrane and an attenuated ECM. In synergy with sinusoidal endothelial cells' abundant and sizable pores, this specialized ECM provides an optimal framework for the rapid bidirectional exchange of macromolecules between blood and hepatocytes [24]. This framework also sustains the differentiated state of the adjacent cells. In normal liver tissue, ECM occupies less than 3% of the relative area in tissue sections and approximately 0.5% of wet weight. Predominantly composed of collagen, fibronectin, laminin, and proteoglycans, the hepatic ECM finds notable presence in the Glisson's capsule, portal tracks, central veins, and the Space of Disse. Among the collagens, types I, III, IV, and V are prominently identified in the liver, with types I, III, and V primarily serving as interstitial ECM components in portal and central areas. Conversely, collagen IV primarily resides in basement membranes [25]. Fibronectin is abundant within the hepatic ECM, notably in subcapsular connective tissue, septa, and portal areas, and as the principal ECM component within the Space of Disse. Laminin is a pivotal element of hepatic basement membranes in parallel with collagen IV.

#### **1.4. Growth factors**

Growth factors, a class of soluble signaling molecules, orchestrate cellular responses by explicitly binding to transmembrane receptors on target cells. Their multifaceted roles encompass cell growth, proliferation, differentiation, and the maintenance of phenotypic characteristics [26]. Among the hundreds of growth factors found within the liver, three wield substantial influence over hepatic function: hepatocyte growth factor (HGF), epidermal growth factor (EGF), and fibroblast growth factor (FGF) [27].

HGF, secreted by HSCs and sinusoidal endothelial cells (SECs), holds the potency of a robust mitogen. It affects both hepatic progenitor cells and differentiated hepatocytes through interaction with the c-MET/HGF receptor, activating subsequent tyrosine kinase pathways in both epithelial and endothelial cells [28]. HGF has implications for liver regeneration, recovery from liver diseases, and the development of specific cancer types. It binds to the ECM via GAGs, heparin, hyaluronan, and collagen, extending its half-life from mere minutes to several hours, enabling prolonged cell exposure

[29].

EGF, produced outside the liver in the Brunner's gland of the duodenum, traverses the portal vein to reach the liver [30]. Upon arrival, it spurs cell division and proves indispensable for normal liver regeneration. The impact of EGF exposure varies based on lobule zonation; hepatocytes positioned in zone 1 (proximate to the portal triad) experience a swifter and more concentrated exposure than those in zone 3. FGF, secreted by perisinusoidal HSCs, governs liver wound healing, regeneration, and angiogenesis [31]. It follows a similar mode of interaction with the liver ECM as HGF. These growth factors interact with the ECM, shaping their function within the intricate liver microenvironment.

### **1.5. Liver regeneration**

The liver is uniquely the sole visceral organ capable of complete regeneration, even rebounding to its total weight and mass after losing up to 60% of its bulk [30]. This remarkable capacity for liver regeneration points to a complex network of control mechanisms often referred to as the "hepatostat" [30]. Understanding liver regeneration, alongside its hemostatic regulation, sheds light on organ development and various disease processes. The intricate interplay among cells, growth factors, and ECM molecules within the liver underpins normal function and governs hepatic development, healing, and regeneration. A sophisticated cascade of signaling molecules orchestrates the cooperation of all these components, culminating in the expansion and organization of new tissue. Nevertheless, despite extensive research, the precise mechanisms governing hepatic regeneration remain enigmatic.

Liver regenerative processes are sparked by the loss or injury of normal liver tissue through physical trauma or chemical insults. Two prevailing models elucidate the orchestration of liver regeneration [32]. In one model, Kupffer cells initiate the process by clearing cellular debris, activating HSCs and hepatocytes to proliferate within the liver parenchyma [33]. This concerted effort restores the liver-to-bodyweight ratio to 100%. An alternative method is proposed when the regenerative potential of hepatocytes is compromised, such as in chronic inflammatory conditions. Here, the biliary compartment assumes the role of a niche harboring facultative stem cells that can transform into hepatocytes. Conversely, when the need arises to repair damaged biliary epithelium and the proliferative

capacity of biliary cells is compromised, the immediate periportal hepatocytes step in as a niche source, trans-differentiating into biliary cells.

The critical role of growth factors in liver regeneration must be considered. Shortly after liver injury, urokinase-type plasminogen activator (uPA) is swiftly released, closely followed by an increase in its receptor, u-PAR. Apart from liberating plasminogen, u-PA releases matrix-associated HGF, immediately triggering surrounding hepatocytes to proliferate. Around one-hour post-injury, HGF release reaches its zenith. During this interval, HSCs, Kupffer cells, and SECs release HGF and EGF to encourage further hepatocyte proliferation [34]. Peaks in growth factor production are observed at 24- and 48-hours post-injury.

ECM remodeling emerges as a pivotal factor in liver regeneration. Matrix metalloproteinases (MMPs) are responsible for degrading most ECM proteins during organogenesis, growth, and average tissue turnover [35]. ECM degradation and remodeling are indispensable in regenerative, enabling unrestricted hepatocyte and other liver cell proliferation [36]. In a healthy, non-inflamed liver, ECM upkeep relies on the coordinated actions of MMPs and HSCs to restore and reshape the hepatic microenvironment [37]. Adult livers in good health exhibit moderate ECM turnover, aligned with the minimal amounts of MMPs persistently identified within these organs. However, in cases of liver injury, various MMPs experience upregulation, aiding in the degradation and replacement of damaged or absent tissue. These MMPs also regulate immune responses by interacting with other growth factors and cytokines, such as TGF- $\beta$  and tumor necrosis factor-alpha (TNF- $\alpha$ ).

## **1.6. Diseases of the Liver**

Liver disease presents a stark and pressing challenge, the sole major cause of death that escalates annually. A sobering fact emerges as the number of liver disease-related deaths has doubled since 1991 [38]. Despite the considerable medical advancements in addressing chronic disorders, liver disease remains an exception. Notably, mortality in this realm has surged by a staggering 400%, with the incidence among individuals under 65 witnessing a dramatic 500% rise since 1970. The landscape encompasses over 100 liver disease types, encompassing a demographic of at least 2 million individuals



in the UK grappling with these conditions [39].

A significant portion, exceeding 75%, of liver tissue must be compromised before a discernible decline in hepatic function materializes [40]. This often results in the belated diagnosis of advanced liver conditions, highlighting the challenge of identifying these diseases at an earlier, more treatable stage. Consequently, liver transplant remains a predominant recourse for those at the end stage of the disease spectrum [41]. However, the landscape of liver transplantation faces pressing constraints. Factors such as an ageing donor population, a higher prevalence of obese donors, and a shift in donor death demographics from sudden trauma to other causes contribute to a chronic scarcity of donor organs.

## Chapter 2

### Liver tissue engineering

#### 2.1. Introduction

The surge in the global burden of advanced liver diseases has intensified the demand for liver transplantation, considered the ultimate curative measure [42]. A vast disparity persists between the available organ donors and the patients awaiting transplantation, leading to a substantial loss of lives among those on the waiting list [43]. Astonishingly, only 10% of the global transplantation needs are met, underscoring a dire need for innovative solutions [44]. Thus, novel bioengineering approaches are imperative to bridge this gap by augmenting citizen donations and optimizing marginal liver utilization.

Liver tissue engineering merges as a promising avenue to uphold and emulate hepatic functions and microstructure [45]. This avenue holds considerable promise within the realm of liver regeneration, aiming to replicate a fully functional liver for *in vivo* applications, encompassing transplantation into patients or implementation as an extracorporeal or *in vitro* system [46]. At present, liver transplantation stands as the sole definitive remedy for chronic liver failure. However, the acute scarcity of donors and the lifelong reliance on immunosuppression impose significant constraints. An alternative therapeutic approach involves hepatocyte infusion, wherein hepatocytes sourced from a healthy donor liver are infused into the portal vein or its vicinity. These infused hepatocytes promptly adhere to the existing ECM *in vivo* [45]. This approach has established itself as a viable method for addressing acute and chronic liver diseases, with over 100 patients receiving treatment. Partial liver hepatectomy to treat the diseased liver from a healthy donor liver. Cell isolation from a healthy donor liver for hepatocyte infusion for *in vivo* treatment of a patient and *in vitro* growth of a 3D implantable tissue.

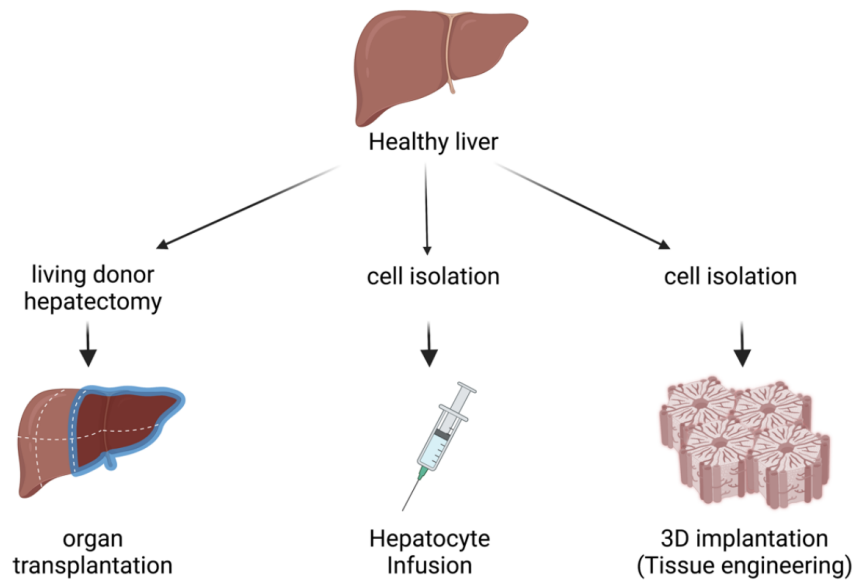


Figure 3. Different approaches toward the liver treatment of a damaged liver from a healthy liver

Innovative strategies, such as the 3D implantation of engineered organs or tissues, exhibit considerable promise and are actively under development [47]. While hepatocyte transplantation holds potential as a less invasive alternative to organ transplantation, it grapples with inherent limitations. These include a restricted availability of donor's livers, compromised cell viability arising from freeze-thaw damage of cryopreserved hepatocytes, and challenges related to poor cell engraftment [48]. As a result, alternative cell sources for infusion are gaining traction, including embryonic stem cells and induced pluripotent stem cells.

Significant advancements in liver functions have been underscored by notable outcomes from phase II clinical trials involving mesenchymal stem cell injection. More recently, endeavors to craft a 3D scaffold that emulates the cellular microenvironment have gained prominence. This avenue aims to realize the implantation of the 3D construct and meet clinical demands within a suitable timeframe. In this innovative approach, either hepatic or stem cells find encapsulation within a 3D biomaterial scaffold, fostering the development of liver-like tissue for subsequent implantation [49]. This bio-engineered *in vitro* platform holds immense promise, enabling comprehensive exploration of disease progression, liver function's biological ramifications, and drug screening studies' facilitation [50]. It stands as a steadfast supporter of liver functions and regeneration. Embracing a broader outlook, the field of liver tissue engineering seeks to present an alternative to organ transplantation by establishing

*in vitro* liver tissue constructs, leveraging recent strides in this direction.

## **2.2. Cell-based approaches for studying the liver**

Multiple methodologies are currently being employed to replicate and investigate the intricacies of the liver, comprehend its biological dynamics, and unravel the mechanisms behind disease progression. These approaches are vital in addressing the escalating scarcity of donor livers for patient treatments. A pivotal player in this narrative is the realm of cell culture studies, serving as a cornerstone in shaping our strategies within liver tissue engineering. The repertoire of liver cells can be sourced from diverse origins and harnessed for cell culture investigations, encompassing both two-dimensional (2D) and three-dimensional (3D) contexts.

### **2.2.1. Primary hepatocytes**

Primary human hepatocytes stand as the gold standard for *in vitro* liver studies, serving as the closest approximation to the behavior of hepatocytes in their natural environment [51]. Their utilization is marred by constraints such as limited availability and challenges linked to their behavior in culture, which have been subjects of scrutiny within the field. Typically sourced from discarded cadaveric donor livers unsuitable for transplantation, these hepatocytes are cryopreserved for later experimental use. However, their applicability could be improved by donor-to-donor variability, phenotypic instability over time in culture, and suboptimal palatability and survival under culture conditions.

Exploring porcine primary hepatocytes offers a remedy to the challenges associated with availability and donor variation [52]. Nonetheless, these cells remain susceptible to the same limitations concerning phenotypic instability and degeneration over extended culture periods. Rat and mouse primary hepatocytes also present options, yet their hepatic profile diverges significantly from that of humans. The consensus recognizes that animal models alone are insufficient for comprehensively studying liver biology. Of the 930 pharmacological compounds withdrawn from the market because of hepatotoxicity, only 17% exhibited comparable toxicity levels in rodent and non-rodent investigations. Certain conditions, such as human Hepatitis C virus infection, remain inexplicable in rodents, affecting only chimpanzees and tree shrews, and their clinical progression deviates from the human ailment.

Rodents metabolize alcohol at a notably accelerated rate compared to humans and do not develop severe liver fibrosis in response to alcohol toxicity. Despite their ready accessibility, primary hepatocytes sourced from animals cannot furnish results that align with human conditions.

### 2.2.2. Cell lines

Researchers turn to cell lines as a pragmatic alternative to surmount the limitations inherent to primary hepatocytes. Cell lines are characterized by their boundless proliferative capacity and stable phenotypes, making them accessible from manufacturers, cost-effective, and straightforward to sustain in culture settings [53]. Researchers employ hepatocyte cell lines derived from tumors, including HepG2, HepC3A, Huh7, HepaRG, and Hep3B. Each has contributed valuable insights through multiple experiments. Cell lines exhibit diminished expression of drug-metabolizing enzymes compared to primary hepatocytes in culture and the human liver *in vivo*, attributed to attenuated transcription of enzyme genes. Marked deviations in the expression of pivotal hepatic transcription factors and nuclear receptors in hepatoma-derived cell lines, compared to primary cells or *in vivo* settings, are presumed to be tied to the reduced CYP expression.

HepG2s, sourced from hepatic carcinoma, exhibit certain requisite phenotypic traits of liver cells [54]. However, microarray studies have unveiled notable alterations in the expression of over 5,000 genes in contrast to primary cells and *in vivo* conditions. Derived from HepG2s, HepC3As display enhanced albumin and nitrogen metabolizing capabilities [55]. Regrettably, their lack of urea enzymes and drug-metabolizing functions restrict their applicability. The HepaRG cell line presents an expression pattern more closely aligned with primaries and *in vivo* conditions, particularly in confluent cultures. By treating proliferating HepaRGs with dimethyl sulfoxide (DMSO), they can be coerced toward a more primary/*in vivo*-like phenotype, displaying elevated levels of CYP3A4 expression.

Their gene expression of CYPs remains lower than that of primary cells. Huh7s, too, can be cultured for several weeks to boost CYP3A4 levels. Unlike HepaRGs, this elevation is achieved without differentiation inducers like DMSO. Non-tumor-derived cell lines also find application. Typically immortalized via gene transfer of the simian virus 40 (SV40) T antigen, these cell lines can also acquire

immortality through co-transfection of albumin-promoter-regulated antisense constructs and transcription factors E2F and D1 cyclin. The THLE-3/2 and Fa2N4 cell lines both exhibit induction of major CYPs. However, their enzyme activity is low, only discernible through susceptible analytical methods.

Advancements in genetic engineering have led to cell lines with reversible immortalization, achieved through Cre-loxP excised oncogenes and suicide genes. The NKNT-3 hepatocyte line and non-parenchymal lines HNNT-2 (endothelial), TWNT-1 (stellate), and MMNK-1 (cholangiocytes) have all been immortalized using these advanced techniques, offering the potential for co-culture studies.

### **2.2.3. Embryonic stem cells and induced pluripotent stem cells**

Researchers prize embryonic stem (ES) cells for their remarkable pluripotency, encompassing indefinite proliferation and the capacity to differentiate into any tissue type [56]. The ethical difficulties associated with human ES cell use compel researchers to employ mouse ES cells predominantly. While these cells have found application in bio-artificial liver (BAL) devices, several differentiation protocols for generating hepatocytes have been reported. However, none have been executed at the scale requisite for replicating a human liver. Furthermore, the reliance on Matrigel in such protocols introduces an additional constraint. Matrigel, a trade name for an ECM product derived from Engelbreth-Holm-Swarm mouse sarcoma cells, poses challenges due to the lack of batch consistency in the product manufacturers offer. The potential risk of introducing mouse viruses from Matrigel raises concerns as well [57].

Induced pluripotent stem cells (iPSCs) offer respite from the apprehensions linked with ES cells [58]. By sidestepping ethical issues tied to cell sourcing and harnessing human cells to avert immunological hurdles associated with animal sources, iPSCs present a potential wellspring of stem cell-derived hepatocytes [59]. Nevertheless, the hepatocytes derived from iPSCs have not reached the primary or *in vivo* cell performance level. Moreover, the differentiation protocols for iPSCs remain arduous, prolonged, and costly.

#### **2.2.4. Adult stem cells**

Adult stem cells have found application in BAL devices and transplantation studies, capitalizing on trans-differentiation. In this process, mesenchymal stem cells (MSCs) derived from various live donor tissues are coaxed into adopting a hepatocyte-like identity [60]. This strategy involves injecting MSCs into the liver, which subsequently undergo trans-differentiation into cells resembling hepatocytes. Using adult stem cells solves alternative cell types' ethical and immunological challenges. Nonetheless, concerns arise from observed improper differentiation into myofibroblast at injection sites.

Researchers have developed multiple *in vivo* differentiation protocols for MSCs. However, akin to iPSCs, these protocols have considerable costs, prolonged timelines, and demanding procedures. They have yet to yield fully differentiated and stable human hepatocytes. This limitation hampers their translation for clinical applications.

#### **2.2.5. Hepatic progenitor cells**

Hepatic progenitor cells, characterized as quiescent stem cells, maintain a sparse presence within the liver in a healthy state [61]. These cells inhabit anatomical structures known as canals of Hering, representing terminal branches of biliary trees. They express a blend of molecular markers shared by adult hepatocytes, cholangiocytes, and fetal hepatoblasts. After prolonged liver injury or inflammation, hepatic progenitor cells transition from quiescence to proliferative activity, subsequently differentiated into hepatocytes and cholangiocytes.

In transplant studies conducted in mice, hepatic progenitor cells exhibit promising outcomes. Marker analysis underscores the heterogeneity within the progenitor cell population. Variability exists among these cells' differentiation capacity, lineage potential, and differentiation stage. This variability, combined with the intricate challenges associated with isolating the limited number of progenitor cells within the liver, poses obstacles to their clinical application. The potential for these cells to give rise to cancer and their associations with hepatocellular carcinoma further constrain their clinical utility.

#### **2.2.6. Human fetal hepatocytes**

In contrast to the limited proliferative capacity of adult hepatocytes, human fetal hepatocytes

exhibit the ability to undergo multiple divisions *in vitro* [62]. Researchers have addressed the potential scarcity of these cells by immortalizing them by introducing SV40 large T antigen and hTERT transfection, thus ensuring an ongoing and virtually inexhaustible supply. While these cells have been employed in both culture and transplantation investigations, they present certain limitations, notably reduced urea production and ammonia clearance compared to primary and *in vivo* hepatocytes. The functional maturation of fetal hepatocytes is insufficient for their clinical utilization in BAL devices.

Transplantation studies involving fetal hepatocytes have shown encouraging preliminary results. However, ethical considerations associated with fetal cells considerably constrain their clinical applicability, particularly when contemplating the significant cell quantities required for transplantation.

### **2.2.7. Hepatoblasts**

Hepatoblasts share similarities with human fetal hepatocytes, although they are obtained at an earlier stage of gestation, granting them a greater capacity for extensive proliferation *in vitro* [63]. Like hepatic progenitor cells, hepatoblasts can differentiate into both hepatocytes and cholangiocytes under *in vivo* conditions. Animal studies further suggest that hepatoblasts can effectively integrate into injured livers, engaging in proliferation to facilitate liver mass regeneration.

However, akin to other stem cells and those derived from the fetal stage, ethical concerns, limited availability, and intricate differentiation protocols *in vitro* introduce notable challenges for the clinical translation of hepatoblasts.

### **2.2.8. Hepatocyte-like cells**

Recent advancements in genetic modification, with a notable emergence of precise techniques like CRISPR gene editing, have empowered researchers to engineer adult cells capable of expressing hepatocyte transcription factors and functional genes. These engineered cells, called hepatocyte-like cells (IHeps) or steps, can express critical hepatic genes and perform crucial functions [64]. IHeps demonstrated successful engraftment and the capacity to reconstruct hepatic tissue within murine models.

Leveraging genetic engineering tools offers a route to circumvent the intricate and resource-



intensive differentiation protocols inherent in stem cell approaches. This innovative approach holds promise for generating an ethically favorable and potentially boundless supply of hepatocytes. However, it is essential to address concerns regarding the durability of gene expression, the potential for phenotypic deviation from a hepatocyte profile, and the recently identified potential for non-target mutations induced by tools like CRISPR. Further investigation is necessary to ascertain the full scope of these considerations.

### **2.3. Biomaterials in liver Tissue engineering**

The ultimate objective of liver tissue engineering is to produce a fully functional liver that can be transplanted into patients or employed as a platform for diverse research endeavors [65]. As hepatocytes and other liver cells rely heavily on the ECM for their survival and functionality, exploring various biomaterials has been pivotal in establishing successful culture systems [24]. The evolution of liver cell culture techniques commenced with developing a collagen sandwich structure, progressing through microencapsulation, and advancing to 2D hydrogel scaffolds [66]. Concurrently, significant strides were achieved in 3D polymer hydrogel scaffolds. Over the past decade, this trajectory culminated in the innovative utilization of decellularized liver extracellular matrix scaffolds.

Currently, most liver models incorporate scaffold biomaterials to create sites for cell attachment, offering increased surface area and structural support for a larger cell mass [67]. The scaffold material chosen for this purpose should be bioactive, biodegradable, and biocompatible, compatible with liver-specific growth factors [68]. In addition to its biological attributes, the scaffold should exhibit favorable physicochemical properties, including mechanical stability, elasticity, and a high level of interconnected porosity that facilitates the diffusion of growth factors, gases, and nutrients. Notably, matrix stiffness is a physical parameter that influences hepatocyte proliferation and the preservation of their functions. Given that hepatocytes can consume oxygen at a rate five to ten times greater than other cells [69], the pore size of the scaffold significantly impacts effective cell growth and function.

An optimal scaffold material should undergo gradual degradation while concurrently being

replaced by regenerated tissue ECM secreted by the cells, thus minimizing the inflammatory response [59]. Furthermore, the biodegradation products must demonstrate biocompatibility as they diffuse out of the cell-scaffold matrix. Additionally, the scaffold should possess controllable pore sizes, facilitating pre-vascularization or angiogenesis and providing ample surface area for cell colonies to proliferate expansively in all directions [70]. Biomaterials can be categorized into three main types: natural (such as gelatin, collagen, and silk), synthetic (including polyethylene glycol and pluronic), and decellularized tissue-based. Natural biomaterials are derived from living organisms and boast attributes such as non-toxicity, biocompatibility, and the absence of an inflammatory response. Synthetic biomaterials, in contrast, offer high customizability based on specific applications, ensuring reproducibility and robustness. Decellularized tissue, although a subset of natural biomaterials, has evolved into a distinct field of study due to rapid advancements in recent years.

Depending on the intended application, these biomaterials can be tailored into various topographies, including coatings, films, sponges, nanofibers, or hydrogels. Notably, hydrogels are widely recognized as the most suitable biomaterial topography in tissue engineering due to their numerous cell-friendly and mechanical properties [71].

Hydrogels are a 3D arrangement of hydrophilic molecules that can absorb and retain water, establishing an aqueous microenvironment [72]. The substantial swelling ratio of hydrogels emulates the natural ECM environment, making them well-suited for encapsulating cells. Remarkably adaptable, hydrogels can be easily fine-tuned to optimize mechanical properties, biodegradability, and biocompatibility [72]. Through crosslinking, they can be reinforced in advanced fabrication techniques such as 3D bioprinting, enhancing their rigidity and viscosity to facilitate the creation of larger-scale 3D structures. The subsequent sections delve into a comprehensive categorization of these hydrogel materials.

### **2.3.1. Natural hydrogels**

In developing liver models, hydrogels serve as essential scaffolds, contributing crucial mechanical properties by offering consistent structural support. They establish a conducive 3D

environment that guides liver regeneration. Hydrogels derived from natural polymers are particularly well-suited for cell interactions, leveraging biopolymers of natural origin [73]. Among these, collagen, the predominant native protein in tissues, is essential. Constituting 25-30% of the total protein content in mammals, collagen plays a vital role in providing structural support in the ECM [74]. As previously mentioned, collagen types I and III are the most abundant in the liver. Collagen is one of the frequently employed biomaterials for scaffold construction, featuring cell-binding motifs that facilitate the growth of liver cells.

Collagen from various sources encompasses a unique composition of 19 amino acids, including hydroxyproline and hydroxylysine, exclusive to collagen proteins. It adopts a repeating sequence of three different amino acids, (Gly-X-Y)<sub>n</sub>, where X frequently represents proline, and Y represents hydroxyproline. These amino acids are connected by peptide bonds, forming hydrogen bond donors and acceptors that maintain a balanced helical conformation, allowing for load-bearing capabilities. In studies focusing on hepatocytes *in vitro*, standard techniques involve cell seeding onto crosslinked collagen hydrogels or cultivating cells within crosslinked collagen sandwich structures. Collagen type I is often employed as a scaffold material, adopted in various forms such as coatings, microspheres, and 3D matrices.

The cross-linking of collagen hydrogels can be initiated through self-assembly at physiological temperatures. This process enhances mechanical properties by stabilizing amino acid side chains, boosting fiber stability and stiffness. This stabilization impedes the sliding of elongated collagen molecules against each other, particularly under stress. Previous research has harnessed collagen for constructing hepatic units with vascularization and promoting the differentiation of bone marrow cells into the hepatic lineage. Despite its numerous advantages, including low antigenicity, collagen faces challenges in 3D cultures due to its relatively low mechanical strength and considerations of cost and rapid degradation.

Gelatin, emerges from the hydrolysis of collagen through exposure to heat. Collagen and gelatin share polypeptide chains held together by hydrogen bonds formed between adjacent amino acid chains

[75]. In hydrolysis, the triple helix structure of chains unravels, resulting in a partial loss of structural conformation. The outcome of this process is a gelatin solution, representing denatured collagen and possessing a sol-gel transition temperature. Upon cooling beneath this transition temperature, the polypeptide chains aggregate, endeavoring to regain their original triple helix structural conformation through non-specific bonds. However, gelatin's reformation is only partial, establishing regions known as junction zones with helical conformation. This gelation process is characterized as thermos reversible, owing to the ease with which non-specific hydrogen or electrostatic bonds can be disrupted by heat.

Consequently, the gelation of gelatin via cooling is regarded as an imperfect reassembly of collagen chains [76]. Notably, gelatin differs from collagen in water solubility, being able to absorb water to 5-10 times its initial volume. While in its gel state, gelatin is adept at entrapping significant quantities of water, thereby contributing to its structural integrity.

Gelatin showcases remarkable biological attributes and can form robust gels and transparent films. Gelatin is already commercially employed in biomedical applications, such as in Gelfoam®, a gelatin-based wound dressing [77]. To investigate biocompatibility and biodegradation over extended culture durations, gelatin hydrogels have been employed, with a notable example being a two-month study where gelatin hydrogel combined with hepatocytes was stacked in layers of 30 or more, showcasing sustained viability and biological functionality. Gelatin scaffolds undergo faster degradation than hybrid scaffolds. Thus, they are frequently amalgamated with other biomaterials to generate hybrid hydrogels, enhancing structural retention and attenuating the degradation rate. A prime illustration of this approach is Gelatin Methacrylate (GelMA) hydrogel, which amalgamates gelatin with the methacrylic group. In liver tissue engineering, GelMA has been leveraged for embedding bioprinted liver spheroids, leading to prolonged functionality characterized by stable albumin, alpha-1 trypsin, ceruloplasmin, and transferrin secretion [78]. Furthermore, an innovative endeavor in liver tissue engineering involved the development of a bioengineered whole liver utilizing gelatin and polyurethane, with meticulous control over interconnectivity and pore size.

Silk stands out as a notably tenacious and robust biomaterial with FDA approval for applications like sutures and various biomedical fields for years [79]. Derived from silkworms and spiders, silk fibroin possesses impressive attributes such as biodegradability, biocompatibility, adjustable mechanical properties, and minimal immunogenicity. Due to its exceptional mechanical strength, silk fibroin has been harnessed to craft load-bearing 3D constructs. However, a shortfall in silk lies in the absence of cell binding motifs, rendering it biologically inert. It is frequently employed with supplementary biomaterials containing Arg-Gly-Asp (RGD) motifs that facilitate cell attachment and sustenance of growth. A recent study, involved the assessment of primary human hepatocytes' functional behavior within porous collagen-incorporated silk sponges. This investigation showed a fivefold augmentation in hepatocyte functions when co-cultured with fibroblasts, underscoring the pivotal role of co-culture in liver tissue engineering.

Natural biomaterials may exhibit relatively modest mechanical properties, yet they evoke an exceptional cell response in tissue engineering. They can adeptly mimic the ECM of liver tissue, thus inciting liver-specific functionalities.

### **2.3.2. Synthetic hydrogels**

Synthetic hydrogels are artificially synthesized polymers crafted using polymerization techniques to precisely manipulate the ultimate properties and functionalities of the resulting hydrogel. The pivotal determinants that govern the ultimate characteristics of synthetic hydrogels encompass molecular weight, molecular structure, stereochemistry architecture, and composition. Molecular weight influences the hydrogel's theology, viscosity, and mechanical attributes, while architecture, whether linear or branched, shapes the physical properties, and stereochemistry plays a role in crystallinity modulation [80]. Synthetic hydrogels are characterized by fixed compositions and structures, rendering them less intricate than their natural counterparts. Consequently, they offer meticulously controlled mechanical properties and reduced reliance on animal-derived components, contributing to a relatively streamlined FDA approval process [81].

Poly(ethylene glycol), often PEG, is a water-soluble, transparent, nontoxic, nonimmunogenic,

colorless, and viscous hydrogel [82]. Its adaptability for mechanical property enhancement, which makes it amenable to technologies like 3D bioprinting, is noteworthy. PEG hydrogels are extensively employed in liver tissue engineering, serving as a biocompatible matrix for encapsulating primary hepatocytes in survival studies [83]. Leveraging its hydrophilic nature, PEG is a modifying agent when combined with other proteins to enhance their long-term stability and diminish immunogenicity. This process, known as PEGylation, finds utility in tissue engineering for polymer conjugation. PEGylation extends to various applications, including drug delivery, cancer-targeting proteins or peptides, and even gene therapy of cells [84]. However, it is essential to note that while PEG is biocompatible, it is not biodegradable. Therefore, its applications necessitate vigilant monitoring to ensure prolonged stability without toxic implications.

Photopolymerized PEG hydrogel has found application in fabricating intricate architectures containing hepatic cells [85]. Additionally, an undegradable PEG hydrogel was employed in a study to create microtissues featuring co-cultured hepatocytes, resulting in sustained hepatic functionalities. Recent research delved into creating PEG-based hydrogels in hexagonally arrayed 3D liver lobules, utilizing primary fetal liver cells to showcase their advanced differentiation over more than five months. Hence, investigations focusing on the scalability and biocompatibility of PEG-based hydrogels emerge as a promising avenue for future therapeutic strategies.

Poly(vinyl alcohol), or PVA, represents a water-soluble biomaterial characterized by remarkable biodegradability and exceptional biocompatibility [86]. Its versatile application spans various tissue types, encompassing cartilage, bone, skin, and even artificial corneas. PVA holds excellent promise as a foundational matrix, bestowing structural integrity. Often employed as a cornerstone for constructing hybrid hydrogels, PVA lacks intrinsic cell adhesion properties [87].

Similarly, other synthetic hydrogels, such as polycaprolactone, poly(lactide), and poly(lactide-co-glycolide) acid, find extensive application in liver tissue models, courtesy of their commendable biocompatibility [88]. These synthetic hydrogels can be meticulously tailored via molecular weight modulation, block structure variation, and manipulation of degradable linkages, allowing precise

control over their chemical and mechanical attributes. Conversely, while natural hydrogels boast unparalleled bioactivity, non-toxicity, and essential ECM components, they often fall short regarding mechanical strength and reproducibility. Hybrid hydrogels have emerged as a strategic countermeasure, effectively mitigating the limitations inherent to natural and synthetic hydrogel counterparts, as elaborated upon in preceding studies within this section [89].

### **2.3.3. Decellularized liver hydrogel**

Decellularization is a meticulous process designed to strip tissues of their resident cells and cellular remnants, yielding a cell-free scaffold only comprising tissue-specific ECM components [89]. This innovative approach has garnered escalating interest within tissue engineering, primarily for its capacity to replicate the intricate microenvironment of native tissues faithfully. The central objective of decellularization revolves around the thorough elimination of both cells and genetic material, such as Deoxyribonucleic acid (DNA), from the ECM [90]. The decellularized ECM finds utility through two distinct avenues: either as a hydrogel or as an intact organ. In the latter scenario, following decellularization, the whole organ can be strategically repopulated with desired cells through the vasculature initially employed for decellularization.

When employing the decellularized organ as a hydrogel, it undergoes enzymatic digestion to yield a free-flowing solution. Since these early milestones, significant strides have been taken in the ongoing refinement and characterization of decellularization methodologies explicitly tailored for liver tissue.

### **2.3.4. Decellularization process**

The decellularization process causes the utilization of a series of detergents capable of lysing cells within the tissue [89]. This procedure, by nature, is harsh and detrimental to the tissue. A delicate equilibrium must be maintained between efficiently removing antigenic material while maximizing the retention of ECM components and crucial biological factors like growth factors. Decellularization encompasses three primary methods: chemical, physical, and enzymatic, frequently employed in tandem to achieve optimal cell removal and the preservation of ECM [91]. It is imperative to underscore

that the choice of decellularization protocol is highly tissue-specific, as each organ varies cell density and protein density. These variables significantly influence the final concentration of decellularized ECM components.

The physical decellularization method is a non-chemical approach often coupled with chemical or enzymatic agents [92]. It involves applying pressure, temperature, and force to the tissue. An example is the application of freeze/thaw cycles, where ice formation occurs around cell plasma membranes. This technique, particularly suitable for thicker tissues like the liver, is typically combined as an initial step with other decellularization approaches to limit the concentration of chemical reagents. The sonication method employs an ultrasonic bath to transmit acoustic power into a solvent containing the tissue, damaging and lysing cell membranes. However, the intense shockwaves that disrupt cells can harm the tissue's structural integrity. Immersing tissues in chemical or enzymatic detergents is another common practice, often accompanied by agitation. Physical decellularization methods are predominantly utilized to complement chemical and enzymatic decellularization agents [90].

The prevailing strategy for liver decellularization predominantly revolves around chemical detergents. Among these, sodium dodecyl sulfate (SDS), an ionic detergent, is frequently employed for cell membrane solubilization and protein denaturation [93]. While SDS effectively dismantles cell-ECM and cell-cell interactions, it can inadvertently damage structural and signaling ECM proteins, particularly GAGs. Its impact on collagen is less severe. Triton X-100, a non-ionic detergent, primarily targets lipid-protein, lipid-lipid, and DNA-protein cellular interactions [94]. Both SDS and Triton X-100 find extensive usage in liver decellularization at varying concentrations, albeit with the potential to adversely affect ECM components [95]. Notably, despite its detrimental effects on GAGs and elastin, SDS efficiently eliminates cellular components, primarily because of its ability to penetrate deeply into dense tissues such as the liver. The exposure time and detergent concentration are meticulously optimized to minimize prolonged contact with the tissues [96]. Following the decellularization process involving detergents, the tissues undergo rigorous washing to eliminate residual cellular and detergent remnants.



In liver decellularization, it is customary to employ enzymes like trypsin and nucleases. These enzymes are typically introduced after the initial treatment with chemical decellularizing agents to enhance the removal of cellular components and augment the efficacy of the chemical agents [94]. As a result, the harmonious combination of all the methods above culminates in the most favorable outcomes while causing minimal disruption to the tissue's microstructure. In all decellularization protocols, the last step entails flushing away any residual reagents by thoroughly washing and sterilizing the decellularized tissue [90]. In many liver decellularization processes, the freeze/thaw cycle precedes the application of chemical and enzymatic agents.

### **2.3.5. Characterization of the decellularized tissue**

With the primary aim of entirely eradicating cells, the decellularized tissue undergoes a comprehensive evaluation to assess the effectiveness of the decellularization process. Decellularization can significantly affect the remodeling and cellular response of biological scaffolds [97]. Therefore, meeting all the requirements and adhering to quantitative and qualitative guidelines that substantiate decellularization is crucial.

The degree of decellularization is typically quantified by measuring the amount of residual DNA in the decellularized tissue [98]. Generally accepted criteria stipulate that the DNA content should be less than 50ng/mg of the decellularized tissue's dry weight, with no visible nuclear material remaining. A low DNA concentration minimizes the decellularized tissue's immunogenicity, thus reducing the risk of inflammation and antigenicity upon implantation in a patient. DNA quantification assays are commonly employed to assess and compare DNA content between native and decellularized tissues.

Histological staining, such as Hematoxylin and Eosin (H&E), is employed to confirm optimal decellularization [99]. This staining method highlights any remaining cell nuclei appearing in shades of purple-blue while the ECM is stained in pink. Additional immunohistochemistry analyses, including Gordon and Sweet's reticulin staining, Periodic Acid-Schiff, or Masson's trichrome staining, are also used to pinpoint crucial liver proteins' presence and location before and after decellularization.

Morphological analysis post-decellularization can be conducted using scanning electron microscopy (SEM) [89]. This approach allows assessing the tissue's porosity, microscopic anatomy, and 3D structures. Proteomic analysis via mass spectrometry offers a comprehensive overview of the various proteins and low-abundance molecules that may influence the decellularized tissue's performance. Quantitative evaluations of ECM proteins furnish comparative data for characterizing the decellularized tissue's influence on cellular physiology. Since collagen is the most prevalent ECM protein in liver tissue, its quantification can provide valuable insights into expected cellular behavior [100].

These morphological and molecular assessments of decellularized liver tissue aim to closely replicate the native tissue components, establishing an *in vivo*-like microenvironment conducive to encapsulated liver cells. Following the successful completion of the decellularization process, the tissue can be further digested to form a hydrogel.

### **2.3.5. dECM hydrogel**

The fully acellular liver decellularized extracellular matrix (dECM) functions as a reservoir rich in growth factors and molecular components, effectively replicating *in vivo* conditions [101]. The applications of decellularized tissue have diversified to include the generation of hydrogels, coatings, and bioinks for 3D bioprinting [102]. Decellularized liver tissue, for instance, can be subjected to digestion using pepsin in an acidic environment to achieve the desired gel concentration [103]. Typically, concentrations ranging from 10-50 mg/ml of dry tissue in an acidic solution are employed, depending on the intended application. A lower concentration of dECM can be utilized for cell growth coatings, while developing a 3D structure necessitates a higher concentration to maintain structural integrity.

Digesting decellularized liver tissue entails using pepsin and an acidic solution, such as acetic acid or hydrochloric acid, at low concentrations to activate the pepsin enzyme. This process spans approximately 48 hours under constant stirring or agitation, forming a free-flowing solution with a pH of around 2-3. This solution is not temperature-sensitive; however, it becomes responsive to temperature

changes in adjustment to a physiological pH of approximately 7. Thus, the pH adjustment process is conducted below 15 °C using sodium hydroxide. Following pH adjustment at a low temperature, the dECM is crosslinked at 37 °C for 20-30 minutes to yield a robust hydrogel. Most dECM hydrogels, even after crosslinking, may lack the structural properties required for utilization in bioengineering techniques [104]. Therefore, supplementary support structures and formulation enhancers are incorporated to enhance the stability of these dECM hydrogels. These hydrogels can be further examined for their permeability, allowing the assessment of aqueous media, solute diffusion, and oxygenation. This study can also be extended to investigate drug diffusion and clearance through specific hydrogel thicknesses, facilitating the creation of tissue models for drug testing. Porcine dECM hydrogel has been integrated into bio-fabrication methods like 3D bioprinting to demonstrate printability and the differentiation of bone marrow-derived mesenchymal stem cells [105]. Studies have showcased enhancements in liver functions within organoids generated in sheep dECM hydrogels compared to collagen type I (rat tail). In summary, incorporating various liver components into hydrogels alongside collagen will likely play a pivotal role in shaping tissue models' remodeling and regenerative capabilities. Liver dECM represents a promising alternative to conventional hydrogels, such as collagen, which have been extensively employed for hepatocyte culture [106]. The future outlook for liver dECM is rapidly evolving, particularly in bioengineering approaches like 3D bioprinting, enabling the inclusion of diverse cell types and intricate geometries to advance liver regeneration [107].

#### **2.4. Fabrication techniques of liver tissue engineering**

Conventional cell culture techniques are typically conducted in 2D, involving the growth of cell monolayers on flat, polystyrene tissue culture plastic dishes. Established since Ross Granville Harrison pioneered cell culture methods in 1910, this approach has contributed significantly to biological research [108]. However, researchers are increasingly acknowledging the limitations of the artificial 2D environment, which significantly affects cell behavior, leading to variations in metabolic profiles and protein production [109].

Hepatocytes, in particular, are responsive to their 3D microenvironment. Changes in factors like albumin and urea production, ammonia clearance, and CYP expression are observed in response to alterations in their culture environment. The rapid functional deterioration of primary hepatocytes and hepatocytes from other sources can be attributed to the artificial conditions of conventional culture methods [110]. This realization has prompted bioengineers to focus on creating specialized microenvironments that optimize and change hepatocyte behavior and performance.

Hepatocyte function is remarkably adaptable and regulated by a combination of factors, including the ECM, extracellular signaling molecules, cell-cell interactions, and mechanical cues from the surrounding environment. While researchers have yet to fully comprehend the effects of these factors, bioengineers are exploring various strategies, some of which may not be strictly "biomimetic" in replicating physiological conditions but still profoundly influence hepatocyte behavior.

Many approaches have been employed to counteract this functional deterioration. These strategies include culturing in arginine-free media, incorporating various growth factors, and using DMSO. Hepatocytes have been cultured on collagen membranes, within Matrigel, and on diverse ECM materials, all of which have significantly shown the capacity to influence hepatocyte function.

The development of devices replicating the hepatic shear environment, architectural designs resembling hepatic lobules and perisinusoidal spaces, and the co-culture of hepatocytes with non-parenchymal cells have shown considerable promise. These methods can be summarized broadly, as outlined in Table 1.

Table 1. Fabrication techniques of liver tissue engineering

Environment	Techniques	Advantages	Disadvantages
Scaffold-free 3D culture	Spheroid formation Sandwich culture Co-culture	No polymers/foreign materials required	High cell densities Necrosis risk in spheroid centers Foreign proteins required
Micropatterning & bioprinting	Bioink printing Cell encapsulation	Rapid bio-patterning Can recapitulate liver	Limited on size

		structures	
Scaffolds	Hydrogels Electrospun polymers ECM scaffolds	Repeatable and structurally stable	Risk of degradation/rejection of foreign materials Necrosis in hydrogel centers
Decellularized organs	Whole organ decellularization	Vasculature and ECM 'bio- recipe' intact	Whole organs are still required Incomplete decellularization Remnant detergents High cell densities for recellularization
Perfusion and microfluidic devices	Shear devices and lobule-mimicking devices	More realistic 'flow' environment Constant oxygen/nutrient exchange	Complex device manufacture and modelling Size limited
Bioartificial livers	Extracorporeal bioreactors	Can actively (via cells) or passively (via adsorption/filtration) support liver function.	High cell densities Current clinical trials unsuccessful in replacing liver function

## **Part II**

### **Over 4500 mm<sup>3</sup> Engineered Liver Scaffold for Implantable Artificial Livers**

## Chapter 1:

# Angiogenesis in Free-Standing Two-Vasculature-Embedded Scaffold Extruded by Two-Core Laminar Flow Device

## I. Background

The vascular network densely permeates organs to provide efficient mass transfer within the body [111]. This branched network of vessels transfers nutrients and oxygen and removes metabolic waste from organs [112]. A functioning vascular network is essential for engineered thick tissues as well. *In vivo*, cells are generally located within 200  $\mu\text{m}$  of blood vessels to avoid ischemic conditions [113]. However, fabricated tissues *in vitro* lack a vasculature network, so cells inside the engineered tissue often receive nutrients by diffusion over 200  $\mu\text{m}$ , with a maximum distance of 1 mm at worst [114].

To fabricate pre-vascular channels, various methods have been proposed, such as electrospinning [115], molding [116], laser degradation [117], coaxial extruding [118-120], acoustofluidic extruding [121], cell sheet stacking [122], and cell coculture [123]. These approaches have shown promise but still require further development because prolonged fabrication times and complex manual processes can damage cell viability. Additionally, limited vasculature layer number and the complex fabrication process of mesovasculatures are other challenges that need to be addressed [124].

Therefore, engineered thick tissues require not only a pre-vascularization method but also a method to promote easy angiogenesis. Some studies have investigated the angiogenic process within microfluidic chips [125-127]. However, there are few reports on angiogenesis in free-standing scaffolds (3D scaffolds without external support) because delivering growth factors (GFs) or implementing a GF gradient inside the 3D scaffolds is challenging. A couple of reports have demonstrated angiogenesis with a single-channel structure. Duong et al. extruded a double-layered, single-vascular scaffold containing human umbilical vein endothelial cells (HUVECs) and human aortic smooth muscle cells (HASMCs) [128]. In their study, the GF secreted from the HASMC layer induced angiogenic sprouting. Gao et al. fabricated a single-layered, single-vascular scaffold with HUVECs and demonstrated angiogenic sprouting using GF-mixed collagen [129]. These methods were not suitable for creating a vascular network within engineered thick tissues.

In this study, we extruded a scaffold embedded with two vascular channels and demonstrated angiogenesis within the pre-vascularized tissue. The scaffold structure consisted of one hollow channel

for flowing GF-mixed media and a core containing HUVECs to form a vascular channel (Fig. 4). A GF gradient from the hollow channel induced angiogenic sprouting from the HUVEC vessel inside the generated scaffold. We compared and quantitatively analyzed angiogenesis under three different culture conditions. The effects of shear stress, perfusibility, cell viability, and core size were also evaluated.

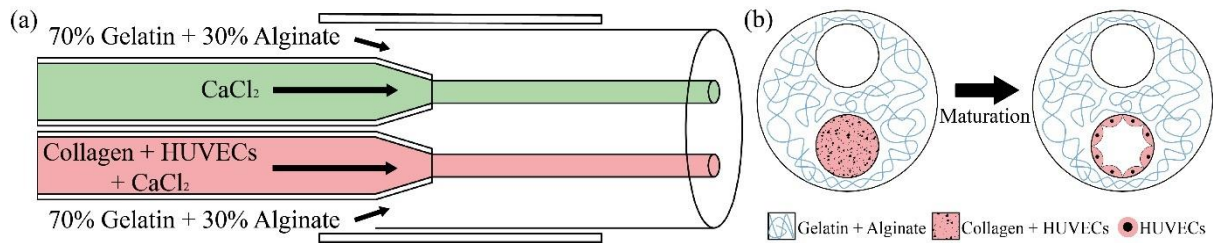


Figure 4. Schematic diagram of the two-vasculature-embedded scaffold. (a) One core (green) consisted only of 0.1 M calcium chloride dihydrate ( $\text{CaCl}_2$ ) for the hollow channel. Another core (pink) was made of HUVECs, 3 mg/mL type-1 collagen, and 0.1 M  $\text{CaCl}_2$  for the vascular channel. The shell layer consisted of gelatin and sodium alginate. (b) Cross-sectional view of the two-vasculature-embedded scaffold immediately after formation and after maturation.

## II. Materials and Methods

### 1. Two-core laminar flow device

Based on our previous device (Figure 5) [130], we designed and fabricated a two-core laminar flow device. It has three inner glass capillaries (580  $\mu\text{m}$  inner diameter [ID], G100-3, Warner Instruments LLC, U.S.A.) that function as inlets and one outer glass capillary (1160  $\mu\text{m}$  inner diameter, G200-3, Warner Instruments LLC, U.S.A.) for an outlet. Two of the three 580  $\mu\text{m}$  ID tubes were tapered to approximately 200  $\mu\text{m}$  using a puller (PC-10, Narishige, Japan) to create the two inner core inlets. The other 580  $\mu\text{m}$  ID tube supplied the outermost layer material to the 1160  $\mu\text{m}$  ID tube without any tapering. All four tubes were then connected within a block of polydimethylsiloxane (PDMS, Dow Corning Corporation, U.S.A.). Before biological experiments, the fabricated device was sterilized at 121°C for 15 minutes.



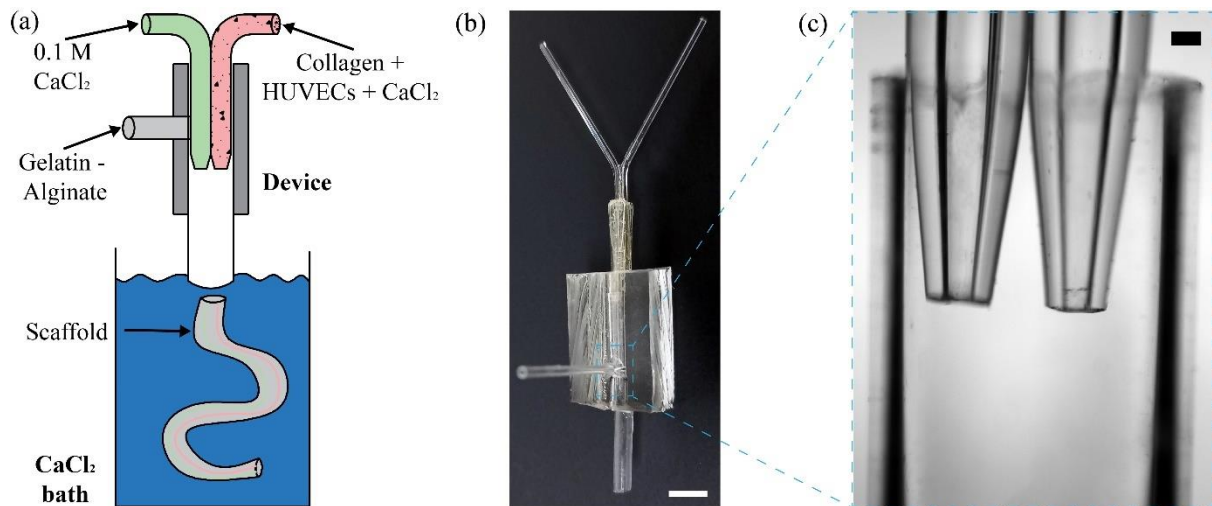


Figure 5. Two-core laminar flow device is presented; (a) A schematic diagram of the two-core laminar flow device and the  $\text{CaCl}_2$  bath; (b) An image of the fabricated device (scale bar: 5 mm); (c) a microscope image of the two-core area among two inlet glasses and the body glass (scale bar: 200  $\mu\text{m}$ ).

## 2. HUVEC culture

HUVECs were purchased from ATCC (U.S.A.) and cultured in their recommended medium (vascular cell basal medium supplemented with Endothelial Cell Growth Kit-VEGF). Media were changed three times a week. The cells were maintained in a humidified incubator at  $37^\circ\text{C}$  with 5%  $\text{CO}_2$  and passaged before reaching 80% confluency. Experiments utilized cells between passages 10 and 15.

## 3. Two-vasculature-embedded scaffold formation

Three syringe pumps (11 Elite C300918, Harvard Apparatus, U.S.A.) were connected to the fabricated device through Tygon tubes (Saint-Gobain, Courbevoie, France). These pumps delivered solutions for the two cores and the outer layer of the scaffold. A mixture of 3 mg/mL collagen,  $2 \times 10^6$  cells/mL HUVECs, and 0.1 M  $\text{CaCl}_2$  (Daejung Chemicals, Republic of Korea) was supplied through one core inlet for the formation of a blood vessel. To create a hollow channel, a solution of 0.1 M  $\text{CaCl}_2$  (Daejung Chemicals, Republic of Korea) was injected through the other core inlet. For the outer layer inlet, a 2% weight/volume (w/v) mixture of gelatin (Sigma-Aldrich, U.S.A.) and alginate (Daejung Chemicals, Republic of Korea) (70:30 ratio) was supplied to form the body of the scaffold. The extruded scaffold was submerged into a 0.1 M  $\text{CaCl}_2$  bath through the outlet and then cross-linked. Calcium ions from the  $\text{CaCl}_2$  solution cross-linked with sodium alginate to form calcium alginate, ensuring that no hydrogel remained in the hollow channel. The gelatin scaffold was then washed with phosphate-buffered saline (PBS, Sigma-Aldrich, U.S.A.). Finally, the washed scaffold was cultured in an incubator at  $37^\circ\text{C}$  with 5%  $\text{CO}_2$ , with fresh medium replacement every 2 days.

#### 4. Laboratory made connecting device

To connect a syringe pump to the fabricated scaffold, a 2.0 mm ID glass tube and a Pasteur pipette (Hilgenberg, Germany) were cut and then bonded together using PDMS (Figure 6A). A hole was punched in a Petri dish (SPL, Republic of Korea), and the assembled glass holder was secured to the Petri dish through the hole using PDMS (Figure 6B). The fabricated leakproof connecting device was then sterilized with 99.9% ethanol for 24 hours before biological experiments.

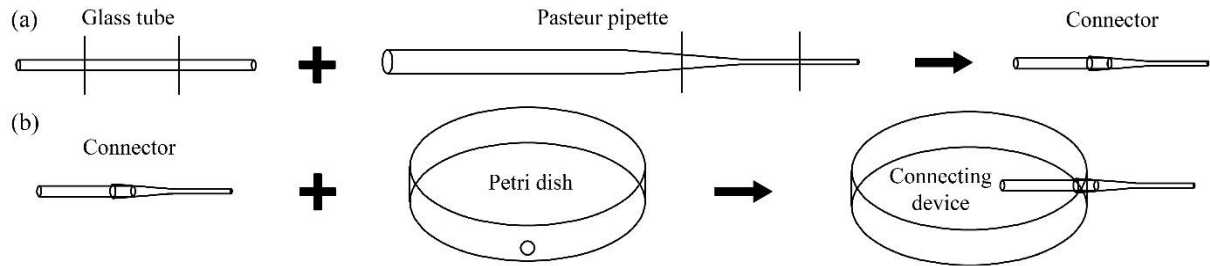


Figure 6. Fabrication process of the connecting device. (a) The holder fabrication process. (b) The attaching process of the hole punched Petri dish and the holder.

#### 5. Three types of culture condition

The fabricated two-vasculature-embedded scaffolds were cultured under three conditions to investigate the effect of media flow: (i) media diffusion obstructed by a glass tube, (ii) static immersion in a media dish, and (iii) media flowing through the scaffold channels (Figure 7).

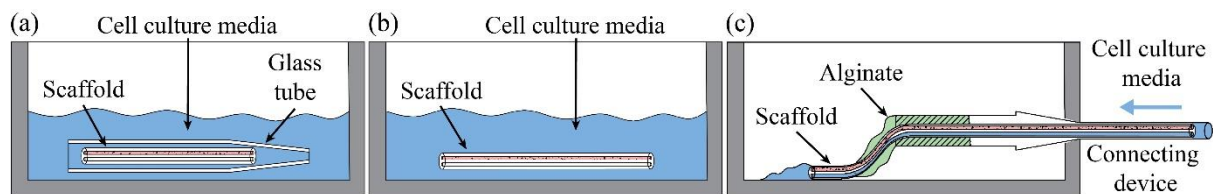


Figure 7. Three types of culture conditions. (a) The obstructing condition. (b) The soaking condition. (c) The flowing condition.

To hinder media diffusion within the fabricated scaffold, it was inserted into a tapered glass tube (narrow end: 1000  $\mu\text{m}$  ID, wide end: 2000  $\mu\text{m}$  ID) and then immersed in culture medium. Using a syringe pump, the 1000  $\mu\text{m}$  OD scaffold was secured by suction into the narrow end of the tapered tube. To create a conventional media diffusion condition for the embedded cells, the fabricated scaffold was simply immersed in culture medium. For flowing media through the scaffold's hollow channel, one end was secured to the holder of the custom-made connecting device using suction. Alginate was used to seal the connection between the holder and the scaffold. Culture medium was continuously delivered to the connected scaffold at a flow rate of 10  $\mu\text{L}/\text{min}$  using a syringe pump. The medium exited the scaffold

from the unconnected end. Initially, no medium flowed out of the scaffold. However, as continuous flow progressed, the exiting medium accumulated around the scaffold, forming a puddle. This accumulated medium was removed from the Petri dish every 24 hours.

## **6. Diffusion from the hollow channel**

To determine an appropriate flow rate within the scaffold's hollow channel, a cell-free two-vasculature-embedded scaffold was fabricated. A red food dye solution was perfused through the cell-free scaffold at varying flow rates ranging from 2  $\mu\text{L}/\text{min}$  to 20  $\mu\text{L}/\text{min}$ . Using a bright-field microscope, the spread and shape (morphology) of the red food dye were observed. Based on these observations of the red food dye, the flow and diffusion of a green fluorescent dye solution (diluted 1:1000 in PBS) were then quantitatively analyzed using a fluorescence microscope.

## **7. Perfusibility in the two vasculatures**

To assess the perfusion of the HUVEC vessel, blue fluorescent microbeads (5.42  $\mu\text{m} \pm 0.09 \mu\text{m}$ , GmbH, Germany) diluted 1:200 in PBS were perfused through the scaffold. Following a 2-day culture period under soaking conditions to promote HUVEC-collagen core development into a blood vessel, the Calcein AM-stained scaffold was connected to a syringe pump using the custom-made connecting device. Blue fluorescent microbeads were then perfused through the scaffold using the syringe pump.

## **8. GFs for angiogenic sprouting**

To stimulate angiogenic sprouting, additional growth factors (GFs) were supplemented to the culture medium, following established protocols [125, 131]. These additional GFs were used at a concentration of 50 ng/mL each of vascular endothelial GF, basic fibroblast GF, and hepatocyte GF (all from Preprotech, U.S.A.). The generated scaffolds were initially cultured in the growth factor-supplemented medium only for the first 2 days to allow for vascular structure development. From day 3 onwards, the culture medium was supplemented with the additional GFs and changed every 2 days.

## **9. Immunofluorescent staining**

To observe migration, morphology, and angiogenesis of the embedded HUVEC, F-actin, CD31, and nuclei were stained using rhodamine-phalloidin, anti-CD31, and DAPI, respectively. First, the formulated scaffold was fixed with 4% paraformaldehyde (P6148, Sigma-Aldrich, U.S.A.) for 40 min at room temperature (RT). The fixed scaffold was immersed in alginate lyase (Sigma-Aldrich, U.S.A.) solution to remove alginate at 37°C. The alginate removed HUVEC core was immersed in a collagen matrix and incubated at 37°C for gelation. Subsequently, the HUVEC core in collagen was

permeabilized with 0.1% Triton X-100 (Sigma-Aldrich, U.S.A.) for 5 min at RT. Primary antibody of anti-CD31 (MA5-13188, Invitrogen, U.S.A.) was incubated at 4°C overnight. Then, secondary antibodies (Alexa Fluor 488, Invitrogen, U.S.A.) and Phalloidin (Alexa Fluor 488, Invitrogen, U.S.A.) were applied for 2 h at RT. Besides, nuclei of the HUVEC core were stained with DAPI (D1396, Invitrogen, U.S.A.) for 5 min. After every chemical treating step, the treated sample was washed 3 times with PBS for 5 min. The stained samples were observed using an IX53 inverted fluorescent microscope (Olympus, Japan) and a FV1000 laser scanning confocal microscope (Olympus, Japan).

## 10. Statistical analysis

The result was represented with a mean value  $\pm$  one standard error from three independent repetitions. To evaluate the statistical significance level, one-way ANOVA and Tukey's post hoc test were utilized. Its significance is remarked as \* for  $P < 0.05$ , \*\* for  $P < 0.01$ , and \*\*\* for  $P < 0.001$ .

## III. Results

### 1. Fabrication of the two-vasculature-embedded scaffold

The two-vasculature-embedded scaffolds without cells were controllably and continuously generated using our two-core-embedded device. After complete gelation, the fabricated scaffolds were uniform and stable with a length of meters (Figure 8a). Various flow rates of the gelatin-alginate fluid, the collagen-CaCl<sub>2</sub> fluid, and the CaCl<sub>2</sub> fluid were explored to select diameters of the shell and two vasculatures for further experiments. In Figure 8c, the graph presented scaffolds' diameter with respect to the shell flow rate at a fixed core flow rate of 0.1 mL/min. As the shell flow rate increased from 1.5 mL/min to 3 mL/min, the shell diameter increased from 948  $\mu\text{m}$  to 1095  $\mu\text{m}$ . Besides, the diameter of the collagen core decreased from 376  $\mu\text{m}$  to 262  $\mu\text{m}$ , and that of the CaCl<sub>2</sub> core also decreased from 331  $\mu\text{m}$  to 203  $\mu\text{m}$ . In addition to the shell flow rate change, the core flow rate shift was also investigated. The shell diameter decreased from 1067  $\mu\text{m}$  to 951  $\mu\text{m}$  in an increment of the core flow rate from 0.05 mL/min to 0.2 mL/min when the shell flow rate was constant with 2 mL/min (Figure 8d). The diameter of the collagen core and CaCl<sub>2</sub> core increased from 191  $\mu\text{m}$  to 409  $\mu\text{m}$  and from 165  $\mu\text{m}$  to 281  $\mu\text{m}$ , respectively. Therefore, the shell flow rate with alginate-gelatin mixture as 2 mL/min and the two-core flow rate with collagen, HUVEC, and CaCl<sub>2</sub> as 0.1 mL/min were designated to fabricate two-vasculature-embedded scaffolds for experiment with cells.

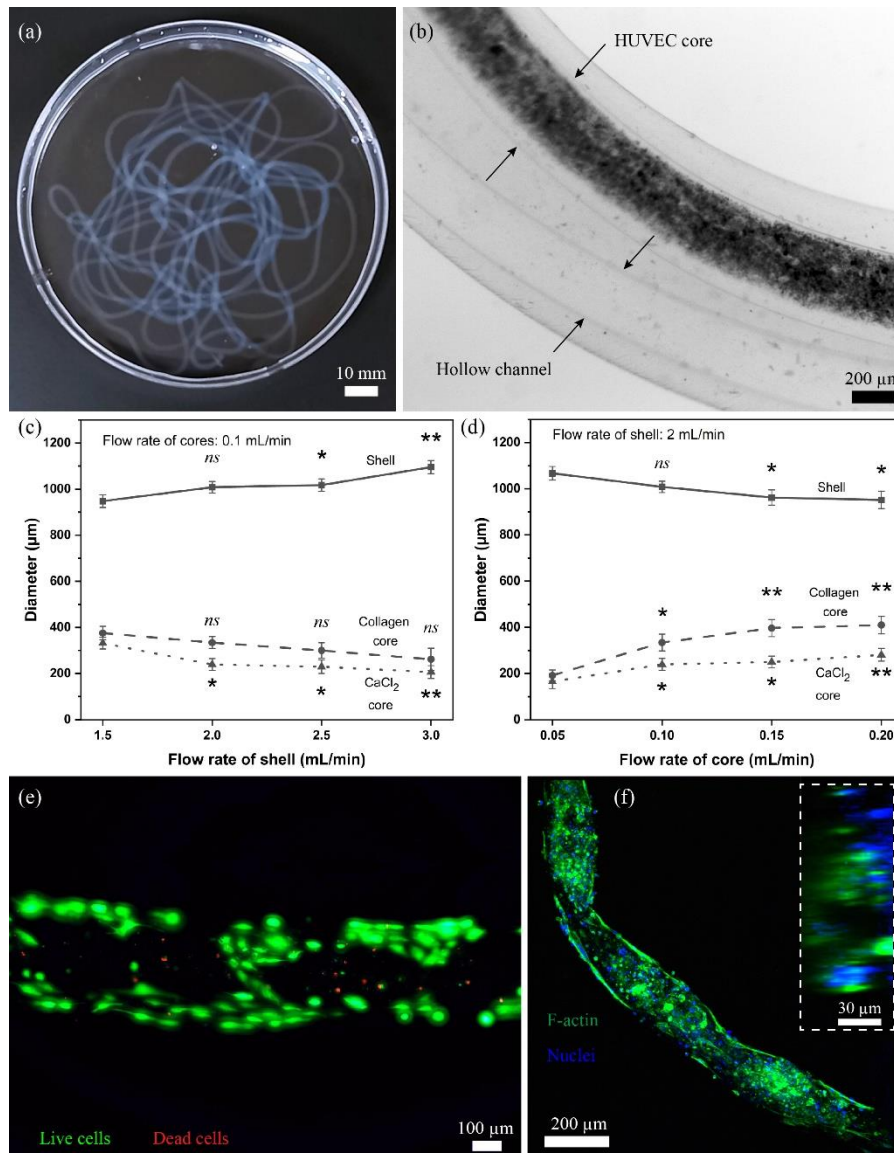


Figure 8. Fabricated two-vasculature-embedded scaffold; (a) the generated scaffold in the Petri dish after the formation (scale bar: 10 mm); (b) The bright-field microscope images of the scaffold with the HUVEC core and the hollow channel after the formation (scale bar: 200  $\mu\text{m}$ ); (c) The diameter of the shell and the two channels with the flow rate of the cores as 0.1 mL/min and various flow rates of the shell; (d) the diameter of the shell and the cores with the flow rate of the shell as 2 mL/min and various flow rates of the cores; (e) the fluorescent image of the stained HUVECs inside the fabricated scaffold after 1-day culture (scale bar: 100  $\mu\text{m}$ ). (f) The confocal image of the HUVECs after 2-day culture (scale bar: 200  $\mu\text{m}$ ) and the cross-sectional view of the lumen structure in the HUVECs (scale bar: 30  $\mu\text{m}$ ).

Figure 8b shows the formulated two-vasculature-embedded scaffold under the bright-field microscope. Two separated cores with a transparent hollow channel and a HUVEC filled channel were observed. Aggregation of individual cells at day 0 (Figure 8b) has gradually stretched, migrated, and



connected to produce ECs' networks after 1 day of culture (Figure 8e). Confocal images of the HUVEC core exhibited a hollow center in cross-section view (Figure 8f). HUVEC has the propensity to form luminal structures in the three-dimensional matrix, which can be perfused [128, 132, 133].

## 2. Perfusability

To optimize flow rate through the hollow channel, the red dye has flowed through the hollow channel of the cell-free two-vasculature-embedded scaffold, as shown in Figure 9. The flow rates over 10  $\mu\text{L}/\text{min}$  have diffused into all parts of the scaffold in 10 min. However, 2  $\mu\text{L}/\text{min}$  and 5  $\mu\text{L}/\text{min}$  required 15 min for the entire diffusion. Even though it diffused at all parts of the scaffold, its color gradient differed according to the flow rate. As the flow rate increased, its red color became deep in less time. However, in our previous study [134], the flow rate over 20  $\mu\text{L}/\text{min}$  has made the linking part from the connecting device to the scaffold loosen in a short time. Therefore, 10  $\mu\text{L}/\text{min}$  was selected for the secure connection in this investigation.

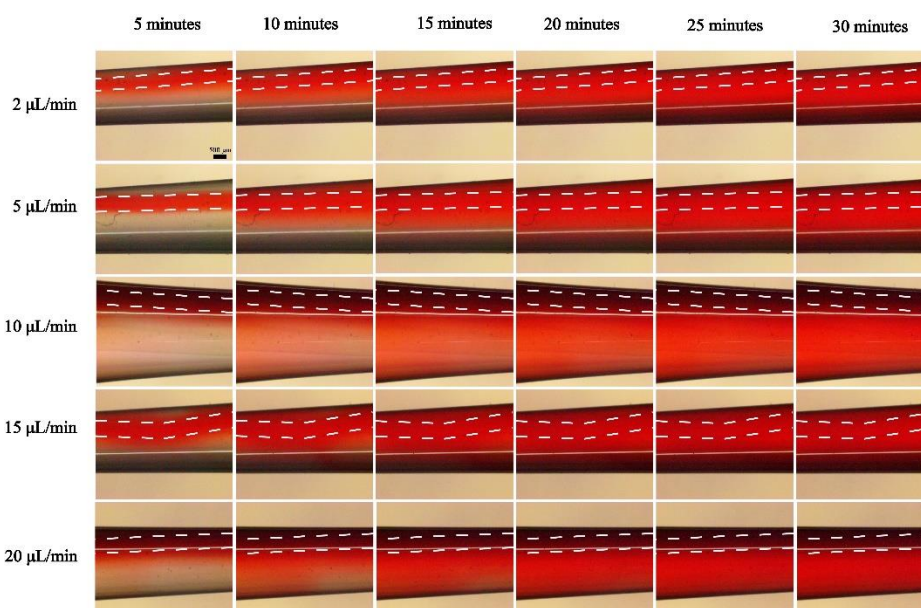


Figure 9. Time-lapse images of the perfused channel from 5 min to 30 min at various flow rates (scale bar: 500  $\mu\text{m}$ ).

Fluorescence fluid was also pumped into the hollow channel with the flow rate of 10  $\mu\text{L}/\text{min}$  until 60 min to understand diffusion in our scaffold. Figure 10 presented the temporal sequence of the fluorescence microscope images. Based on the temporal images, fluorescence intensity was analyzed. The most gray value at 1 time point showed an increasing tendency as time went (Figure 10b). The integrated density exhibited a similar tendency with the most gray value (Figure 10b). Considering these two graphs, 15 min was a meaningful time to diffuse significantly up to about 100  $\mu\text{m}$  apart from the edge of the channel.

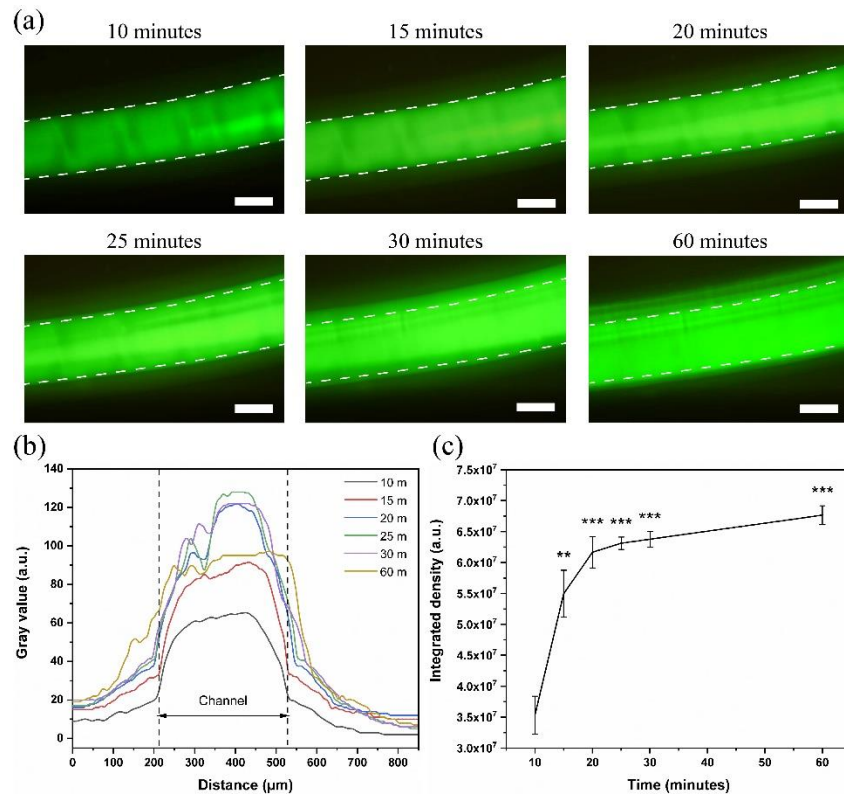


Figure 10. Perfusion assay; (a) The time-lapse fluorescence images of the channel from 0 min to 60 min at  $10 \mu\text{L}/\text{min}$  of fluorescence fluid (scale bar:  $200 \mu\text{m}$ ). (b) The fluorescent intensity profile in the channel was graphed according to the distance. (c) The integrated density was analyzed with respect to the time.

Perfusibility of the HUVEC vessel was evaluated with blue fluorescence microbead, as shown in Figure 11. The blue fluorescence microbead flowed continuously in the HUVEC vessel. It showed that the embedded HUVECs have well developed into the vascular structure. Even though the syringe pump drove the blue microbead identically to both channels at the flow rate of  $10 \mu\text{L}/\text{min}$ , the hollow channel flowed much more microbeads than the HUVEC vessel (Figure 11b). It was presumed that the HUVEC vessel had much more bumpy structures than the hollow channel for the microbead to pass through.

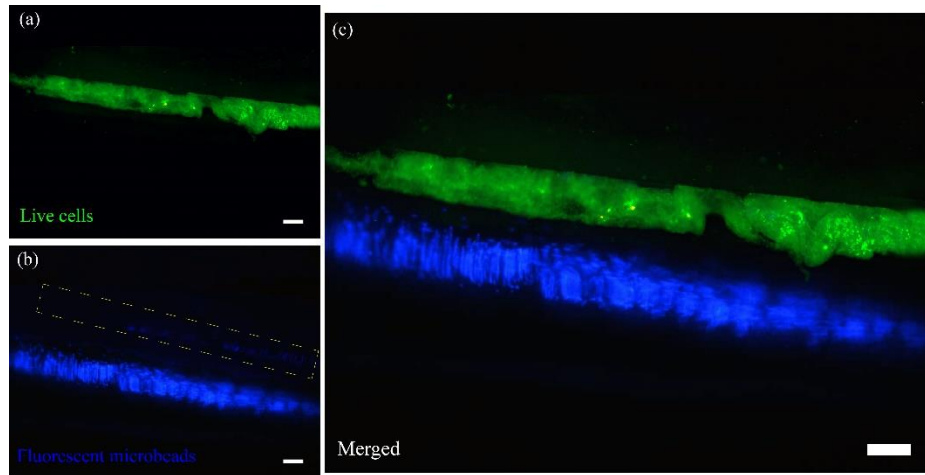


Figure 11. Fluorescence images of the two-vasculature-embedded scaffold during pumping; (a) the fluorescence images of the live-/dead-stained HUVEC channel. (b) The hollow channel with the blue fluorescent microbeads. (c) The fluorescence images of the two vasculatures (green: Live cell, blue: Microbeads, scale bar: 200  $\mu\text{m}$ ).

### 3. Cell morphology according to the culture condition

Different F-actin expression of the embedded HUVECs was observed according to the culture condition, as shown in Figure 12. The cells in the obstructing condition exhibited arbitrary size and cobblestone-like morphology with random orientation (Figure 12a). The soaking condition showed spindle-like morphology doped in the cobblestone-like morphology with random orientation (Figure 12b). Particularly, the cells in the flowing condition presented uniform spindle-like morphology with the arrangement in the flow direction (Figure 12c). These results indicated that cell elongation and alignment of the flowing condition are similar *in vivo* [135]. For further quantitative analysis, three morphometric parameters of the embedded HUVECs, namely, perimeter, elongation ratio, and orientation deviation (Figure 12d-f), were investigated. The orientation deviation was calculated from the standard deviation of cell orientation, the direction of the longer part in the embedded HUVEC morphology. The cells in the flowing condition exhibited the longest perimeter, the highest elongation ratio, and the lowest orientation deviation. It means that the cells in the flowing condition were mostly elongated and aligned among three culture conditions.



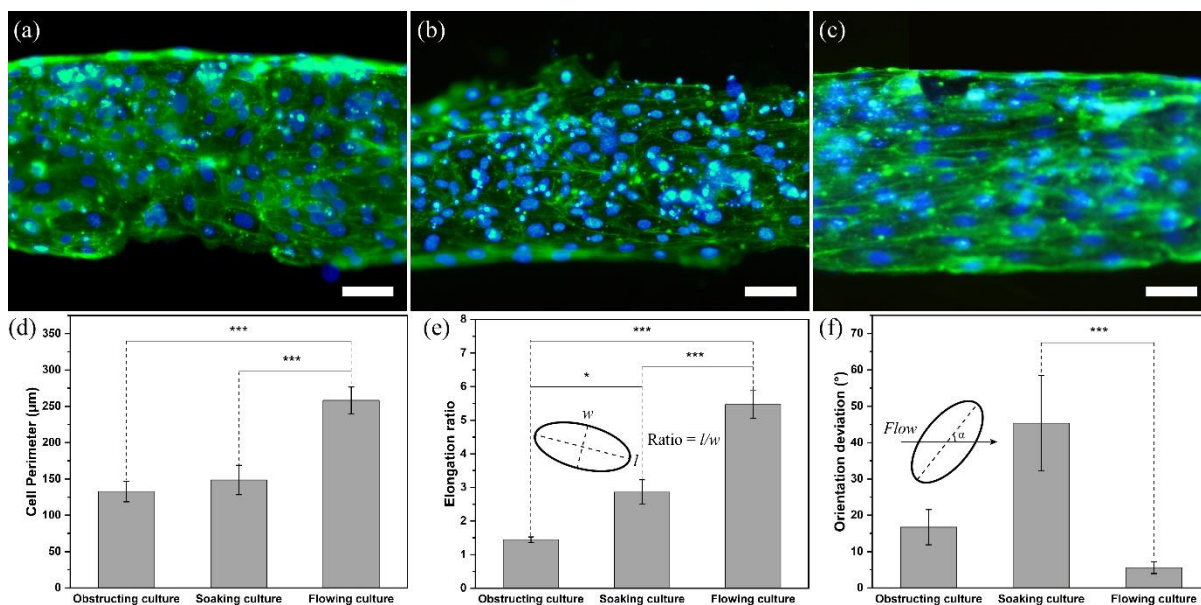


Figure 12. Morphology characterization in the HUVEC channel on day 2; the stained HUVECs in (a) the obstructing condition, (b) the soaking condition, and (c) the flowing condition (scale bar: 50  $\mu\text{m}$ ). The quantification of (d) the perimeter, (e) the elongation ratio, and (f) the orientation deviation of the stained HUVECs.

#### 4. Angiogenic sprouting

Figure 13 exhibited the angiogenic sprouting of the embedded HUVECs in the generated two-vasculature-embedded scaffold up to day 10 with F-actin (Figure 13a-c) markers. The cells in the obstructing condition angiogenically sprouted from day 3 to day 7 (Figure 13a). Those sprouting looked no significant directionality. On day 10, all the sprouts disappeared, and no new sprouts were recognized. The cells in the soaking condition presented the angiogenic sprouting from day 3 to day 10 (Figure 13b). Considerate directionality was not observed as well. The cells in the flowing condition angiogenically sprouted during all the time points from day 1 to day 10 (Figure 13c). In particular, significant directionality of all the new sprouts to the hollow channel was observed, which diffused the high GF media into the HUVEC vessel. Furthermore, connections among adjacent sprouts were found on day 7 and day 10.

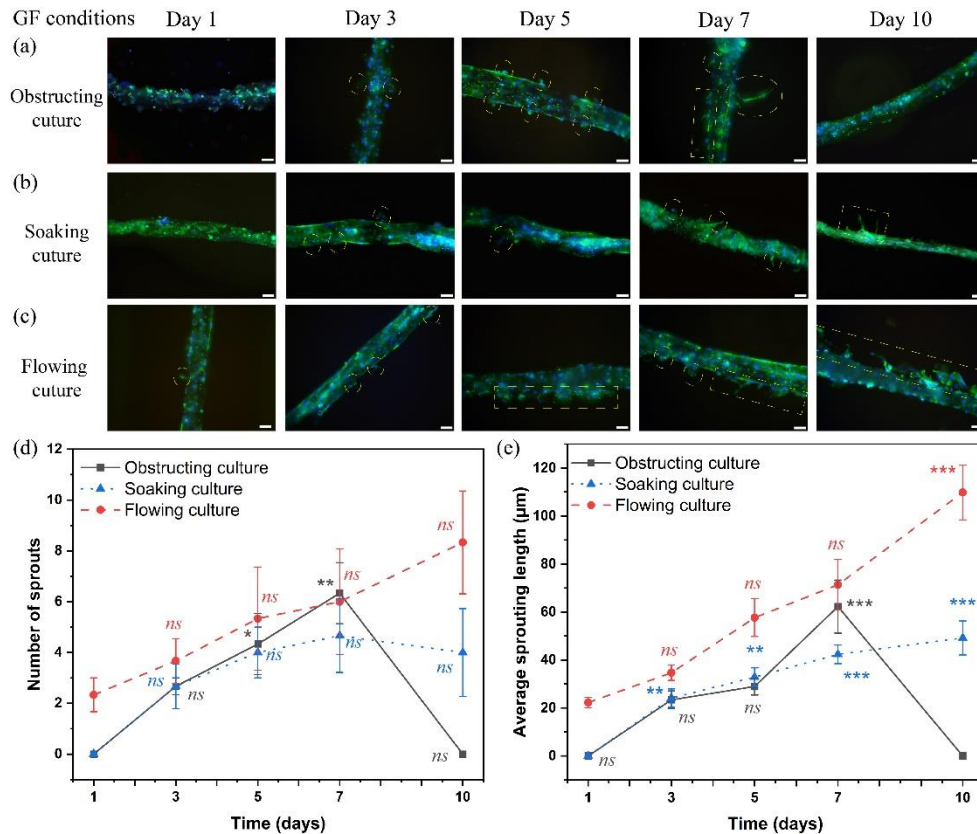


Figure 13. Angiogenic sprouting in all three culture conditions. The immunofluorescence images with F-actin signal of (a) the obstructing condition, (c) the soaking condition, and (c) the flowing condition (green: F-actin, blue: Nuclei, scale bar: 100  $\mu\text{m}$ ). (d) The sprouting number was graphed. (e) The average length of the sprout was analyzed.

Sprouting number and length were quantitatively analyzed, as shown in Figure 13d and e. The flowing media inside presented an increasing tendency in both the number and the length. Except for the sprouting number at day 7, the cells in the flowing condition showed the highest number, the longest length among all the three conditions. On day 7, the sprouting number of the obstructing condition was slightly higher than that of the flowing condition. On day 7, the obstructing condition exhibited the highest number and the longest length among all the time points in the same culture condition. The sprouting number of the soaking condition showed the highest number at day 7 among all the time points in the same culture condition. In the case of the length, it presented a gradual increasing tendency.

The flowing condition showed the most active angiogenesis. It was assumed that the GF diffusion from the near hollow channel stimulated HUVECs more than the GF diffusion from the outside media. The glass capillary of the obstructing condition looked restricting the GF diffusion into the embedded HUVECs. It was demonstrated that below 65% cell viability in the obstructing condition could affect no angiogenesis at day 10.

## IV. Discussion

The formulated scaffolds consisted of two separated channels and the outer shell. One channel was filled with the mixture of HUVECs and type I collagen. The other channel was the hollow channel. The outer shell material was the composite of gelatin and alginate. The laboratory made connecting device linked the generated scaffold to a syringe pump for 10 days without any leakage. The flowed media diffused from the hollow channel to the embedded HUVECs. Due to the diffused media, aggregation of the individual HUVECs developed into the vascular structure. The angiogenic sprouting was induced from the HUVEC vessels to the hollow channel by the gradient of the additional GFs.

Scaffold material could be divided into natural, synthetic, hybrid, and decellularized extracellular matrix. Each group has its own advantages and disadvantages. Gelatin, a natural polymer, has been used in tissue engineering due to its high biocompatibility and biodegradability. However, the poor mechanical properties of gelatin restrict its application. Fortunately, alginate is generally used to improve its mechanical characteristics. Taking into consideration the previous investigations [136-138], the composite of gelatin-alginate with weight ratio of 70:30 was chosen to enhance biocompatibility and mechanical properties.

In this study, the outer shell thickness and the distance between the two cores were approximately 280 – 290  $\mu\text{m}$  and 140 – 150  $\mu\text{m}$ , respectively. Rouwkema et al. demonstrated that cells show similar biological behavior at a distance < 200  $\mu\text{m}$  due to the supply of adequate culture medium by diffusion [139]. The maximum distance between capillaries is approximately 200  $\mu\text{m}$ , usually < 150  $\mu\text{m}$  [140, 141]. Therefore, our structure could be a potential model to investigate perfusion efficiency from one channel to another in a thick three-dimensional structure.

The developed HUVEC vessel showed to flow microbeads (Figure 11). Lots of microbeads on most surface area of the hollow channel and some microbeads in the HUVEC vessel have not flowed or flowed relatively slowly. These not moving or slow-moving microbeads were supposed to attach to the channel surface like the flow-enhanced cell adhesion [142-144]. The hollow channel was made continuously and uniformly by the microfluidic laminar flow device. However, the HUVEC vessel was formulated by HUVEC's natural tendency so that its structure would be much more complex and variable.

The HUVECs in the flowing condition have elongated much more in their shapes and aligned much more with each other (Figure 12) than into two other conditions. ECs recognize minor variations in the direction, magnitude, and shear stress and respond by directing vasculature remodeling [145, 146]. ECs are continuously contacted *in vivo* to shear stress from blood flow to maintain vascular homeostasis [147, 148]. Mechanical stimulation is an integral component of tissue development, in which it can distinctly influence cell behavior by inducing morphological and transcriptional changes

[149, 150]. ECs tend to respond to fluid shear stress to minimize resistance, modifying the ECs phenotype [151, 152]. ECs align and elongate due to the mechanically affected distribution of cytoskeleton proteins when shear stress occurs with the perfusion process [153-155]. Besides, ECs become more elongated with long-term culture related to the stable cell-cell junction and higher motility capacity [156, 157]. Interestingly, the lumen structure could be more expanded than the initial status based on the perfused process through the HUVECs core with hydrodynamic forces from the medium flow.

The cells in the flowing condition showed the most active angiogenesis during all the time points (Figure 13). All the sprouting of the flowing condition were toward the hollow channel, which flowed the additional GFs media (Figure 13c). It was supposed that the concentration gradient from the hollow channel (Figure 10) affected the sprouting directionality of the flowing condition. None of the sprouting reached the hollow channel (Figure 13 a-c). Two reasons are suspected for this not reaching phenomenon. First, the outer shell material (mixture of gelatin and alginate) between the two vasculatures inside the formulated scaffold could hinder sprouting. Because animal cells do not produce endogenous alginases to enzymatically degrade alginate scaffolds [158], the sprouting from the HUVEC vessel could not invade into the outer shell. The second reason might be the additional GF stimulating time. The flowing and soaking conditions exhibited the sprouting length's increasing tendency up to day 10, the last observation day. Considering this inclination, longer additional GF stimulating time could grow the sprouting up to the hollow channel.

All the sprouting of the obstructing condition have disappeared at day 10, different from the other two culture conditions. Melly et al. also mentioned that the new vessels are unstable and depend on continued GFs stimulation until 4 weeks [159]. If the expression is lost before this time, sprouting will regress and disappear [159]. Shin et al. noticed that direct tip cell connections principally regulated the life cycle of stalk cells [160]. Stalk cells became disorganized, regressed, and finally disappeared with the disconnection between stalk cells and tip cells, independent of the GF gradient type [160]. Considering these reports, the low diffusion in the obstructing condition might cause the sprouting disappearance at day 10.

## V. Conclusion

Our two-core-embedded device enabled the fabrication of a scaffold containing two embedded vascular channels. One channel became populated with human umbilical vein endothelial cells (HUVECs), forming a functional vessel. The other channel allowed for continuous flow of culture medium. This perfusion of culture media through the adjacent hollow channel significantly enhanced HUVEC behavior, particularly their ability to sprout new vessels (angiogenic sprouting). This

innovative scaffold and device hold great promise for applications in vascular research, 3D bioprinting, and drug discovery.

## Chapter 2:

# Bioinspired Liver dECM Scaffold using Sacrificial Calcium Alginate for Artificial Liver

## I. Background

Biomaterials play a crucial role in liver tissue engineering by providing a supportive environment for the growth and function of liver cells. These materials can be natural hydrogels, synthetic hydrogels, liver-decellularized extracellular matrix, or a mixture of them and are used to create scaffolds that mimic the natural condition of the liver [49]. Alginate is a natural hydrogel extensively used in tissue engineering due to its biocompatibility, low toxicity, and ease of gelation. Alginate is commonly used as a scaffold material in liver tissue engineering to provide 3D structural support. Alginate hydrogels have also been used as a platform for the co-culture of multiple liver cell types, such as hepatocytes and endothelial cells, to mimic the *in vivo* liver microenvironment. However, it has a rigid structure and cannot deform, making it difficult for cells to change their morphology when cultured. Additionally, alginate's pore size and mechanical properties can limit cell migration and proliferation. Therefore, cells can survive and function in the alginate matrix, but they may not be able to mimic their 3D environment fully [79]. dECM is obtained by removing the cells from a tissue, leaving behind the ECM, the natural scaffold supporting and directing cell growth and function. In liver tissue engineering, the dECM of a healthy liver can be used as a scaffold to support the growth and differentiation of liver cells. This approach has several advantages over other techniques, as it provides a natural and biologically relevant environment for the cells and can preserve the complex architecture and composition of the liver tissue. The use of a mixture of liver dECM and alginate has been explored as a potential biomaterial in tissue engineering [161-163]. The dECM provides a natural and complex microenvironment for liver cells, while alginate provides mechanical support and facilitates cell encapsulation. The combination of these two materials can create a 3D structure that mimics the natural liver environment and supports liver cell growth and differentiation.

There are various methods to create 3D artificial engineered liver tissue. Some standard methods include self-assembly/spheroid formation, bioprinting, hydrogel-based approaches, decellularized extracellular matrix, and co-culture [164, 165]. It is worth noting that some of these methods overlap or combine. Among that, 3D bioprinting is a promising technology for liver tissue engineering because it allows for precise control over the placement and organization of cells and

biomaterials in a 3D space. It can also enable the fabrication of complex structures that mimic the heterogeneous architecture of liver tissue, including incorporating blood vessels and bile ducts. Additionally, 3D bioprinting can overcome the limitations of other methods, such as low cell viability and poor mechanical properties. Nonetheless, 3D bioprinting holds great potential for advancing liver tissue engineering and regenerative medicine.

Recently, a study proved that 3D liver spheroids were more functionally stable and exhibited increased sensitivity after a long-term period [166-169]. Although the 3D hepatocyte spheroid is an ideal model of hepatotoxicity, the limited size of spheroids due to hypoxic conditions at the spheroidal core impedes the creation of thicker liver tissues. Unable to maintain tissues less than 500  $\mu\text{m}$  in diameter for an extended period. This led to central necrosis in the liver spheroids because spheroids are analogous to avascular tissues or tumor masses and have a diffusion limitation of about 150–200  $\mu\text{m}$  for many molecules, particularly oxygen. Hence, hepatocyte spheroids are unsuitable for forming tissues with uniform cell quality. As the spheroid grows, the structure's core may become limited in terms of oxygen and nutrient availability due to limited diffusion into the center of the structure. This can lead to cell necrosis in the spheroid's center, limiting its growth and functionality. In addition, while spheroids allow for the formation of 3D cell structures, they may not fully recapitulate the complex cell-cell interactions seen in native liver tissue. This can limit the functionality of the resulting tissue construct. Spheroids are typically small and difficult to scale to create larger tissue constructs. This can limit their usefulness in creating clinically relevant tissue replacements.

This study investigated the characteristics of engineered liver tissue using extrusion bioprinting. We fabricated a long, thin, and flexible scaffold with a solid fiber structure using a mixture of liver decellularized extracellular matrix (dECM), alginate, and HepG2-EA.hy926 cells. After allowing the fibers to form for one day, we removed the alginate component using alginate lyase. The primary goal was to evaluate vascular network formation within the engineered tissue. To achieve this, we conducted *in vivo* experiments (Figure). The findings from this study have the potential to provide valuable insights into the development of 3D liver tissue engineering and its potential applications in clinical settings.

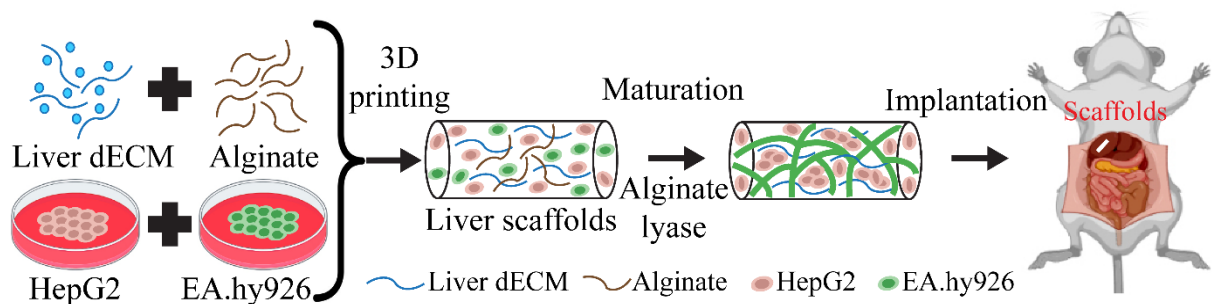


Figure 14. Schematic diagram of the liver fiber scaffold.



## **II. Materials and Methods**

### **1. Hydrogel mixture**

#### **1.1. Liver dECM synthesis**

The porcine liver tissue was sliced into 1 mm thick sections and thoroughly rinsed twice with cold PBS for an hour at 500 rpm. Three detergent solutions were prepared to treat the sliced liver tissue. First, SDS (Sigma-Aldrich, U.S.A.) was diluted in DI water to create concentrations of 0.1%, 1%, and 2%. Second, 1% Triton X-100 (Sigma-Aldrich, U.S.A.) and a combination of 1% SDS and 1% Triton X-100 were diluted in DI water to form the second and third treatment solutions. Next, the tissue sections were immersed in each chemical solution for 48 hours at room temperature with constant agitation at 500 rpm, replacing the detergent every 8 hours. After decellularization, the tissue was flushed thrice with PBS for 2 hours each to eliminate residual detergent and cellular debris. The samples were sterilized using 100% and 70% ethyl alcohol for 30 minutes and 3 hours, respectively. Lastly, the scaffolds were rinsed thrice with PBS containing 1% penicillin/streptomycin for 2 hours each.

The decellularized samples were freeze-dried for 72 hours and ground into powder using a blender. 3.5 g of liver-decellularized extracellular matrix was solubilized with 100 mg of pepsin (Sigma-Aldrich, U.S.A.) in 100 ml of 5% acetic acid (Sigma-Aldrich, U.S.A.). The mixture was stirred at room temperature for four days. After complete digestion, the dECM solution was acquired by centrifuging at 3,000 rpm for 15 minutes to remove particles and then stored at 4 °C for future use.

#### **1.2. Bioink preparation (Liver dECM-Alginate)**

A 35 mg/mL solution of dECM was prepared by diluting it in 10X PBS (Sigma-Aldrich, U.S.A.) and neutralizing it with 10 M and 1 M sodium hydroxide (NaOH). DI water was added to achieve a 30 mg/mL liver dECM concentration. This process was conducted on ice to prevent dECM gelation. Sodium alginate powder (Daejung Chemicals, Republic of Korea) was dissolved in DI water to create a 1.5% wt solution, which was then sterilized at 110°C for 30 minutes before biological experiments. A bioink was formulated by combining liver dECM (30 mg/mL) and sodium alginate (1.5% wt) at a 70:30 volume ratio and stored at 4°C before constructing scaffolds.

### **2. Cell culture**

HepG2 and EA.hy926 were purchased from the American Type Culture Collection (ATCC, U.S.A.) and cultured in DMEM High Glucose (Dulbecco's Modified Eagle Medium, Welgene, Republic of Korea) supplemented with 10% fetal bovine serum (Gibco, Thermo Scientific, U.S.A.). Fresh culture medium was changed every 2-3 days. They were cultured in a humidified incubator at 37°C with 5% CO<sub>2</sub> and were passaged before reaching approximately 80% surface coverage.

### **3. Scaffold generation**

A device for creating fiber scaffolds was assembled from a glass capillary (1160  $\mu\text{m}$  ID, G200-3, Warner Instruments LLC, U.S.A.) and Tygon tubing (Saint-Gobain, Courbevoie, France), and sterilized at 121°C for 15 min before use. This device was then connected to a syringe pump for injecting bioink, a mixture of chosen materials and cells, at a flow rate of 0.5 mL/min. The extruded fiber scaffold was submerged in a calcium chloride bath for crosslinking. Notably, the cell-laden scaffold received an 0.05 IU/mL alginate lyase (Sigma-Aldrich, U.S.A.) treatment after 1 day in culture to remove the alginate component. Finally, all scaffolds were cultured in an incubator at 37°C with 5% CO<sub>2</sub>, and daily media changes.

### **4. Immunofluorescence staining**

To observe the morphology of the liver scaffolds, staining for albumin, CD31, and nuclei was performed using anti-albumin, anti-CD31, and DAPI, respectively. The formulated scaffold was initially fixed with 3.5% paraformaldehyde (PFA, P6148, Sigma-Aldrich, U.S.A.) for 40 minutes at RT. The fixed scaffold was then immersed in a 3% gelation solution and incubated at 37°C for gelation. Subsequently, the scaffolds in gelatin were permeabilized with 0.5% Triton X-100 (Sigma-Aldrich, U.S.A.) for 5 minutes at RT. A mixture of primary antibodies, including anti-albumin (Abcam, United Kingdom) and anti-CD31 (Abcam, United Kingdom), was incubated overnight at 4°C. Afterward, secondary antibodies (Abcam, United Kingdom) were applied for 2 hours at RT. The cell nuclei were stained with DAPI (D1396, Invitrogen, U.S.A.) for 5 minutes. Following each chemical treatment, the samples were washed 3 times with PBS for 5 minutes. The stained samples were observed using an IX53 inverted fluorescent microscope (Olympus, Japan) and an FV1000 laser scanning confocal microscope (Olympus, Japan).

### **5. *In vivo* experiment**

The Sprague Dawley male rat (5 weeks old, 95 - 135 g) was purchased from Hana company (Busan, Republic of Korea). The rats were kept in a facility with 60% humidity at 24 °C, a 12-hour light/dark cycle, and free access to drinks and food. Animal studies were performed per the principles and guidelines of laboratory animal care and ethics, with permission from the University of Ulsan's Institutional Animal Care and Use Committee (GIG-22-010, University of Ulsan, Ulsan, Republic of Korea). The experiment was conducted three times using a total of nine rats.

A rat was placed in an individual box without feeding for 1 day in a noise-free area before surgery. All surgical instruments were sterilized by an autoclave at 121°C for 30 min. Rats were divided into three groups: SHAM, hepatectomy, and implantation. Three groups were followed on days 7, 14,



and 21. It was anesthetized using 20 mg/mL 2,2,2-Tribromoethanol (Sigma-Aldrich, U.S.A.). The sedative period typically lasts for 60 min. The hair was removed by Nair gel (Church & Dwight, United Kingdom), and povidone-iodine 10% (Forson, Republic of Korea) was applied for disinfection before surgery. The skin on the abdomen was incised appropriately 5 cm in length and 3 cm in width from the cartilaginous section at the lower end of the sternum with scissors and forceps. An eye speculum was put in the opened area to observe the abdominal cavity. A dissection forceps was used to extract the left liver lobe and place it on a glass slide. A sterile scalpel blade (#15) to perform a hepatectomy ( $1 \times 3$  mm). A swab was used to maintain the cutting liver area for 5 min to prevent liver bleeding.

The right liver lobe was opened in the implantation groups, and 3D engineered liver scaffold ( $1 \times 3$  mm) was inserted into this site. Then, the connection between the opened liver lobe and the liver scaffold was sutured using 7-0 silk sutures (Ailee, Republic of Korea) to avoid the displacement of the scaffold. After that, the liver was returned to the abdominal cavity, and the abdominal wall and skin were sutured with 3-0 nylon sutures (Ailee, Republic of Korea). The surgical incision was cleaned with a surgical iodine-soaked swab twice. The surgical rats were placed in an individual box in a noise-free area. The animals were observed in the recovery and monitored their food and water consumption for 3 hours.

Blood samples were collected from the lateral tail veins of rats for three groups on evaluation days 7, 14, and 21. These samples were centrifuged at  $2000 \times g$  for 10 mins at RT to gather the serum. The liver function tests (albumin and urea) were performed using the collected serum with an ALISA and Urea assay kit. The surgical rats were anesthetized again on days 7, 14, and 21 to harvest the implanted liver region. After harvesting, the anesthetized mouse was performed cervical dislocation until respiration stopped for euthanasia.

## **6. Histological analysis**

The cell scaffolds were fixed overnight in 3.5% PFA before dehydrating in ethanol. Before wax infiltration, xylene was used to displace the ethanol in the sample. Then, the samples were sliced into thicknesses of 10  $\mu\text{m}$  using an RM2255 microtome (Leica Biosystems, Germany). Before staining, the paraffin wax in the sections was removed using xylene before rehydrating in ethanol and water. These processes were performed at the Bio-Medical Institute at Kyungpook National University Hospital, Dae-gu, Republic of Korea. For H&E staining, the slices were stained with Harris Haematoxylin (3801561, Leica Biosystems, Germany) and Alcoholic Eosin Y515 (3801610, Leica Biosystems, Germany). Then, they were treated with ammonia buffer (50mL deionized water + 0.15mL ammonia solution [ $\text{NH}_4\text{OH}$ ]). The H&E-stained slices were observed under a bright-field microscope (IX71, Olympus Corp., Tokyo, Japan).

## 7. Statistical analysis

The result was represented with a mean value  $\pm$  one standard error from more than three independent repetitions. One-way ANOVA and Tukey's post hoc test were utilized to evaluate the statistical significance level. Its significance is remarked as \* for  $P < 0.05$ , \*\* for  $P < 0.01$ , and \*\*\* for  $P < 0.001$ .

## III. Results

### 1. The formation of vascular networks and hepatocyte cluster

Immunofluorescence images demonstrate the formation of a vascular network within a liver dECM scaffold co-cultured with HepG2 and EA.hy926 cells over 10 days. Green fluorescence (CD31) marks endothelial cells, red (albumin) marks hepatocytes, and blue (nuclei) highlighting all cells. A unique phenomenon unfolded, where the development of a vascular network commenced on day 1, primarily extending outside the scaffold structure. Concurrently, the generation of hepatocyte clusters was observed internal to the scaffolds. Clear visualization of these dynamics was achieved through confocal imaging, as visually demonstrated in Figure 15. Day 7 shows a more established network with intricate endothelial connections and functional hepatocytes. Finally, by day 10, a well-defined vascular network is evident, marked by extensive green fluorescence from endothelial cells, and red fluorescences from functional hepatocytes producing albumin. The distribution of blue nuclei throughout the scaffold indicates overall cell viability and distribution.

These divergent responses highlight the interplay between the vascularization strategy and scaffold's microenvironment. The cluster expansion suggests the potential for sustained cell proliferation and self-organization, indicative of a conducive environment for cellular activity. The emergence of a vascular network underscores the scaffold's ability to prompt angiogenesis, fostering external connections that hold significant promise for nutrient and oxygen exchange. Overall, these images demonstrate the successful formation and maturation of a vascular network within the liver dECM scaffold, highlighting its potential for complex liver tissue engineering and regenerative medicine applications.

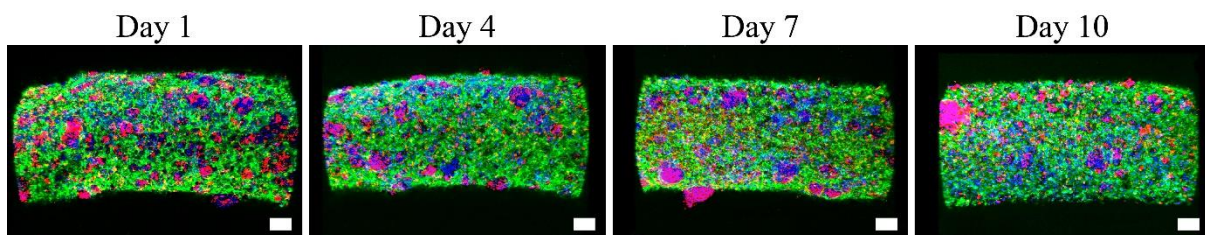


Figure 15. Immunofluorescence images of the vascular network formation of the liver dECM scaffold over 10 days (red: albumin, green: CD-31, blue: nuclei), scale bar: 100  $\mu$ m.

## 2. *In vivo* implanted experiment

The animal experiment in Fig. 16 shows the implantation process and subsequent analysis. Following controlled liver excision, the native liver received the 10-day matured liver-engineered tissue. This tissue was skillfully inserted and sutured for firm anchoring (Fig. 16a,b). Macroscopic and microscopic images (Fig. 16c,d) confirmed the appropriate size of the scaffold for the excised liver fragment.

After designated intervals (days 7, 14, and 21), rats were euthanized for tissue and blood sample collection. Figure 16e shows the implantation site with H&E and Masson's Trichrome staining. Both the artificial and native liver tissues demonstrated development until 21 days. The connections and integration were observed on days 7 and 14. By day 14, and 21, the artificial tissue showed noticeable expansion and infiltration into the native liver, exceeding the rate on day 7. Notably, holes throughout the artificial tissue in all samples indicated ongoing blood vessel growth, which is crucial for delivering nutrients and oxygen for survival. The consistency of findings was confirmed by the agreement between H&E and Masson's trichrome staining. Notably, loose connective tissue, essential for tissue integrity, organ support, and communication, emerged by day 3. Additionally, progressive enrichment of the 3D extracellular matrix within the artificial tissue was observed throughout the study.

Blood samples from SHAM, hepatectomy, and implantation groups were analyzed for albumin and urea secretion (Fig. 16f,g). Levels remained within the healthy range across all groups for the observation period. However, the hepatectomy group on day 7 showed altered levels, reflecting the liver's response to surgery. These levels returned to normal by day 14, indicating recovery. The implantation group showed no significant deviations, suggesting successful implantation. Throughout the 21 days, the rats maintained regular activity and vitality. The artificial and native liver tissues exhibited harmonious growth and integration with no adverse symptoms. This confirms the safety of the approach over three weeks. Importantly, positive liver function in implanted rats from day seven onward highlights the effectiveness of this method for liver tissue engineering applications.

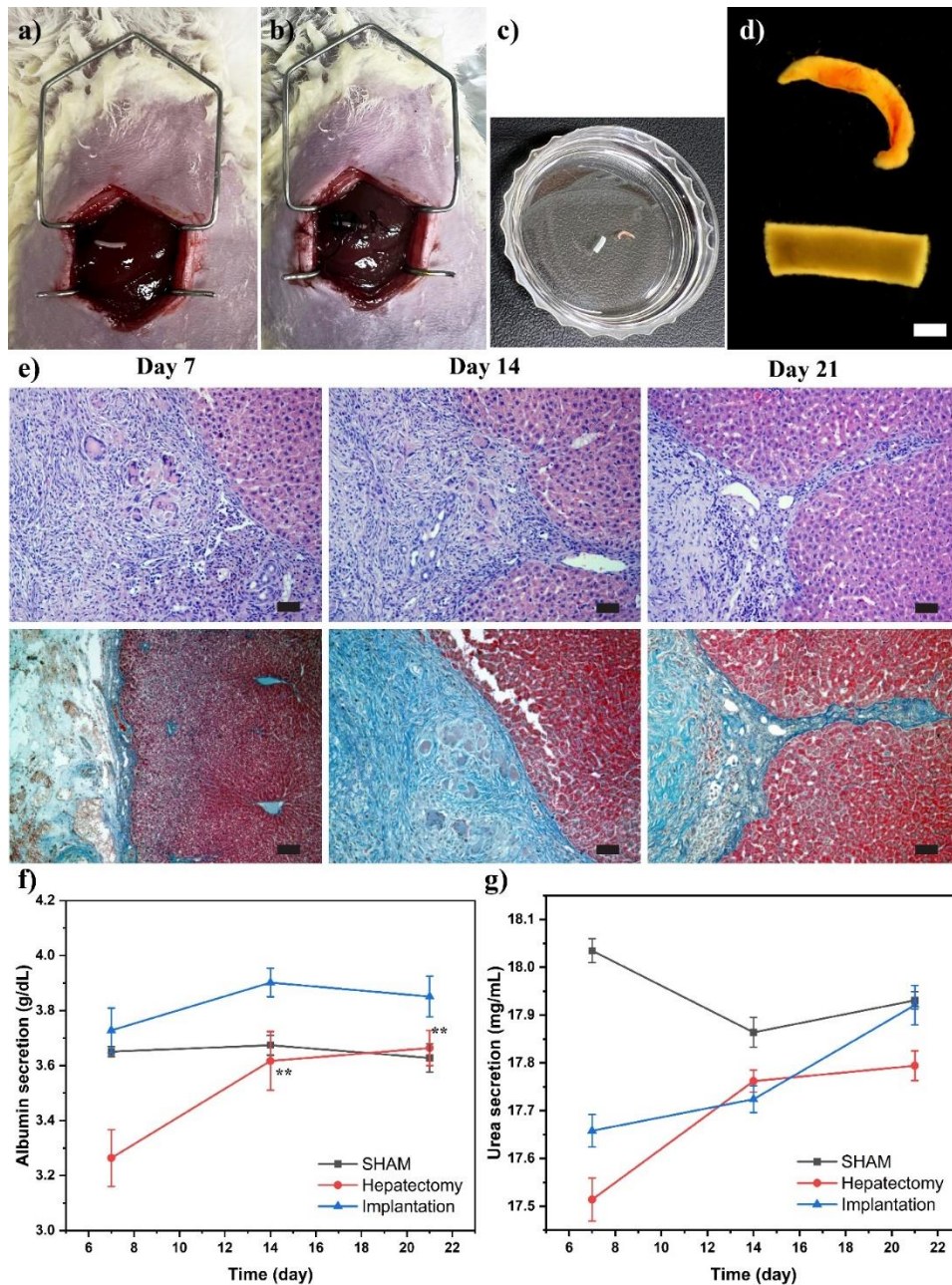


Figure 16. Animal experiment investigate the implantation of liver-engineered tissue; (a) Positioning the engineered tissue for implantation, (b) suturing the tissue into the native rat liver, (c) comparing the engineered tissue with the excised rat liver, (d) The microscope image provided a detailed comparison between two tissues (scale bar: 500  $\mu\text{m}$ ), (e) tissue sections from day 7, 14, and 21 post-implantation were stained with Hematoxylin and Eosin (H&E) and Masson's Trichrome (scale bar: 50  $\mu\text{m}$ ), (f) the albumin secretion, and (g) the urea secretion level of animal over 21-day implantation.

#### IV. Discussion

The dimension of a tissue construct holds paramount significance in tissue engineering applications, exerting a pivotal influence on its overall function and performance. The diameter



primarily refers to the tissue construct's size, which can influence various aspects of its behavior. Our methodology encompassed the utilization of alginate lyase to effectuate the removal of the alginate component. The observed scaffold diameter directly influences diffusion processes and nutrient supply [139, 170]. As the diameter increases, the distance for nutrients and oxygen to diffuse into the tissue and waste products to diffuse out becomes larger. Consequently, this phenomenon imposes a constraint on the achievable thickness of the tissue construct. An insufficient supply of nutrients and oxygen can precipitate cellular demise within the core region of the tissue construct, thereby impinging on the functional integrity and viability of constituent cells [171].

This hierarchical impact can lead to a scenario wherein the outer cellular layers exhibit superior functionality compared to their inner counterparts. Moreover, the size of the tissue construct emerges as a determinant of transplantation feasibility. Constructs of smaller dimensions inherently present enhanced manageability during implantation, facilitating seamless integration within the recipient's anatomical framework. Furthermore, successful integration hinges on the scaffold's ability to assimilate with the host's vasculature and liver tissue upon transplantation. In this regard, smaller diameter constructs are deemed advantageous, as their assimilation into the host's physiological milieu is potentially more expedient when contrasted with larger counterparts.

Regarding the dimensions of tissue constructs, the interplay between size and efficient nutrient diffusion is a pivotal factor in tissue engineering, underscoring the critical role of optimizing construct dimensions to ensure adequate cellular viability and functionality. The key differentiator in our fabrication process was the deliberate removal of the alginate component after 1 day. Alginate, while beneficial for scaffold fabrication due to its biocompatibility and gel-like properties, can hinder the diffusion of molecules due to its dense structure [172]. The utilization of co-culture conditions involving multiple cell types has been shown to enhance the establishment of physiological interactions and signaling, thereby potentially aiding diffusion [173, 174]. Additionally, incorporating liver dECM provides a biomimetic environment, promoting cellular attachment and migration, further contributing to efficient nutrient and waste exchange [175, 176]. The strategic removal of alginate after a brief incubation period aligns with previous research demonstrating improved porosity and permeability of the scaffold matrix, favorably impacting nutrient transport [177].

Implementing alginate lyase to remove alginate also positively affects optimal cell development and morphological features within artificial liver tissue constructs. This approach offers multifaceted advantages that contribute to enhancing cellular behavior and tissue functionality. The integration of liver dECM, recognized for its native biochemical cues and structural integrity, further complements the benefits of alginate removal. The combination of alginate lyase treatment and liver dECM promotes cell-matrix interactions that closely mirror physiological conditions. This encourages cells to adopt more authentic morphologies, exhibit enhanced functionalities, and form intricate cellular networks,

mimicking the complex structures found in native liver tissue. The synergy between alginate removal and the presence of liver dECM significantly influences cellular behavior. This combined approach fosters the development of hepatocyte-like phenotypes and guides the establishment of vascular networks critical for nutrient supply and waste removal.

The successful implantation of artificial liver tissue generated through our approach into the healthy rat liver is critical in assessing its biocompatibility, cellular viability, tissue maturation, and liver functionality within an *in vivo* context. The biocompatibility evaluation is paramount when considering engineered tissues' long-term viability and integration. The compatibility of our artificial liver tissue with the host rat liver environment underscores the absence of adverse immune responses or rejection, indicative of a construct well-tolerated by the host system. The retention of cellular viability within the implanted artificial liver tissue indicates the construct's ability to adapt and thrive within the host microenvironment. The three-week observed cellular viability implies that the fabricated tissue maintains a supportive milieu that sustains cellular health and function. This suggests the effective integration of cells within the artificial liver tissue, facilitated by our approach's consideration of biomimetic cues and appropriate microenvironmental conditions.

Furthermore, the assessment of tissue development over the three-week duration offers valuable insights into the construct's maturation and potential for further growth. The compatibility of the artificial liver tissue with the host rat liver environment fosters the establishment of supportive interactions and growth cues, enabling the tissue to progress toward more native-like states. An integral facet of our investigation involves monitoring the liver function of the implanted rat over the study period. The sustained liver functionality within the host system substantiates our approach's capacity to generate functional artificial liver tissue that can participate in the metabolic processes vital for maintaining host health. These findings accentuate the potential clinical relevance of our tissue engineering approach, offering promising prospects for addressing liver-related pathologies or dysfunction through a regenerative and functional strategy.

## V. Conclusion

We developed a method for building liver-engineered tissue using 3D bioprinting with a liver dECM-alginate mixture. Notably, removing the alginate after scaffold formation shaped dense vascular networks, and hepatocytes clusters within the liver dECM microenvironment. Finally, successful implantation in animal models yielded promising outcomes.

## Chapter 3:

# Double-layered blood vessels over 3 mm in diameter extruded by the inverse-gravity technique

## I. Background

Vascular bypass surgery, a common treatment for severe large-vessel disease using donated blood vessels [178], faces limitations due to donor availability and complications at the donor site [179, 180]. Consequently, synthetic vascular grafts (TEVGs) have been developed and clinically utilized as an alternative [181-183]. However, acellular TEVGs made from biodegradable polymers like polyester are limited in diameter due to risks of calcification and blockage below 6 mm [184-186]. Additionally, they lack regenerative abilities, making them unsuitable for use in growing children [187, 188]. Cell-sheet and tubular casting techniques offer promising methods for creating cellular TEVGs, but their product dimensions, particularly length, are limited by the size of the cell sheet or mold [189-192]. This restricts their application to larger vessels, such as the radial artery or superior epigastric artery, which can range from 0.7 to 3.3 mm in diameter and 2.2 to 24.7 cm in length [193-196]. Similarly, while 3D bioprinting can create vessels with branches, the high cost of equipment remains a hurdle [197-199].

Direct extrusion offers a cost-effective way to create long blood vessel scaffolds using microfluidic devices [120, 121, 200, 201]. These devices promote a laminar flow pattern that encapsulates vascular cells within various hydrogels [128, 129, 134, 202]. Despite success in generating long scaffolds, this technique is limited to diameters under 2 mm when cells are included [200, 203, 204]. While Liang *et al.* (2020) achieved larger diameters (around 3.5 mm) by significantly increasing the viscosity of a biomaterial [205], this approach resulted in a very stiff material potentially unsuitable for cell growth needed in blood vessel walls [206]. Enlarging the nozzle diameter alone won't create larger scaffolds. The flow rate needed to fill a wider nozzle disrupts the laminar flow crucial for forming a proper tube. This can lead to two issues: increased flow rates can disrupt the laminar flow, or a flow rate sufficient to maintain laminar flow becomes too fast, causing material waste and incomplete gelation (especially for light-cured materials). These challenges limit the creation of long, large-diameter blood vessels using extrusion techniques.

This study introduces an inverse-gravity (IG) extrusion technique to facilitate fabricate long blood vessels exceeding 3 mm in diameter. Our method generates coaxial, triple-layered scaffolds with outer sacrificial layers exceeding 8 mm in diameter. The advantages of this IG technique are supported by both theoretical and numerical analyses, ensuring the validity of our experimental results.

## II. Materials and Methods

### 1. Simulation

COMSOL Multiphysics (version 5.6, COMSOL, USA) software was used to perform 3D numerical simulations of a device designed to create a double-coaxial laminar flow. The geometry and fluid parameters for the simulation were defined as shown in Figure 17. The governing equations for this simulation were the Navier-Stokes equations [209].

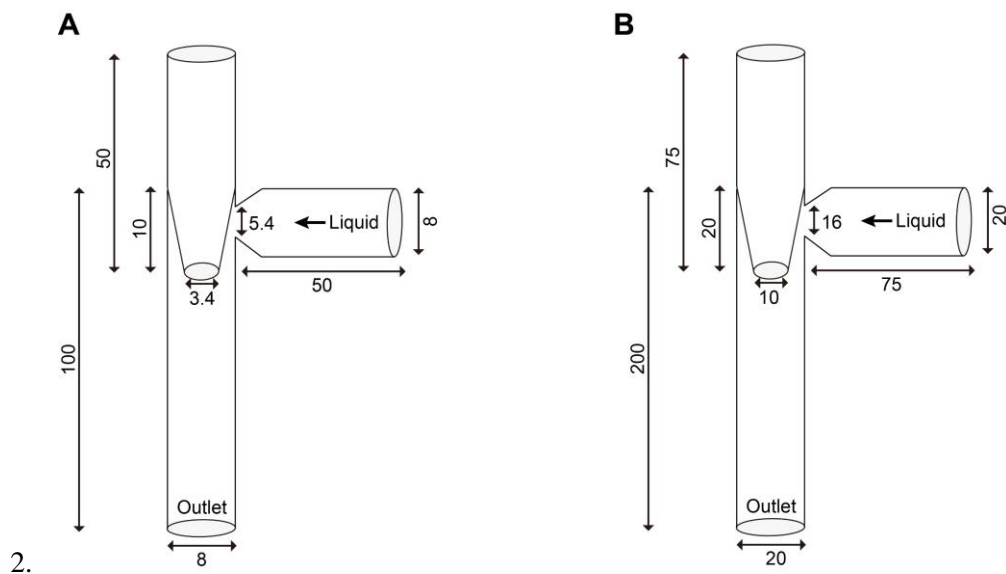


Figure 17. Geometries used for the simulations are shown (unit: millimeter). (a) An 8-mm-diameter geometry. (b) A 20-mm-diameter geometry. A liquid with a density of  $998.23 \text{ kg/m}^3$  and a viscosity of  $8.90 \times 10^{-4} \text{ Pa}\cdot\text{s}$  was defined at  $20 \text{ }^\circ\text{C}$  for the simulations.

### 2. Extrusion device

A double-coaxial flow device was fabricated to test the formation of coaxial laminar scaffolds. The device comprised two inlets and one outlet made from glass Pasteur pipettes (8 mm diameter) and serological pipettes (20 mm diameter). The inlets had tapered ends that were partially inserted into the outlet for coaxial assembly (Figure 18a). PDMS was used to ensure the integrity of the inlets and outlet.

Building upon the double-coaxial design, triple- and quadruple-coaxial laminar flow devices were further developed to directly extrude multilayered scaffolds for fabricating double-layered blood vessels exceeding 3 mm in diameter. The triple device comprised five glass tubes with three inlets, one link, and one outlet (Figure 18b). The quadruple device comprised seven glass tubes with four inlets, two links, and one outlet (Figure 18c). All glass tubes were 8 mm in diameter. One end of the inlets and links were tapered to a diameter narrower than 5.5 mm, and these tapered sections were partially



inserted into the links and the outlet, as shown in Figure 18b-c. All glass tubes were tightly assembled using cuboid-shaped PDMS bodies.

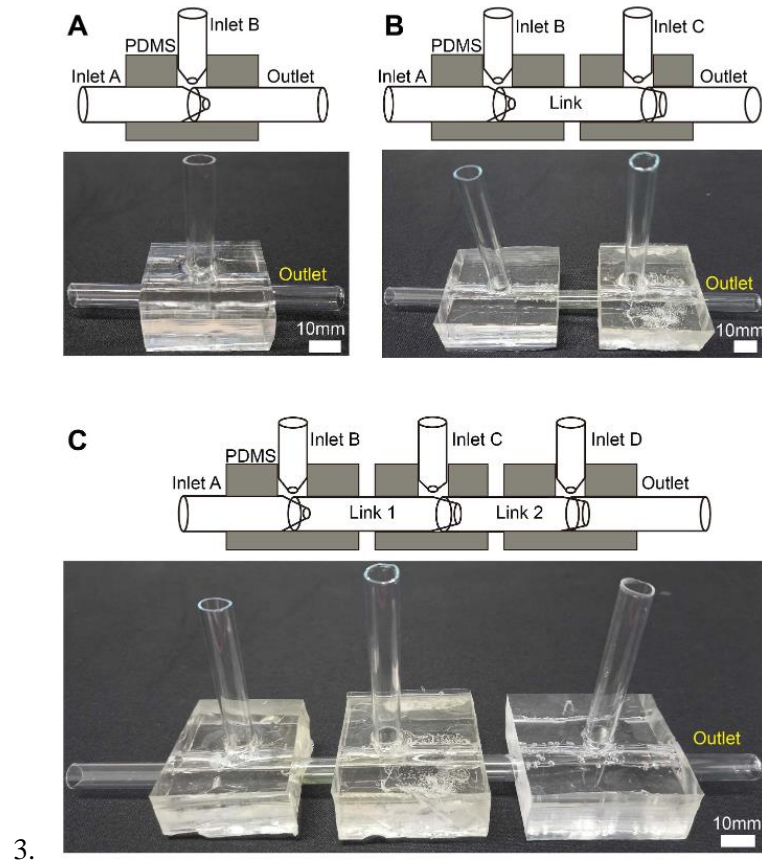


Figure 18. Schematic sketch and picture of extrusion devices for multilayered scaffolds. (a) Double-layer device, (b) Triple-layer device, (c) Quadruple-layer device.

### III. Results and Discussion

Creating multilayered structures requires an extrusion device that generates a stable coaxial laminar flow. Laminar flow is known to occur at a Reynolds number ( $Re$ ) below 2100 [207]. As described in Equation:

$$Re = \frac{\rho V D}{\mu}$$

$Re$  depends on the fluid's density ( $\rho$ ), flow speed ( $V$ ), characteristic linear dimension ( $D$ , often the nozzle diameter), and the inverse of its viscosity ( $1/\mu$ ) [208]. While density and viscosity are typically determined by the pre-hydrogel material properties, increasing the nozzle diameter necessitates a decrease in flow velocity to maintain a stable  $Re$ .

As a fluid flows along the gravitational direction inside a circular nozzle, some of the fluid near the wall experiences a frictional drag from the inner surface. This frictional drag slows down the fluid

near the wall. The severity of this drag depends on the viscosity, density, and pressure of the fluid. As the nozzle diameter increases with the same initial flow velocity (i.e., the same initial pressure), the effect of the wall surface friction on the velocity of the fluid far from the wall decreases. Over a certain diameter, the velocity of the fluid far from the wall is accelerated by gravitational force with little effect from the wall friction. This acceleration causes the fluid far from the wall to flow not in parallel with the fluid near the wall, leading to a chaotic stream so that the fluid cannot fully fill the nozzle to the end. Therefore, as the nozzle diameter  $D$  increases, the initial flow velocity should increase to fully fill the inside of the nozzle (denoted hereafter as the full-filling velocity).

This increased full-filling velocity for enlarged nozzles in the gravitational direction is contradictory to extruding coaxial tubular scaffolds. However, the IG extrusion technique is not hindered by gravity in the full-filling of the nozzle. In contrast, gravity contributes to slowing down the fluid, resulting in the full-filling of the nozzle in the inverse gravitational direction. Consequently, with the IG extrusion technique, a wider range of nozzle diameters and fluid viscosities can be used to achieve full filling at a manageable initial velocity. This is demonstrated in Figure 17, which compares the two methods using an 8 mm-diameter nozzle. In the gravitational direction, 300 ml min<sup>-1</sup> of water from a perpendicular inlet barely fully filled the nozzle (Figure 19a). In contrast, 3 ml min<sup>-1</sup> of water in the inverse gravitational direction fully filled the nozzle (Figure 19b).

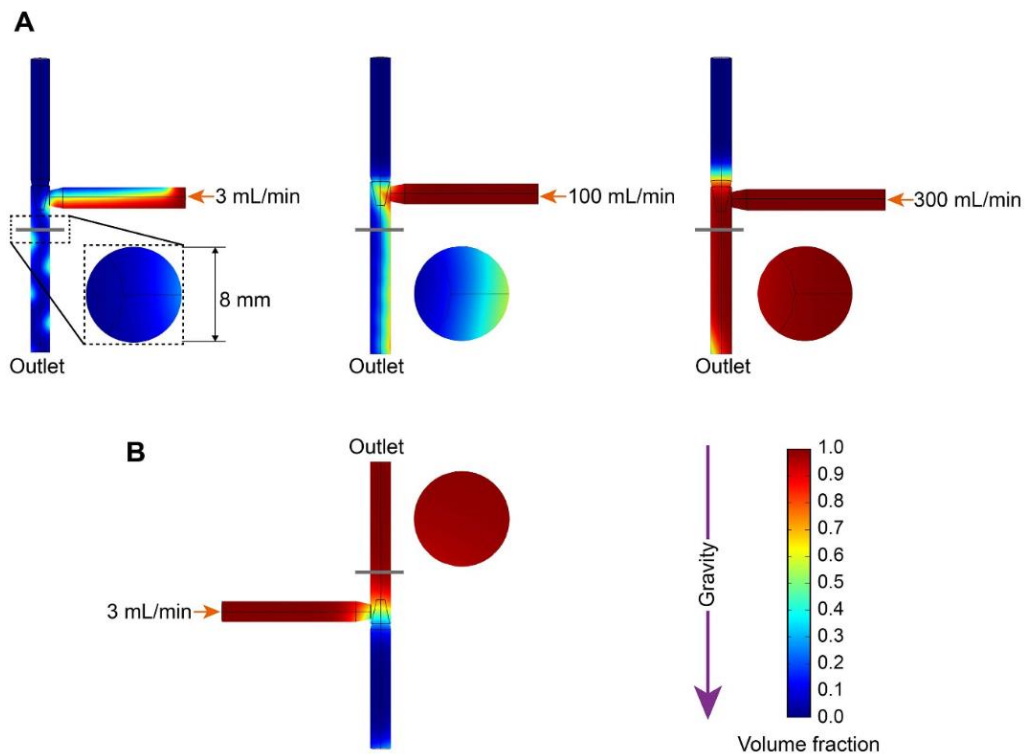


Figure 19. Simulating water flow into a main pipe via a single-branched inlet. The figure shows contours visualizing the liquid distribution (liquid/air volume fraction) within the geometry. The circle insets are

cross-sections of the pipe at 10 mm from the branched inlet. (a) 3 ml/min, 100 ml/min flow rates of water along the gravitational direction cannot fully fill the 8 mm-diameter nozzle. The 300 ml/min flow rate of water can fully fill the pipe. (b) Low flow rate of 3 ml/min of water along the inverse gravitational direction fully fills the 8 mm-diameter nozzle.

In the gravitational direction (Figure 20a), both the 1.5% w/v alginate solution and the 10 mg/ml type-I collagen solution failed to fully fill the 8 mm-diameter nozzle at flow rates of 3.0 ml/min and 1.5 ml/min, respectively. However, the proposed method fully filled the 8 mm-diameter nozzle and extruded a coaxial double-layered hydrogel at the same fluid velocities (Figures 20b-c). Another double-layered scaffold from the 10 mm-diameter nozzle (Figure 20d), triple-layered scaffold from the 8 mm-diameter nozzle (Figure 3e), and quadruple-layered scaffold from the 8 mm-diameter nozzle (Figure 20f) were extruded along the inverse gravitational direction. In the gravitational direction, the maximum flow rate (65 ml/min alginate and collagen) of the syringe pump (Pump 11 Elite, Harvard Apparatus, USA) cannot fully fill the 8 mm-diameter nozzle of the double-layer extruding device

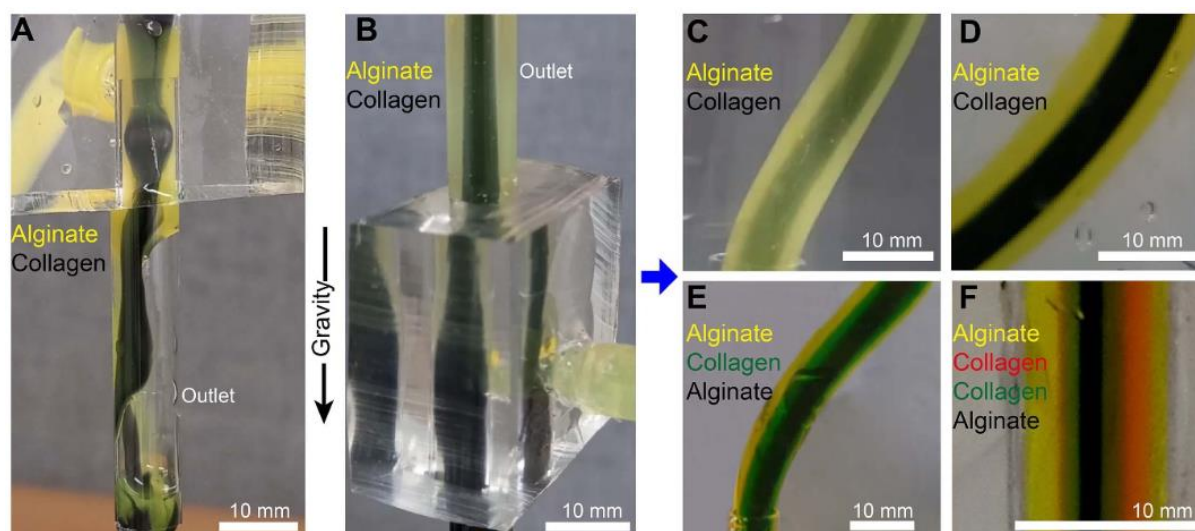


Figure 20. Coaxial laminar scaffold formation using alginate and collagen. (a) At flow rates of 1.5 ml/min for yellow alginate and 3.0 ml/min for black collagen, the solution cannot fully fill the nozzle in the gravitational direction. (b) The same flow rates (1.5 ml/min alginate, 3.0 ml/min collagen) in the inverse gravitational direction fully fill the nozzle and form a coaxial laminar flow. (c) Double-layered scaffold extruded with an 8 mm-diameter nozzle. (d) Double-layered scaffold extruded with a 10 mm-diameter nozzle using IG extrusion. (e) Triple-layered scaffold and (f) quadruple-layered scaffold prepared by IG extrusion.

#### IV. Conclusion

By simply reversing the extrusion direction, this study overcame the conventional limitations of achieving coaxial laminar flow in large-diameter nozzles. This reversal harnesses gravity to aid,

rather than hinder, the formation of laminar flow, allowing the IG extrusion technique to demonstrate the formation of multilayered scaffolds. The significance of this technique extends far beyond blood vessels. The IG extrusion technique has the potential to create complex tissue structures for various organs. This versatility could significantly advance the field of biofabrication by enabling the creation of functional tissue mimics for regenerative medicine applications. Beyond the initial success of this study, further research and development are needed to fully optimize the IG extrusion technique for clinical use.

## **Chapter 4:**

# **Over 4500 mm<sup>3</sup> Engineered Liver Scaffold for Implantable Artificial Livers**

## **I. Background**

The liver, a crucial organ for detoxification, metabolism, and protein synthesis, faces significant threats from global liver disease. According to recent statistics, liver disease is responsible for two million deaths yearly, making it a leading cause of death [210]. Liver transplantation, the only curative treatment for end-stage disease, is limited by donor shortages, rejection risks, immunosuppressive drugs, and high costs [211]. Liver tissue engineering offers a promising solution to address these limitations, potentially reducing rejection risk and eliminating immunosuppressive drugs, with lower costs than transplantation.

Liver tissue engineering is an exciting and rapidly advancing field that aims to develop functional liver tissue using engineering and biological approaches. Creating a supportive biological environment – utilizing scaffolds, biomaterials, and growth factors to mimic the natural liver – is critical. However, engineering functional liver tissue presents several challenges, including replicating liver structure and function, ensuring long-term stability, vascularization, immunogenicity, scaling up, and clinical integration [62]. Achieving long-term functionality involves optimizing cell culture conditions to maintain cell viability and function, essential for developing effective therapies for liver disease.

While researchers have developed a process for fabricating alginate microfibers using microfluidic laminar flow systems to build liver macroscopic tissues, these microfibers present limitations due to their small size [212, 213]. Their small size restricts them from fully replicating the metabolic capacity and cell interactions needed for complete functionality, achieving optimal alignment and organization to mimic natural tissue structure, and efficiently delivering nutrients and removing waste products compared to a single large fiber. Furthermore, ensuring consistent and adequate vascularization becomes more complex in structures composed of numerous small fibers. To overcome these limitations, a large-volume liver engineered tissue offers a promising solution. Such a tissue could potentially contain more cells and better mimic the natural size and architecture of livers, leading to improved function after implantation. Moreover, a single, large-volume implant could significantly simplify surgery and replace a large damaged tissue area.

Engineering large-volume tissues presents additional challenges. Delivery systems and vascularization strategies need development to ensure efficient oxygen and nutrient supply throughout the entire construct. Fabrication techniques for large-scale constructs should be explored to promote uniform cell distribution and maturation. This study utilizes extrusion bioprinting to fabricate large-volume, liver-engineered constructs. These scaffolds feature a sophisticated internal structure: a large central chamber, two peripheral vascular channels mimicking blood flow, and a hollow channel within the central chamber designed to perfuse the construct with cell culture media (Figure 21). To address the challenge of maintaining viability and function within these large constructs, we investigated the use of a direct media perfusion system. Three groups were compared: large-volume scaffolds without an internal channel, large-volume scaffolds with an internal channel but no perfusion (soaked in cell culture media), and large-volume scaffolds with an internal channel perfused with cell culture media. We believe the results of this study could provide valuable insights into the development of 3D large-volume liver-engineered tissue for potential clinical applications.

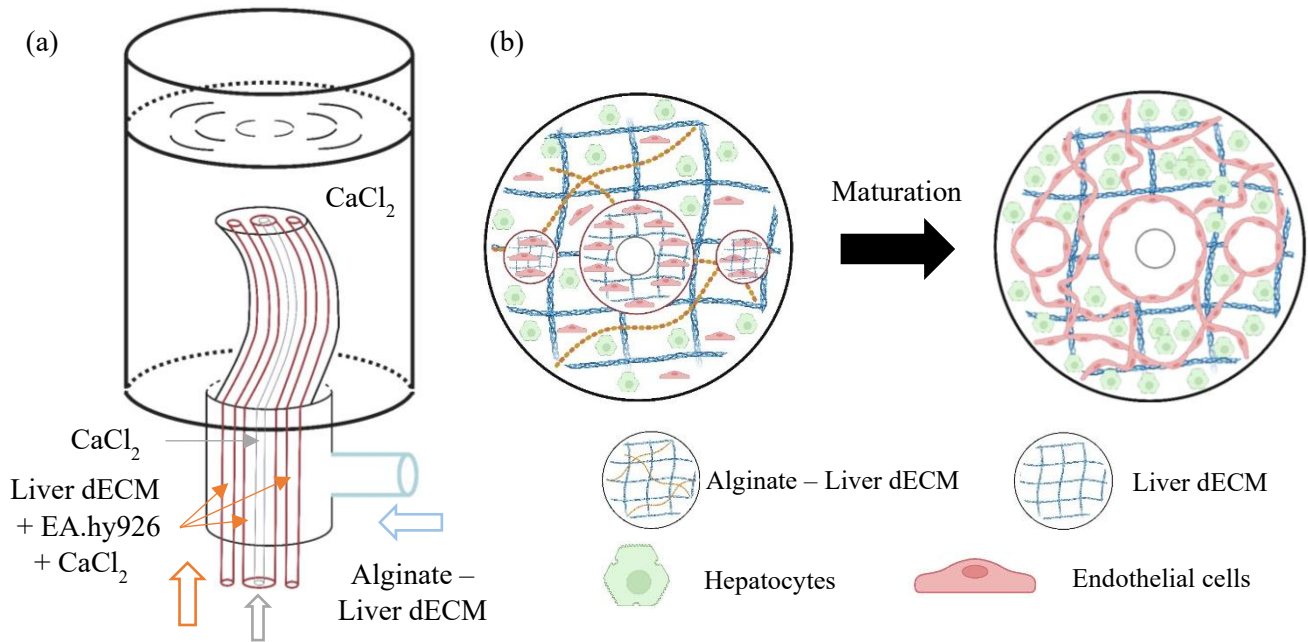


Figure 21. Schematic diagram of the large-volume liver engineered scaffold. (a) Three red cores were made of EA.hy926, 30 mg/mL liver dECM, and 0.1 M  $\text{CaCl}_2$  for the vascular channel. One gray core consisted of 0.1 M  $\text{CaCl}_2$  only for the hollow channel. The shell layer included a mixture of liver dECM and sodium alginate was supplied by blue inlet. (b) The cross-sectional view of the large-volume liver scaffold right after the formation and after the maturation.

## II. Materials and Methods

### 1. Bioink preparation (Liver dECM-Alg)

To prepare a 35 mg/mL solution of dECM, the dECM was initially diluted in 10X PBS. This mixture was carefully neutralized using 10 M and 1 M sodium hydroxide (NaOH) solutions. Following this, DI water was added to the mixture until a final concentration of 30 mg/mL liver dECM was achieved. The entire process was meticulously carried out on ice to prevent premature gelation of the dECM, ensuring that the matrix remained in its intended liquid state throughout the preparation phase. In a parallel step, sodium alginate powder was dissolved in DI water to form a 1.5% weight/volume solution. This solution was then sterilized by heating it to 110°C for 30 minutes.

The next phase involved formulating a bioink by blending the prepared liver dECM solution (at a concentration of 30 mg/mL) with the sterilized sodium alginate solution (at 3% wt/vol). These components were mixed at a 70:30 volume ratio. This formulation was designed to leverage the biological properties of dECM while benefiting from the structural support provided by sodium alginate. The resultant bioink was then stored at 4°C to maintain its stability and functionality before its application in constructing tissue-engineered scaffolds.



## 2. Cell culture

HepG2 and EA.hy926 were purchased from the American Type Culture Collection (ATCC, U.S.A.) and cultured in Dulbecco's Modified Eagle Medium (DMEM, Gibco, U.S.A.) supplemented with 10% Fetal Bovine Serum (FBS, Gibco, U.S.A.), and 1% penicillin/streptomycin (Gibco, U.S.A.). Fresh culture media were changed every 2 – 3 days. They were cultured in a humidified incubator at 37°C with 5% CO<sub>2</sub> and were passaged before reaching approximately 80% surface coverage.

## 3. Laminar device

The device for generating large-volume liver scaffold consists of two parts: a large part and a small part (Figure 22). The large part includes a triple-nozzle device, a large inlet, a large polydimethylsiloxane (PDMS) body, and an outlet. The small part includes two inlets, a small PDMS body. In the large part, a triple-nozzle device was designed and modified based on our previous device [201]. The structure of the device comprises a large central nozzle containing a smaller inner nozzle, surrounded by two smaller outer nozzles evenly spaced. To achieve a uniform distribution of these cores, a mold was designed and then printed using CAD software and a 3D printer, as illustrated in figure b. In the large part, a glass capillary (2 mm OD, 1.1 mm ID) was employed for the central nozzle, while two glass capillaries (1 mm, 0.58 mm ID) were assembled for the surrounding outer nozzles within the 3D mold. The smaller tubes were tapered as approximately 250 μm using a puller.

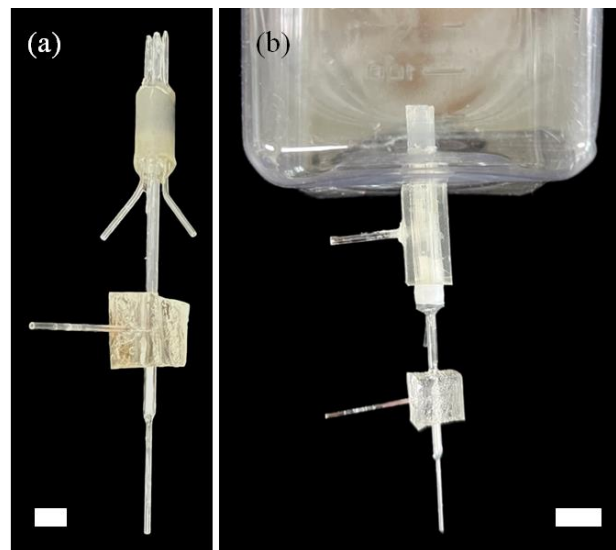


Figure 22. Laminar flow device. (a) Triple-nozzle device designed to fabricate three pre-vascular channels, with a small part to fabricate the empty channel for supplying cell culture medium, (b) Laminar flow device connected to a reservoir bath to collect the extruded scaffold

Then, the device was inserted into a PDMS block. The PDMS block within 6.6 mm hollow inside was made as body of the device. PDMS was used as glue to fix the position of these tube within

the 3D mold. A glass tube (2 mm OD, 1.1 mm ID), and a plastic tube (6.6 mm OD, 5 mm OD) were utilized for the inlet of the outermost layer, and the outlet, respectively. In the small part, two glass tubes (1 mm OD, 0.58 mm ID) were utilized for the two inlets. The small PDMS block within 2 mm hollow inside was made as body of the device. The outlet of the small part is the central nozzle of the multiple-nozzle device of the large part. The whole device was sterilized at 121°C for 30 min before biological experiments.

#### **4. Large-volume liver engineered scaffold formation**

The scaffold has a large central vasculature channel with an empty inner channel and two small peripheral vascular channels. All three channels were covered by an outer hepatocyte – endothelial cells layer, that mimicking in the human liver. The liver scaffold was printed using inverse-gravity technique [214].

Therefore, a single syringe pump (11 Elite C300918, Harvard Apparatus, U.S.A.) was used to supply a combination of 30 mg/mL liver dECM – 3% sodium alginate (ratio: 70/30), and  $5 \times 10^6$  cells/mL HepG2 –  $1.5 \times 10^6$  cells/mL EA.hy926 into the plastic inlet tube of the large part in the device for culturing the body of the scaffold. Another single syringe pump and a multiple syringe pump were used to deliver a mixture of 30 mg/mL liver dECM,  $5 \times 10^6$  cells/mL EA.hy926 cells/mL, and 0.1 M  $\text{CaCl}_2$  into the large central channel, and two small peripheral channels of the large compartment of the device to promote their development into blood vessels, respectively. For the empty channel, 0.1 M  $\text{CaCl}_2$  solution was injected to create a hollow channel inside the large central vasculature channel.

The scaffold was extruded from bottom to top vertically, and then was submerged into a 0.1 M  $\text{CaCl}_2$  bath through the outlet and cross-linked. Calcium ions of the  $\text{CaCl}_2$  cross-linked with sodium alginate into calcium alginate so that no hydrogel in the hollow channel remained. The gelled scaffold was washed with phosphate-buffered saline (PBS, Sigma-Aldrich, U.S.A.). The washed scaffold was cultured in an incubator at 37°C with 5%  $\text{CO}_2$ .

#### **5. The formation of vascular networks in large-volume liver scaffold**

The extruded large-volume scaffolds were initially cultured in fresh DMEM supplemented with 10% FBS for one day (24 hours). Following this initial culture period, an alginate lyase solution was prepared by mixing the enzyme with DMEM and 10% FBS. This solution was formulated to achieve a final concentration of 0.1 units/mL of alginate lyase. The primary function of this enzyme is to degrade the alginate components within the scaffolds. This removal of alginate is a crucial step as it facilitates the formation of vascular networks by clearing the scaffold's matrix, thereby creating pathways that can be utilized for vascularization.



The alginate lyase solution was then applied to the scaffolds for a duration of 24 hours. During this period, the alginate lyase acted on the alginate within the scaffolds, breaking it down and thereby aiding in the scaffold's restructuring towards a more vascularized architecture. This process is crucial for establishing a well-developed vascular network, which is essential for nutrient and oxygen diffusion throughout the scaffold, ultimately supporting sustained cell viability and function.

After the 24-hour enzyme treatment, the alginate lyase solution was carefully replaced with fresh cell culture medium. This step ensures the removal of any residual enzyme and the provision of a nutrient-rich environment for further cell growth and scaffold maturation. By continually supplying fresh medium, the cells within the scaffold are maintained in an optimal growth state, promoting the overall health and functionality of the engineered tissue.

## 6. Pumping culture system

A connecting device was 3D-printed to link a syringe pump to the fabricated scaffold. The device includes a reservoir with a hole, designed to hold the scaffold while submerged in cell culture media. A Pasteur pipette (Hilgenberg, Germany) was cut and then bonded to the hole of the 3D reservoir using PDMS (Figure 3A). After confirming no leakage, the fabricated connecting device was submerged with 99.9% ethanol in 24 h, and then sterilized at 110°C for 30 min for biological experiments.

To supply culture media through the hollow channel of the scaffold, one end was secured to the holder of the custom-made connecting device. Alginate was used to fill any gaps and ensure a tight connection. Culture medium was provided at a flow rate of 10  $\mu\text{L}/\text{min}$  from a syringe pump to the connected scaffold and then flowed out the unconnected end. Initially, no medium flowed out of the scaffold. However, as the medium flow continued, the excess medium accumulated as a puddle around the scaffold. This accumulated medium was removed from the 3D reservoir every 24 hours.

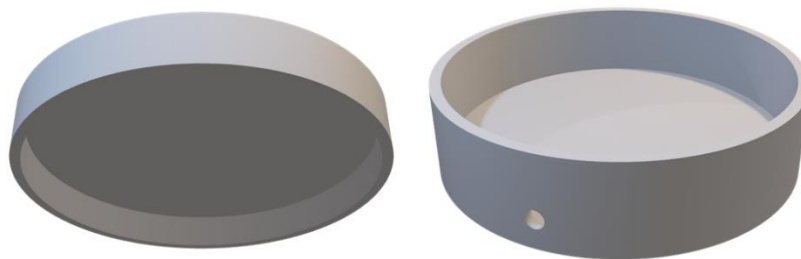


Figure 23. 3D-printed reservoir for the connecting device.

## 7. Three types of culture condition

Three types of scaffolds were fabricated under two distinct culture conditions to assess the development of large-volume, functional liver-engineered tissues, as shown in Figure 24.

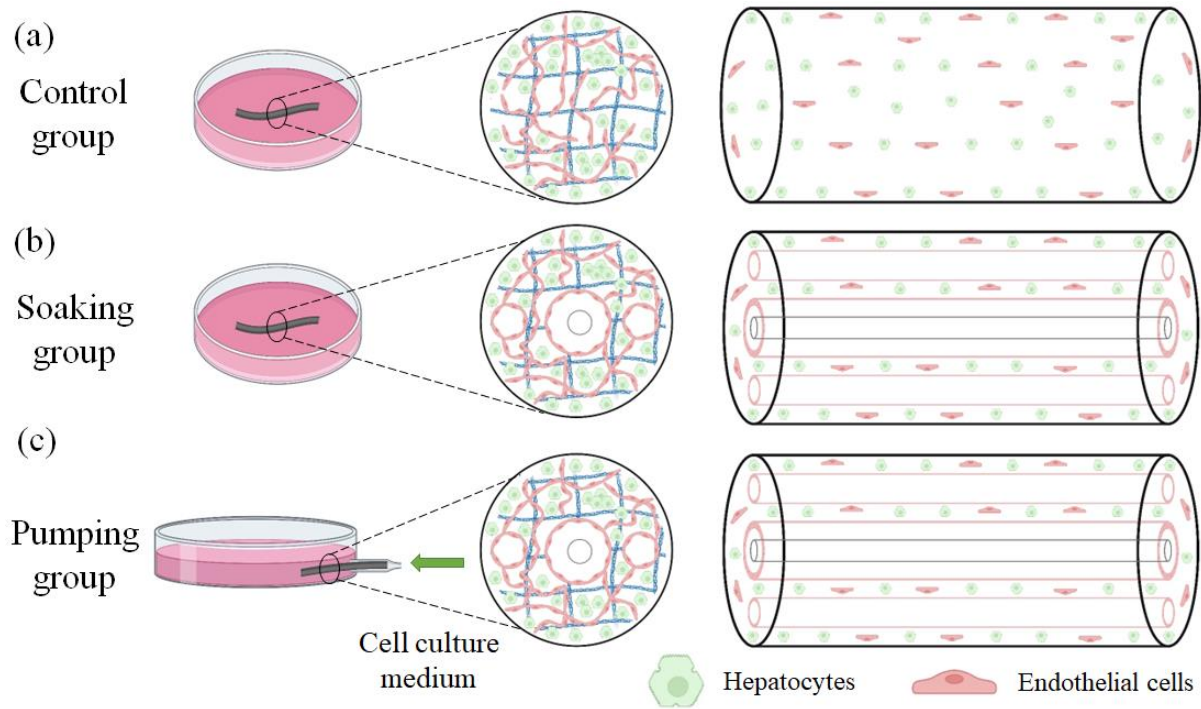


Figure 24. Three types of culture conditions. (a) Control group, (b) Soaking group, (c) Pumping group

The static culture condition involved submerging two groups of scaffolds in the cell culture medium. These groups rely on conventional diffusion for nutrient exchange as the cells grow on the scaffold. The first group, designated as the control, consists of scaffolds without any internal vascular channels. The second group, termed the soaking group, possesses the structure depicted in Figure 3.

In contrast, the dynamic culture condition employed a "pumping group" with a structure similar to the soaking group in the static culture. However, this group utilizes a pumping culture system to deliver the cell culture medium directly through the hollow channel within the scaffold, promoting a different mechanism of nutrient and waste exchange compared to the static approach.

## 8. Cell viability

The viability of the formulated scaffold was evaluated at days 1, 4, 7, and 14 using a live/dead viability kit for mammalian cells (L3224, Thermo Scientific, U.S.A.). The staining solution consisted of 0.05% Calcein AM (4 mM) in anhydrous dimethyl sulfoxide (DMSO) and 0.2% ethidium homodimer-1 (2 mM) in a 1:4 (v/v) mixture of DMSO and water. The stained scaffold was washed three times with PBS for 5 minutes each and then observed under a fluorescent microscope. The fluorescent

intensity of live cells (green channel) and dead cells (red channel) was analyzed using ImageJ software (Fiji, NIH Image, U.S.A.). The percentage of cell viability was calculated as the ratio between the green intensity and the sum of the green and red intensities.

$$Cell\ viability = \frac{Green\ intensity}{Green\ intensity + red\ intensity} \times 100$$

## 9. Cell proliferation

The CellTiter 96 AQueous One Solution Cell Proliferation Assay system (Promega) was used according to the manufacturer's instructions on days 1, 4, 7, and 14. A 5 mm scaffold with 100  $\mu$ L of cell culture media was plated into each well of a 96-well plate, and 20  $\mu$ L of CellTiter 96 AQueous One Solution reagent was added to each well. After a 4-hour incubation in a humidified 5% CO<sub>2</sub> atmosphere, absorbance at 490 nm was measured using a SpectraMax i3 microplate reader (Molecular Devices, Sunnyvale, CA, U.S.A.). Three replicate wells per time point were used to obtain measurements of cell proliferation.

## 10. Liver function

The amount of albumin and urea secreted by the cell scaffolds into the culture medium within 24 hours was analyzed on days 1, 4, 7, and 14 using human albumin ELISA kit and Urea assay kit (Abcam, United Kingdom) according to the manufacturer's instructions.

## 11. Immunofluorescence staining

To observe the morphology of the liver scaffolds and their protein expression, the formulated scaffolds were fixed with 3.5% paraformaldehyde (PFA) for 40 minutes at room temperature (RT) followed by staining for albumin, CD31, and nuclei. It was then immersed in a 3% gelatin solution and incubated at 37°C for gelation. Subsequently, the scaffolds in gelatin were permeabilized with 0.5% Triton X-100 for 5 minutes at RT. A mixture of primary antibodies, including anti-albumin (Abcam, United Kingdom) and anti-CD31 (Abcam, United Kingdom), was incubated overnight at 4°C. Afterward, secondary antibodies (Abcam, United Kingdom) were applied for 2 hours at RT. The cell nuclei were stained with DAPI (D1396, Invitrogen, U.S.A.) for 5 minutes. Following each chemical treatment, the samples were washed 3 times with PBS for 5 minutes. The stained samples were observed using an IX53 inverted fluorescent microscope (Olympus, Japan).

## 12. Statistical analysis

The result was represented with a mean value  $\pm$  one standard error from more than two independent repetitions. One-way ANOVA and Tukey's post hoc test were utilized to evaluate the

statistical significance level. Its significance is remarked as \* for  $P < 0.05$ , \*\* for  $P < 0.01$ , and \*\*\* for  $P < 0.001$ .

### III. Results and Discussion

#### 1. Fabrication of the two-vasculature-embedded scaffold

Our flow device with an IG technique enabled the controlled and continuous generation of large-volume, three-channel scaffolds without cells (Figure 25). After complete gelation, the fabricated scaffolds exhibited uniformity and stability, reaching meter-long lengths. The printability allows for fabrication of meter-long scaffolds with a diameter of approximately 5 mm and a length of 230 mm for a 1-minute printing time. The volume of the scaffold is  $4510 \text{ mm}^3$ , and this volume can be increased by fabricating longer scaffolds. By varying the flow rates of the outer layer fluid and the inner channel fluid, we could precisely control the diameters of the shell, the large central channel, and the two peripheral channels, allowing for customization for further experiments. Notably, the flow rates could also be adjusted to modify the shape of the three inner channels, enabling the creation of straight, wavy, helical, or coil structures.

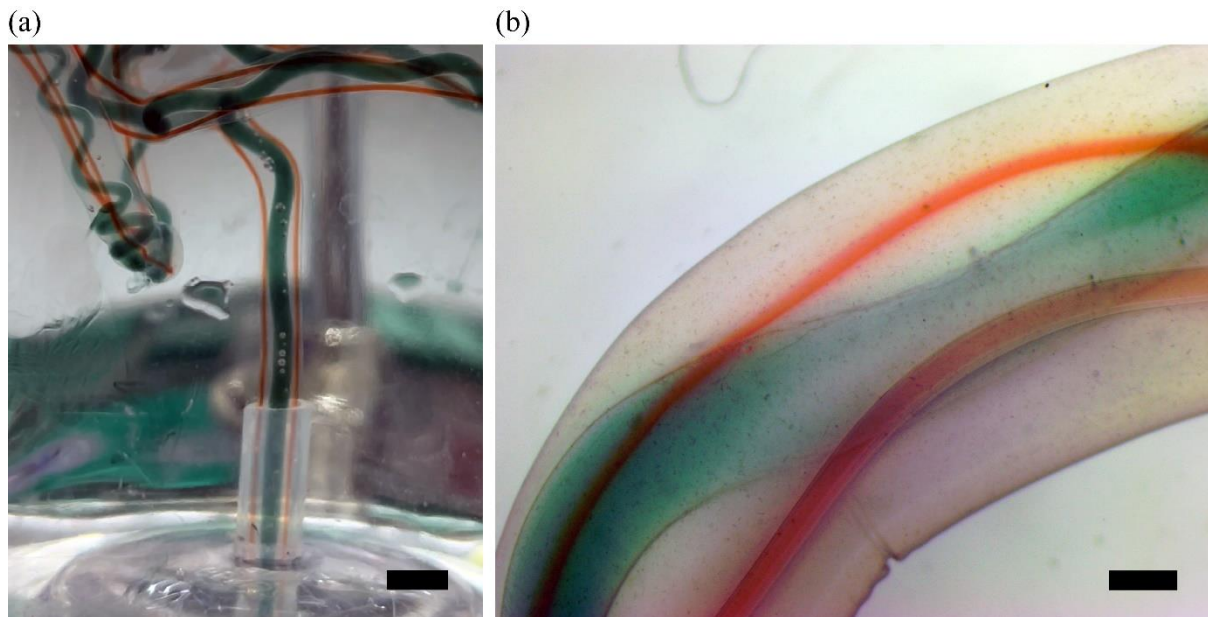


Figure 25. The fabricated large-volume scaffold. (a) The formation of generated cell-less scaffold (scale bar: 5 mm), (b) the bright-field microscope image of the scaffold (scale bar: 1 mm)

#### 2. Impact of different culture conditions on cell viability

The figure 26 and 27 illustrate the effects of different culture conditions on cell viability within scaffolds over 14 days. Initially, the control and soaking groups show high cell viability, over 80%,



indicating successful initial seeding and cell health. The pumping group exhibits slightly lower initial viability (75%) at day 1, due to the extended time required for fabrication and connection.

By day 4, the control and soaking groups show a decline in viability to approximately 70%, due to limitations in nutrient and oxygen diffusion within the large scaffolds. This is further supported by the observation that the outer layers maintain higher viability compared to the inner regions. In contrast, the pumping group exhibits significantly higher viability (70%) at day 4, highlighting the effectiveness of the dynamic culture system in overcoming diffusion limitations.

This trend continues through day 14. The control and soaking groups experience a further decline in viability, reaching below 40%. Static culture conditions fail to sustain cell health over time due to inadequate nutrient and oxygen supply. The pumping group, however, maintains a relatively stable viability around 70%, demonstrating the long-term benefits of the dynamic culture system with its hollow channels for continuous nutrient and oxygen delivery.

The results clearly demonstrate the advantage of dynamic culture conditions. Fluorescence microscopy and cell viability data show that the pumping group maintained superior cell viability over 14 days. This is likely attributed to the improved nutrient and oxygen delivery facilitated by the dynamic system, promoting cell health and functionality. Conversely, static conditions in the control and soaking groups limit nutrient and oxygen diffusion, leading to a more rapid decline in cell viability due to hypoxia and nutrient deprivation. This underscores the importance of dynamic culture systems in tissue engineering for maintaining cell viability within scaffolds, which is crucial for successful tissue construct development and function *in vivo*.

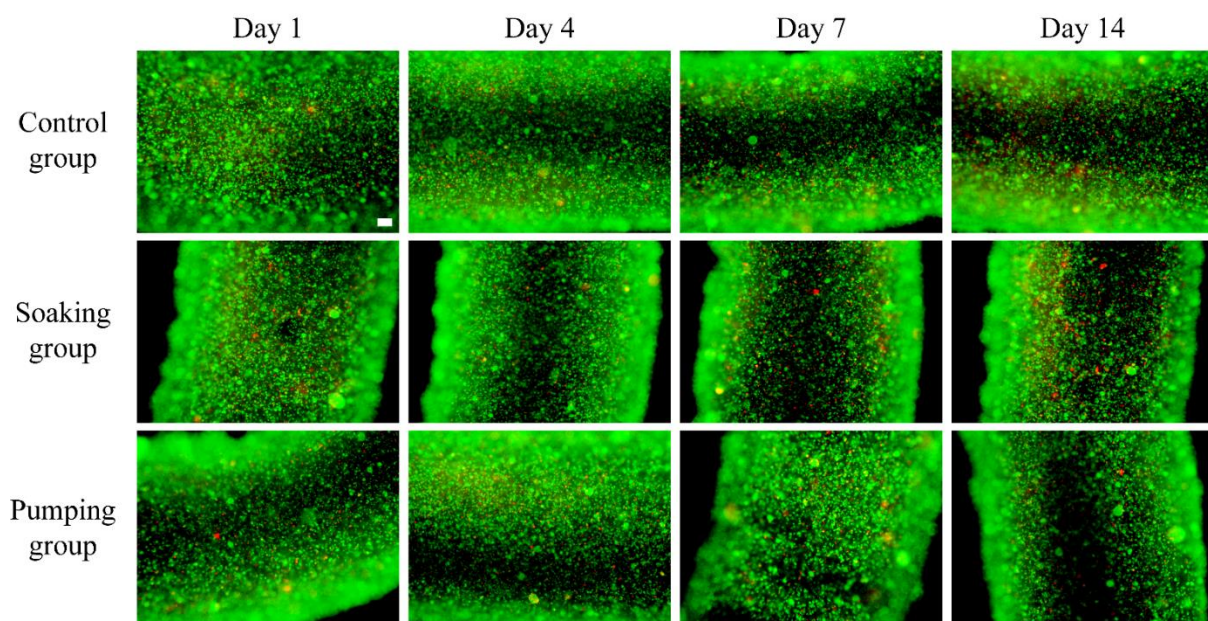


Figure 26. The fluorescence images of the live-/dead-stained liver scaffold over 14 days according to the control group, the soaking group, and the pumping group (scale bar: 200  $\mu\text{m}$ ).

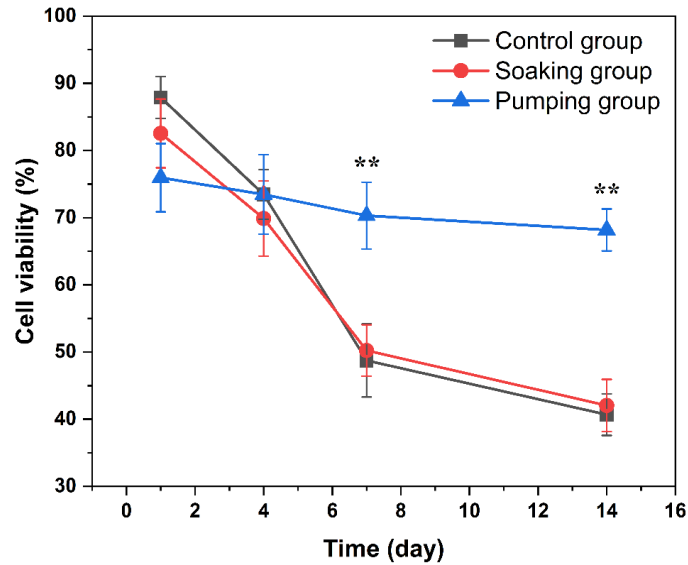


Figure 27. Cell viability of the liver scaffold over 14 days according to the control group, the soaking group, and the pumping group.

### 3. Impact of different culture conditions on cell proliferation

Figure 28 shows the absorbance at 490 nm, representing cell proliferation over a 14-day period under three different culture conditions. On day 1, all three groups exhibit similar absorbance levels, indicating comparable initial cell densities. By day 4, all groups exhibit a significant increase in absorbance, reflecting robust cell proliferation. From day 4 onwards, the proliferation patterns diverge. The absorbance for the control and soaking groups starts to decline gradually, indicating a reduction in cell proliferation. By day 14, the absorbance for these groups falls to around 1.8, showing a significant drop from their peak levels.

Conversely, the pumping group maintains a higher absorbance, peaking at day 4 and sustaining elevated levels through day 14. The absorbance for the pumping group on days 7 and 14 remains significantly higher than that of the control and soaking groups. Over a 14-day period, the pumping group displays significantly greater cell proliferation compared to the control and soaking groups. The initial proliferation up to day 4 is robust across all groups, likely due to the sufficient availability of nutrients and optimal culture conditions. However, as time progresses, the static conditions in the control and soaking groups result in nutrient depletion and accumulation of waste products, leading to a decline in cell proliferation. In contrast, the pumping group, which employs a dynamic culture system, sustains higher cell proliferation rates. The continuous nutrient flow and effective waste removal in this system likely contribute to maintaining a conducive environment for cell growth. The sustained high absorbance levels in the pumping group indicate that dynamic culture conditions significantly enhance cell proliferation in large-volume engineered tissues.

These findings underscore the importance of dynamic culture systems in tissue engineering. The ability to maintain high cell proliferation rates is crucial for the development of functional tissue constructs. The pumping group's performance highlights the potential of dynamic culture methods to overcome the limitations of static culture, such as nutrient diffusion barriers and waste accumulation, which are particularly challenging in large-volume tissues. Overall, the results suggest that dynamic culture systems are more effective in promoting cell proliferation and sustaining tissue health, thereby enhancing the viability and functionality of engineered tissues. This has significant implications for the field of tissue engineering, especially in developing large-scale tissue constructs for clinical applications.

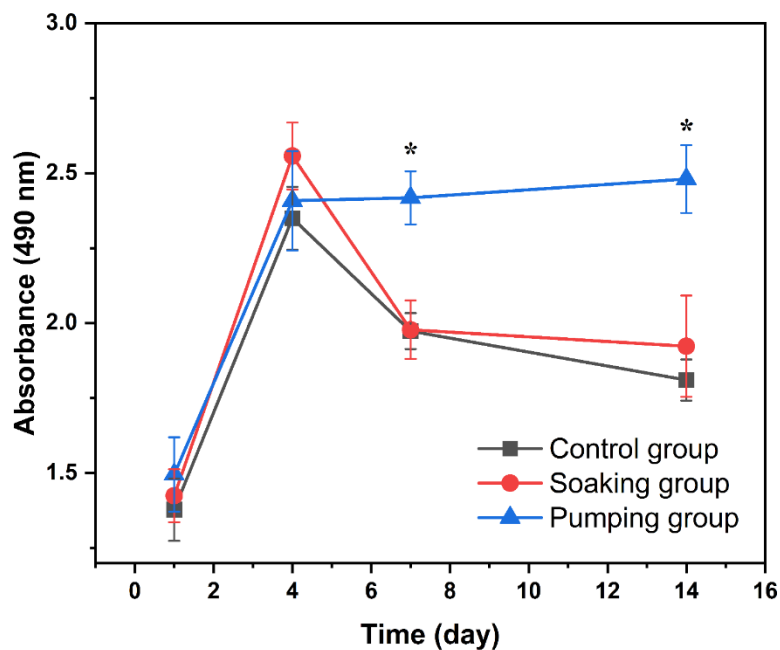


Figure 28. Cell proliferation in liver scaffolds. Proliferation of cells within large-volume liver-engineered scaffold across three groups is shown following 14 days in culture. CellTiter 96 AQueous One Solution Cell Proliferation Assay was used to quantify proliferation.

#### 4. Morphological Analysis of Liver Scaffold Architecture

The control group showed a gradual development of vascular networks and hepatocyte function over time, as shown in figure 29. However, this development was mainly restricted to the outer layer, where efficient nutrient and oxygen supply was available. By day 4, the presence of endothelial cells and albumin suggested early stages of liver cell function. Nuclei exhibited a fairly uniform distribution, indicating good cell health. Day 7 showed enhanced endothelial cell proliferation and network formation, marked by increased CD31 staining. More pronounced albumin staining confirmed improved hepatocyte function and nuclei remained uniformly distributed. Finally, day 14 revealed well-

developed vascular networks (green) and robust albumin production (red) on the outer layer. Uniform DAPI staining again confirmed sustained cell viability and function.

The soaking group, also static but with internal vascular channels, exhibited a similar pattern to the control group according to the cell viability, but with some initial enhancement. Similar to the control group at day 4, endothelial cells and albumin production were observed. However, slightly denser CD31 staining suggested a potential early advantage in endothelial cell proliferation due to the presence of the channels. Nuclei were uniformly distributed. By day 7, denser vascular networks indicated significant endothelial cell proliferation and network formation. Increased albumin staining suggested enhanced hepatocyte function. Nuclei remained uniformly distributed. Day 14 revealed a well-established vascular network and robust albumin production on the outer layer.

The pumping group, representing a dynamic culture condition with continuous flow, demonstrated the most rapid initial development but faced limitations in long-term stability. Day 4 and day 7 showed very intense CD31 staining, indicating substantial endothelial cell proliferation and network formation driven by the flow. Increased albumin staining suggested enhanced hepatocyte function. Nuclei remained uniformly distributed. However, day 14 revealed a concerning trend. Green fluorescence (CD31) decreased compared to day 7, suggesting a reduction in endothelial cell proliferation or network stability. Red fluorescence (albumin) indicates the presence of large, uniformly distributed hepatic aggregates aligned with the flow. This observation suggests the effect of dynamic culture conditions on the large-volume engineered tissue.

Compared to the control and soaking groups (both static cultures), the pumping group (dynamic culture) exhibited the most significant initial improvement in vascular networks and hepatocyte function. However, this group faced limitations in long-term stability, as indicated by the decrease in green fluorescence intensity by day 14. In conclusion, immunofluorescence analysis revealed that while dynamic culture conditions can significantly enhance initial tissue formation. These findings suggest that optimizing dynamic culture systems to balance rapid initial development with long-term cell health is crucial for successful applications.



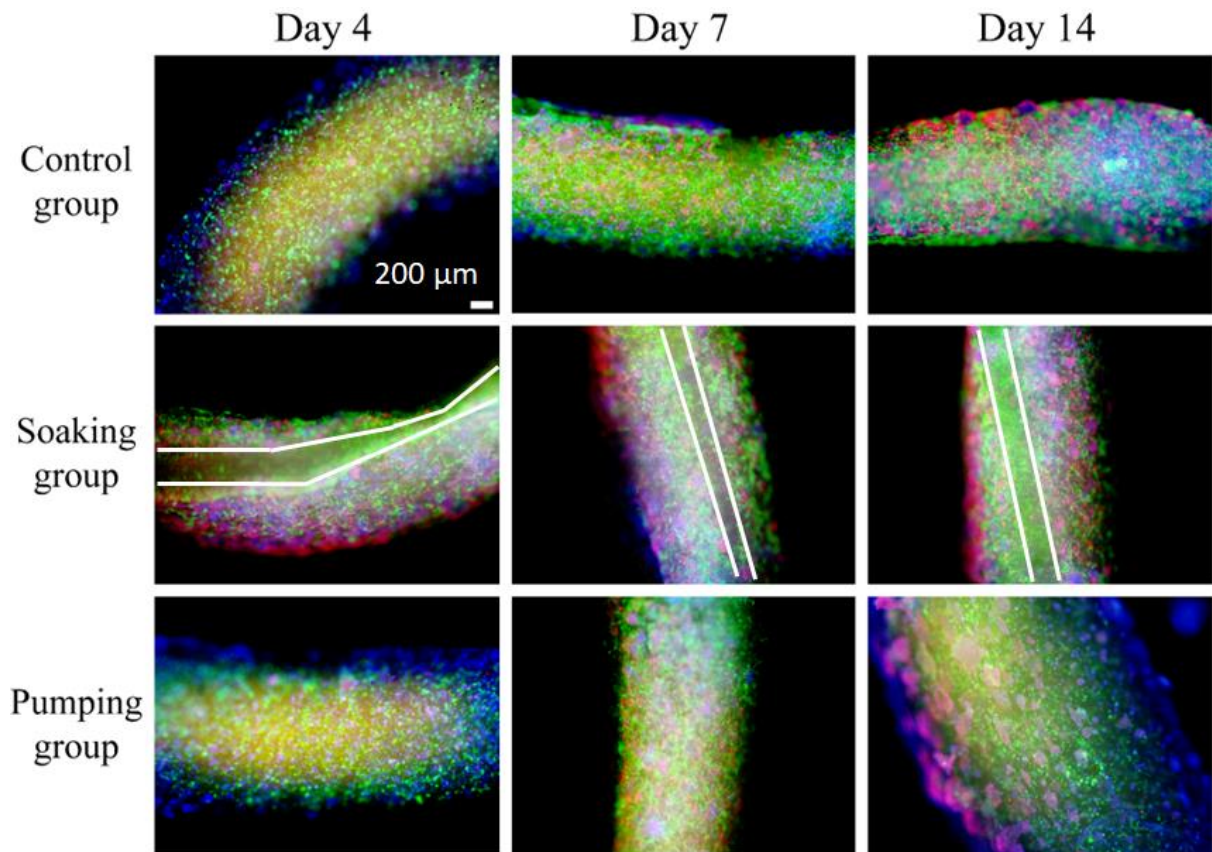


Figure 29. Liver scaffold morphology by immunofluorescence imaging. Immunofluorescence (IF) images depict the morphology of liver scaffolds across three groups at days 4, 7, and 14 of culture. Specific markers were used to visualize (green: CD31, red: albumin, blue: nuclei), scale bar: 200  $\mu\text{m}$ .

## 5. Evaluating liver synthetic function in liver scaffolds

Figure 30 presents liver function of 3D large-volume engineered tissue over 14 days, as measured through albumin and urea secretion in three different culture groups.

For albumin secretion, all groups exhibit similar albumin levels on day 1. By day 4, the control and soaking groups begin to show a decline in albumin production. This decline becomes more pronounced over time, with both groups exhibiting a significant reduction by day 14. In contrast, the pumping group demonstrates a steady increase in albumin secretion from day 4 onwards. By day 14, the pumping group shows a significantly higher level of albumin secretion compared to the control and soaking groups. This suggests that the dynamic pumping conditions with inner vascular channels are more conducive to maintaining and even enhancing the hepatic function of the engineered tissues.

For urea secretion, the control and soaking groups experience a decline in urea production over time. Starting from similar levels on day 1, both groups exhibit a decrease in urea secretion, with the soaking group showing a more pronounced drop. By day 14, urea secretion in both the control and

soaking groups is significantly lower compared to their initial levels. In contrast, the pumping group exhibits a steady increase in urea secretion throughout the 14-day period. By the end of the study, the pumping group's urea secretion is significantly higher than that of the control and soaking groups, indicating high metabolic activity.

The marked differences in albumin and urea secretion between the groups highlight the critical impact of culture conditions on the functional performance of engineered liver tissues. The pumping group's high performance can be attributed to the dynamic culture conditions that promote better nutrient distribution and waste removal, mimicking the natural physiological environment more closely than static conditions. The enhanced secretion of albumin and urea suggests that the cells in the pumping group not only survive better but also maintain their hepatic functions more effectively.

These findings underscore the importance of dynamic culture systems in tissue engineering. By providing a more favorable microenvironment, dynamic systems like the pumping method used in this study can significantly improve the functionality of engineered tissues. This is particularly crucial for liver tissues, where the ability to perform metabolic, synthetic, and detoxifying functions is essential. The dynamic pumping culture system enhances the functional performance of large-volume engineered liver tissues, as evidenced by higher and sustained levels of albumin and urea secretion. This suggests that dynamic culture conditions should be considered in the design and development of tissue-engineered constructs for liver regeneration and other clinical applications.

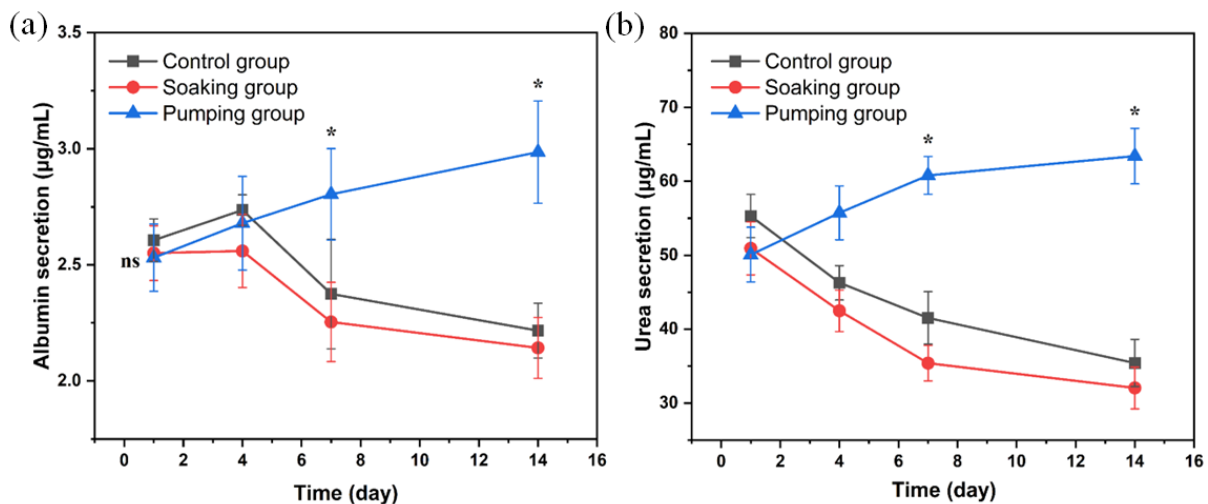


Figure 30. Assessment of liver synthetic function in liver scaffolds through albumin and urea secretion assays with three groups over 14 days. Secretion levels were quantified to evaluate the synthetic and metabolic activities of the engineered liver tissues.

## IV. Conclusion

This study presents a novel approach for constructing large-volume, liver-engineered tissues using 3D extrusion bioprinting with an inverse-gravity technique. This technique enables the easy and stable fabrication of centimeter-scale scaffolds. Initially, a bioink composed of sodium alginate and liver decellularized extracellular matrix (dECM) was used. The liver dECM component provides a natural scaffold that mimics the native liver tissue and supports favorable cellular behavior, while the sodium alginate component ensures printability and maintains the overall structure during the initial stages. After two days, the alginate component is removed, allowing for improved cell function within the liver dECM microenvironment. A crucial aspect of this strategy involves delivering the culture medium through a hollow channel within the scaffold by a direct pumping system. Compared to static culture conditions, our findings demonstrate promising results for our large-volume engineered tissue. These results include stable cell viability (~70%, representing a 30% increase), elevated liver function (35% higher albumin secretion and 80% higher urea secretion) over 14 days, and potentially improved initial vascularization. However, further optimization of the dynamic culture conditions is necessary to ensure long-term maintenance of the vascular network. Addressing this limitation holds the potential for the implantation of these engineered liver tissues in patients with damaged livers.

## References

- [1] S. R. Abdel-Misih and M. Bloomston, "Liver anatomy," (in eng), *Surg Clin North Am*, vol. 90, no. 4, pp. 643-53, Aug 2010, doi: 10.1016/j.suc.2010.04.017.
- [2] A. Kalra, E. Yetiskul, C. J. Wehrle, and F. Tuma, "Physiology, Liver," in *StatPearls*. Treasure Island (FL): StatPearls Publishing
- Copyright © 2023, StatPearls Publishing LLC., 2023.
- [3] S. B. Nayak *et al.*, "A peculiar liver with surgically and radiologically important variations: a case report," (in eng), *Anat Cell Biol*, vol. 46, no. 1, pp. 82-4, Mar 2013, doi: 10.5115/acb.2013.46.1.82.
- [4] C. Eipel, K. Abshagen, and B. Vollmar, "Regulation of hepatic blood flow: the hepatic arterial buffer response revisited," (in eng), *World J Gastroenterol*, vol. 16, no. 48, pp. 6046-57, Dec 28 2010, doi: 10.3748/wjg.v16.i48.6046.
- [5] T. L. Kline, M. Zamir, and E. L. Ritman, "Relating function to branching geometry: a micro-CT study of the hepatic artery, portal vein, and biliary tree," (in eng), *Cells Tissues Organs*, vol. 194, no. 5, pp. 431-42, 2011, doi: 10.1159/000323482.
- [6] K. Wake and T. Sato, ""The sinusoid" in the liver: lessons learned from the original definition by Charles Sedgwick Minot (1900)," (in eng), *Anat Rec (Hoboken)*, vol. 298, no. 12, pp. 2071-80, Dec 2015, doi: 10.1002/ar.23263.
- [7] E. Trefts, M. Gannon, and D. H. Wasserman, "The liver," (in eng), *Curr Biol*, vol. 27, no. 21, pp. R1147-r1151, Nov 6 2017, doi: 10.1016/j.cub.2017.09.019.
- [8] T. Kietzmann, "Metabolic zonation of the liver: The oxygen gradient revisited," (in eng), *Redox Biol*, vol. 11, pp. 622-630, Apr 2017, doi: 10.1016/j.redox.2017.01.012.
- [9] R. P. Cunningham and N. Porat-Shliom, "Liver Zonation – Revisiting Old Questions With New Technologies," (in English), *Frontiers in Physiology*, Review vol. 12, 2021-September-09 2021, doi: 10.3389/fphys.2021.732929.
- [10] Q. Su *et al.*, "Single-cell RNA transcriptome landscape of hepatocytes and non-parenchymal cells in healthy and NAFLD mouse liver," *iScience*, vol. 24, no. 11, p. 103233, 2021/11/19/ 2021, doi: <https://doi.org/10.1016/j.isci.2021.103233>.
- [11] W. Du and L. Wang, "The Crosstalk Between Liver Sinusoidal Endothelial Cells and Hepatic Microenvironment in NASH Related Liver Fibrosis," (in English), *Frontiers in Immunology*, Review vol. 13, 2022-June-28 2022, doi: 10.3389/fimmu.2022.936196.
- [12] W. Seo and W. I. Jeong, "Hepatic non-parenchymal cells: Master regulators of alcoholic liver disease?," (in eng), *World J Gastroenterol*, vol. 22, no. 4, pp. 1348-56, Jan 28 2016, doi: 10.3748/wjg.v22.i4.1348.
- [13] S. R. Nagarajan, M. Paul-Heng, J. R. Krycer, D. J. Fazakerley, A. F. Sharland, and A. J. Hoy, "Lipid and glucose metabolism in hepatocyte cell lines and primary mouse hepatocytes: a comprehensive resource for in vitro studies of hepatic metabolism," *American Journal of Physiology-Endocrinology and Metabolism*, vol. 316, no. 4, pp. E578-E589, 2019, doi: 10.1152/ajpendo.00365.2018.
- [14] V. Natarajan, E. N. Harris, and S. Kidambi, "SECs (Sinusoidal Endothelial Cells), Liver Microenvironment, and Fibrosis," (in eng), *Biomed Res Int*, vol. 2017, p. 4097205, 2017, doi: 10.1155/2017/4097205.
- [15] N. Luo, J. Li, Y. Wei, J. Lu, and R. Dong, "Hepatic Stellate Cell: A Double-Edged Sword in the Liver," (in eng), *Physiol Res*, vol. 70, no. 6, pp. 821-829, Dec 30 2021, doi: 10.33549/physiolres.934755.
- [16] C. Yin, K. J. Evason, K. Asahina, and D. Y. Stainier, "Hepatic stellate cells in liver development, regeneration, and cancer," (in eng), *J Clin Invest*, vol. 123, no. 5, pp. 1902-10, May 2013, doi: 10.1172/jci66369.
- [17] L. J. Dixon, M. Barnes, H. Tang, M. T. Pritchard, and L. E. Nagy, "Kupffer cells in the liver," (in eng), *Compr Physiol*, vol. 3, no. 2, pp. 785-97, Apr 2013, doi: 10.1002/cphy.c120026.
- [18] H. W. Zimmermann, C. Trautwein, and F. Tacke, "Functional role of monocytes and macrophages for the inflammatory response in acute liver injury," (in eng), *Front Physiol*, vol. 3, p. 56,

- 2012, doi: 10.3389/fphys.2012.00056.
- [19] J. M. Banales, R. C. Huebert, T. Karlsen, M. Strazzabosco, N. F. LaRusso, and G. J. Gores, "Cholangiocyte pathobiology," (in eng), *Nat Rev Gastroenterol Hepatol*, vol. 16, no. 5, pp. 269-281, May 2019, doi: 10.1038/s41575-019-0125-y.
- [20] C. Frantz, K. M. Stewart, and V. M. Weaver, "The extracellular matrix at a glance," (in eng), *J Cell Sci*, vol. 123, no. Pt 24, pp. 4195-200, Dec 15 2010, doi: 10.1242/jcs.023820.
- [21] T. Rozario and D. W. DeSimone, "The extracellular matrix in development and morphogenesis: a dynamic view," (in eng), *Dev Biol*, vol. 341, no. 1, pp. 126-40, May 1 2010, doi: 10.1016/j.ydbio.2009.10.026.
- [22] F. Gattazzo, A. Urciuolo, and P. Bonaldo, "Extracellular matrix: a dynamic microenvironment for stem cell niche," (in eng), *Biochim Biophys Acta*, vol. 1840, no. 8, pp. 2506-19, Aug 2014, doi: 10.1016/j.bbagen.2014.01.010.
- [23] N. K. Karamanos *et al.*, "A guide to the composition and functions of the extracellular matrix," (in eng), *Febs j*, vol. 288, no. 24, pp. 6850-6912, Dec 2021, doi: 10.1111/febs.15776.
- [24] W. Lv *et al.*, "Constructing biomimetic liver models through biomaterials and vasculature engineering," (in eng), *Regen Biomater*, vol. 9, p. rbac079, 2022, doi: 10.1093/rb/rbac079.
- [25] K. M. Mak and R. Mei, "Basement Membrane Type IV Collagen and Laminin: An Overview of Their Biology and Value as Fibrosis Biomarkers of Liver Disease," (in eng), *Anat Rec (Hoboken)*, vol. 300, no. 8, pp. 1371-1390, Aug 2017, doi: 10.1002/ar.23567.
- [26] Y. I. Tarasenko, Y. Yu, P. M. Jordan, J. Bottenstein, and P. Wu, "Effect of growth factors on proliferation and phenotypic differentiation of human fetal neural stem cells," (in eng), *J Neurosci Res*, vol. 78, no. 5, pp. 625-36, Dec 1 2004, doi: 10.1002/jnr.20316.
- [27] P. B. Limaye, W. C. Bowen, A. V. Orr, J. Luo, G. C. Tseng, and G. K. Michalopoulos, "Mechanisms of hepatocyte growth factor-mediated and epidermal growth factor-mediated signaling in transdifferentiation of rat hepatocytes to biliary epithelium," (in eng), *Hepatology*, vol. 47, no. 5, pp. 1702-13, May 2008, doi: 10.1002/hep.22221.
- [28] G. Yu *et al.*, "Hepatic stellate cells secreted hepatocyte growth factor contributes to the chemoresistance of hepatocellular carcinoma," (in eng), *PLoS One*, vol. 8, no. 9, p. e73312, 2013, doi: 10.1371/journal.pone.0073312.
- [29] J. C. Silva *et al.*, "Compositional and structural analysis of glycosaminoglycans in cell-derived extracellular matrices," (in eng), *Glycoconj J*, vol. 36, no. 2, pp. 141-154, Apr 2019, doi: 10.1007/s10719-019-09858-2.
- [30] G. K. Michalopoulos, "Liver regeneration," (in eng), *J Cell Physiol*, vol. 213, no. 2, pp. 286-300, Nov 2007, doi: 10.1002/jcp.21172.
- [31] L. J. Kitto and N. C. Henderson, "Hepatic Stellate Cell Regulation of Liver Regeneration and Repair," (in eng), *Hepatol Commun*, vol. 5, no. 3, pp. 358-370, Mar 2021, doi: 10.1002/hep4.1628.
- [32] C. Hadjittofi, M. Feretis, J. Martin, S. Harper, and E. Huguet, "Liver regeneration biology: Implications for liver tumour therapies," (in eng), *World J Clin Oncol*, vol. 12, no. 12, pp. 1101-1156, Dec 24 2021, doi: 10.5306/wjco.v12.i12.1101.
- [33] G. Kolios, V. Valatas, and E. Kouroumalis, "Role of Kupffer cells in the pathogenesis of liver disease," (in eng), *World J Gastroenterol*, vol. 12, no. 46, pp. 7413-20, Dec 14 2006, doi: 10.3748/wjg.v12.i46.7413.
- [34] H. Makino *et al.*, "Changes in growth factor and cytokine expression in biliary obstructed rat liver and their relationship with delayed liver regeneration after partial hepatectomy," (in eng), *World J Gastroenterol*, vol. 12, no. 13, pp. 2053-9, Apr 7 2006, doi: 10.3748/wjg.v12.i13.2053.
- [35] T. Sorsa, L. Tjäderhane, and T. Salo, "Matrix metalloproteinases (MMPs) in oral diseases," (in eng), *Oral Dis*, vol. 10, no. 6, pp. 311-8, Nov 2004, doi: 10.1111/j.1601-0825.2004.01038.x.
- [36] A. Abu Rmilah, W. Zhou, E. Nelson, L. Lin, B. Amiot, and S. L. Nyberg, "Understanding the marvels behind liver regeneration," (in eng), *Wiley Interdiscip Rev Dev Biol*, vol. 8, no. 3, p. e340, May 2019, doi: 10.1002/wdev.340.
- [37] C. E. McQuitty, R. Williams, S. Chokshi, and L. Urbani, "Immunomodulatory Role of the Extracellular Matrix Within the Liver Disease Microenvironment," (in eng), *Front Immunol*, vol.



- 11, p. 574276, 2020, doi: 10.3389/fimmu.2020.574276.
- [38] H. Paula, S. K. Asrani, N. C. Boetticher, R. Pedersen, V. H. Shah, and W. R. Kim, "Alcoholic liver disease-related mortality in the United States: 1980-2003," (in eng), *Am J Gastroenterol*, vol. 105, no. 8, pp. 1782-7, Aug 2010, doi: 10.1038/ajg.2010.46.
- [39] R. Williams *et al.*, "Unacceptable failures: the final report of the Lancet Commission into liver disease in the UK," *The Lancet*, vol. 395, no. 10219, pp. 226-239, 2020/01/18/ 2020, doi: [https://doi.org/10.1016/S0140-6736\(19\)32908-3](https://doi.org/10.1016/S0140-6736(19)32908-3).
- [40] K. Hassan, V. Bhalla, M. E. El Regal, and A. K. HH, "Nonalcoholic fatty liver disease: a comprehensive review of a growing epidemic," (in eng), *World J Gastroenterol*, vol. 20, no. 34, p. 12082-101, Sep 14 2014, doi: 10.3748/wjg.v20.i34.12082.
- [41] R. Arulraj and J. Neuberger, "Liver transplantation: filling the gap between supply and demand," (in eng), *Clin Med (Lond)*, vol. 11, no. 2, pp. 194-8, Apr 2011, doi: 10.7861/clinmedicine.11-2-194.
- [42] D. Mikulic and A. Mrzljak, "Liver transplantation and aging," (in eng), *World J Transplant*, vol. 10, no. 9, pp. 256-266, Sep 18 2020, doi: 10.5500/wjt.v10.i9.256.
- [43] N. Ghahramani, "Living organ donation: an ethical evolution or evolution of ethics?," (in eng), *Int J Organ Transplant Med*, vol. 1, no. 2, pp. 57-62, 2010.
- [44] B. Ekser, D. K. C. Cooper, and A. J. Tector, "The need for xenotransplantation as a source of organs and cells for clinical transplantation," (in eng), *Int J Surg*, vol. 23, no. Pt B, pp. 199-204, Nov 2015, doi: 10.1016/j.ijsu.2015.06.066.
- [45] V. Hosseini *et al.*, "Current progress in hepatic tissue regeneration by tissue engineering," *Journal of Translational Medicine*, vol. 17, no. 1, p. 383, 2019/11/21 2019, doi: 10.1186/s12967-019-02137-6.
- [46] G. Mazza, W. Al-Akkad, K. Rombouts, and M. Pinzani, "Liver tissue engineering: From implantable tissue to whole organ engineering," (in eng), *Hepatol Commun*, vol. 2, no. 2, pp. 131-141, Feb 2018, doi: 10.1002/hep4.1136.
- [47] K. Dzobo *et al.*, "Advances in Regenerative Medicine and Tissue Engineering: Innovation and Transformation of Medicine," (in eng), *Stem Cells Int*, vol. 2018, p. 2495848, 2018, doi: 10.1155/2018/2495848.
- [48] G. S. P. Hsia, J. Esposito, L. A. da Rocha, S. L. G. Ramos, and O. K. Okamoto, "Clinical Application of Human Induced Pluripotent Stem Cell-Derived Organoids as an Alternative to Organ Transplantation," (in eng), *Stem Cells Int*, vol. 2021, p. 6632160, 2021, doi: 10.1155/2021/6632160.
- [49] M. Ali and S. L. Payne, "Biomaterial-based cell delivery strategies to promote liver regeneration," *Biomaterials Research*, vol. 25, no. 1, p. 5, 2021/02/25 2021, doi: 10.1186/s40824-021-0206-w.
- [50] G. H. Underhill and S. R. Khetani, "Bioengineered Liver Models for Drug Testing and Cell Differentiation Studies," (in eng), *Cell Mol Gastroenterol Hepatol*, vol. 5, no. 3, pp. 426-439.e1, Mar 2018, doi: 10.1016/j.jcmgh.2017.11.012.
- [51] K. Zeilinger, N. Freyer, G. Damm, D. Seehofer, and F. Knöspel, "Cell sources for in vitro human liver cell culture models," (in eng), *Exp Biol Med (Maywood)*, vol. 241, no. 15, pp. 1684-98, Sep 2016, doi: 10.1177/1535370216657448.
- [52] C. Hu and L. Li, "In vitro culture of isolated primary hepatocytes and stem cell-derived hepatocyte-like cells for liver regeneration," (in eng), *Protein Cell*, vol. 6, no. 8, pp. 562-74, Aug 2015, doi: 10.1007/s13238-015-0180-2.
- [53] G. Kaur and J. M. Dufour, "Cell lines: Valuable tools or useless artifacts," (in eng), *Spermatogenesis*, vol. 2, no. 1, pp. 1-5, Jan 1 2012, doi: 10.4161/spmg.19885.
- [54] M. Štampar, B. Breznik, M. Filipič, and B. Žegura, "Characterization of In Vitro 3D Cell Model Developed from Human Hepatocellular Carcinoma (HepG2) Cell Line," (in eng), *Cells*, vol. 9, no. 12, Nov 28 2020, doi: 10.3390/cells9122557.
- [55] K. Nakamura, N. Kato, K. Aizawa, R. Mizutani, J. Yamauchi, and A. Tanoue, "Expression of albumin and cytochrome P450 enzymes in HepG2 cells cultured with a nanotechnology-based culture plate with microfabricated scaffold," (in eng), *J Toxicol Sci*, vol. 36, no. 5, pp. 625-33, Oct 2011, doi: 10.2131/jts.36.625.

- [56] S. Yamanaka *et al.*, "Pluripotency of embryonic stem cells," (in eng), *Cell Tissue Res*, vol. 331, no. 1, pp. 5-22, Jan 2008, doi: 10.1007/s00441-007-0520-5.
- [57] E. A. Aisenbrey and W. L. Murphy, "Synthetic alternatives to Matrigel," (in eng), *Nat Rev Mater*, vol. 5, no. 7, pp. 539-551, Jul 2020, doi: 10.1038/s41578-020-0199-8.
- [58] L. Ye, C. Swingen, and J. Zhang, "Induced pluripotent stem cells and their potential for basic and clinical sciences," (in eng), *Curr Cardiol Rev*, vol. 9, no. 1, pp. 63-72, Feb 1 2013, doi: 10.2174/157340313805076278.
- [59] Y. L. Zheng, "Some Ethical Concerns About Human Induced Pluripotent Stem Cells," (in eng), *Sci Eng Ethics*, vol. 22, no. 5, pp. 1277-1284, Oct 2016, doi: 10.1007/s11948-015-9693-6.
- [60] R. S. Tuan, G. Boland, and R. Tuli, "Adult mesenchymal stem cells and cell-based tissue engineering," (in eng), *Arthritis Res Ther*, vol. 5, no. 1, pp. 32-45, 2003, doi: 10.1186/ar614.
- [61] R. C. Lo and I. O. Ng, "Hepatic progenitor cells: their role and functional significance in the new classification of primary liver cancers," (in eng), *Liver Cancer*, vol. 2, no. 2, pp. 84-92, Apr 2013, doi: 10.1159/000343844.
- [62] A. A. Palakkan, D. C. Hay, A. K. PR, K. TV, and J. A. Ross, "Liver tissue engineering and cell sources: issues and challenges," *Liver International*, vol. 33, no. 5, pp. 666-676, 2013, doi: <https://doi.org/10.1111/liv.12134>.
- [63] M. Zhang *et al.*, "Generation of Self-Renewing Hepatoblasts From Human Embryonic Stem Cells by Chemical Approaches," (in eng), *Stem Cells Transl Med*, vol. 4, no. 11, pp. 1275-82, Nov 2015, doi: 10.5966/sctm.2015-0051.
- [64] N. R. Hannan, C. P. Segeritz, T. Touboul, and L. Vallier, "Production of hepatocyte-like cells from human pluripotent stem cells," (in eng), *Nat Protoc*, vol. 8, no. 2, pp. 430-7, Feb 2013, doi: 10.1038/nprot.2012.153.
- [65] T. Agarwal, B. Subramanian, and T. K. Maiti, "Liver Tissue Engineering: Challenges and Opportunities," *ACS Biomaterials Science & Engineering*, vol. 5, no. 9, pp. 4167-4182, 2019/09/09 2019, doi: 10.1021/acsbmaterials.9b00745.
- [66] P. Godoy *et al.*, "Recent advances in 2D and 3D in vitro systems using primary hepatocytes, alternative hepatocyte sources and non-parenchymal liver cells and their use in investigating mechanisms of hepatotoxicity, cell signaling and ADME," *Archives of Toxicology*, vol. 87, no. 8, pp. 1315-1530, 2013/08/01 2013, doi: 10.1007/s00204-013-1078-5.
- [67] S. Kazemnejad, "Hepatic tissue engineering using scaffolds: state of the art," (in eng), *Avicenna J Med Biotechnol*, vol. 1, no. 3, pp. 135-45, Oct 2009.
- [68] S. Croce, A. Peloso, T. Zoro, M. A. Avanzini, and L. Cobianchi, "A Hepatic Scaffold from Decellularized Liver Tissue: Food for Thought," (in eng), *Biomolecules*, vol. 9, no. 12, Dec 2 2019, doi: 10.3390/biom9120813.
- [69] C. H. Cho, J. Park, A. W. Tilles, F. Berthiaume, M. Toner, and M. L. Yarmush, "Layered patterning of hepatocytes in co-culture systems using microfabricated stencils," (in eng), *Biotechniques*, vol. 48, no. 1, pp. 47-52, Jan 2010, doi: 10.2144/000113317.
- [70] I. Bružauskaitė, D. Bironaitė, E. Bagdonas, and E. Bernotienė, "Scaffolds and cells for tissue regeneration: different scaffold pore sizes-different cell effects," (in eng), *Cytotechnology*, vol. 68, no. 3, pp. 355-69, May 2016, doi: 10.1007/s10616-015-9895-4.
- [71] S. Maji and H. Lee, "Engineering Hydrogels for the Development of Three-Dimensional In Vitro Models," *International Journal of Molecular Sciences*, vol. 23, no. 5, doi: 10.3390/ijms23052662.
- [72] T. C. Ho *et al.*, "Hydrogels: Properties and Applications in Biomedicine," (in eng), *Molecules*, vol. 27, no. 9, May 2 2022, doi: 10.3390/molecules27092902.
- [73] N. H. Thang, T. B. Chien, and D. X. Cuong, "Polymer-Based Hydrogels Applied in Drug Delivery: An Overview," *Gels*, vol. 9, no. 7, doi: 10.3390/gels9070523.
- [74] K. K. K. S. Silvipriya, A. R. Bhat, B. Dinesh Kumar, Anish John, Panayappan lakshmanan, *Collagen: Animal Sources and Biomedical Application*. Issue: 3, 2015, pp. 123-127.
- [75] L. G. Gonzalez and T. J. Wess, "The effects of hydration on the collagen and gelatine phases within parchment artefacts," *Heritage Science*, vol. 1, no. 1, p. 14, 2013/04/24 2013, doi: 10.1186/2050-7445-1-14.
- [76] M. Meyer, "Processing of collagen based biomaterials and the resulting materials properties,"

- (in eng), *Biomed Eng Online*, vol. 18, no. 1, p. 24, Mar 18 2019, doi: 10.1186/s12938-019-0647-0.
- [77] S. P. Ndlovu, K. Ngece, S. Alven, and B. A. Aderibigbe, "Gelatin-Based Hybrid Scaffolds: Promising Wound Dressings," (in eng), *Polymers (Basel)*, vol. 13, no. 17, Aug 31 2021, doi: 10.3390/polym13172959.
- [78] M. Rothbauer *et al.*, "A Decade of Organs-on-a-Chip Emulating Human Physiology at the Microscale: A Critical Status Report on Progress in Toxicology and Pharmacology," (in eng), *Micromachines (Basel)*, vol. 12, no. 5, Apr 21 2021, doi: 10.3390/mi12050470.
- [79] A. Bandyopadhyay, S. K. Chowdhury, S. Dey, J. C. Moses, and B. B. Mandal, "Silk: A Promising Biomaterial Opening New Vistas Towards Affordable Healthcare Solutions," *Journal of the Indian Institute of Science*, vol. 99, no. 3, pp. 445-487, 2019/09/01 2019, doi: 10.1007/s41745-019-00114-y.
- [80] A. Lupu, L. M. Gradinaru, V. R. Gradinaru, and M. Bercea, "Diversity of Bioinspired Hydrogels: From Structure to Applications," *Gels*, vol. 9, no. 5, doi: 10.3390/gels9050376.
- [81] F. Xu *et al.*, "Hydrogels for Tissue Engineering: Addressing Key Design Needs Toward Clinical Translation," (in eng), *Front Bioeng Biotechnol*, vol. 10, p. 849831, 2022, doi: 10.3389/fbioe.2022.849831.
- [82] H. T. Tee, R. Zipp, K. Koynov, W. Tremel, and F. R. Wurm, "Poly(methyl ethylene phosphate) hydrogels: Degradable and cell-repellent alternatives to PEG-hydrogels," *European Polymer Journal*, vol. 141, p. 110075, 2020/12/05/ 2020, doi: <https://doi.org/10.1016/j.eurpolymj.2020.110075>.
- [83] E. S. Mirdamadi, D. Kalhori, N. Zakeri, N. Azarpira, and M. Solati-Hashjin, "Liver Tissue Engineering as an Emerging Alternative for Liver Disease Treatment," *Tissue Engineering Part B: Reviews*, vol. 26, no. 2, pp. 145-163, 2020/04/01 2019, doi: 10.1089/ten.teb.2019.0233.
- [84] P. Mishra, B. Nayak, and R. K. Dey, "PEGylation in anti-cancer therapy: An overview," *Asian Journal of Pharmaceutical Sciences*, vol. 11, no. 3, pp. 337-348, 2016/06/01/ 2016, doi: <https://doi.org/10.1016/j.ajps.2015.08.011>.
- [85] S. Ye, J. W. B. Boeter, L. C. Penning, B. Spee, and K. Schneeberger, "Hydrogels for Liver Tissue Engineering," (in eng), *Bioengineering (Basel)*, vol. 6, no. 3, Jul 5 2019, doi: 10.3390/bioengineering6030059.
- [86] S. Sau, S. Pandit, and S. Kundu, "Crosslinked poly (vinyl alcohol): Structural, optical and mechanical properties," *Surfaces and Interfaces*, vol. 25, p. 101198, 2021/08/01/ 2021, doi: <https://doi.org/10.1016/j.surfin.2021.101198>.
- [87] J. M. Ino, P. Chevallier, D. Letourneur, D. Mantovani, and C. Le Visage, "Plasma functionalization of poly(vinyl alcohol) hydrogel for cell adhesion enhancement," (in eng), *Biomatter*, vol. 3, no. 4, Oct-Dec 2013, doi: 10.4161/biom.25414.
- [88] S. Liu, S. Qin, M. He, D. Zhou, Q. Qin, and H. Wang, "Current applications of poly(lactic acid) composites in tissue engineering and drug delivery," *Composites Part B: Engineering*, vol. 199, p. 108238, 2020/10/15/ 2020, doi: <https://doi.org/10.1016/j.compositesb.2020.108238>.
- [89] A. Neishabouri, A. Soltani Khaboushan, F. Daghigh, A. M. Kajbafzadeh, and M. Majidi Zolbin, "Decellularization in Tissue Engineering and Regenerative Medicine: Evaluation, Modification, and Application Methods," (in eng), *Front Bioeng Biotechnol*, vol. 10, p. 805299, 2022, doi: 10.3389/fbioe.2022.805299.
- [90] A. Gilpin and Y. Yang, "Decellularization Strategies for Regenerative Medicine: From Processing Techniques to Applications," (in eng), *Biomed Res Int*, vol. 2017, p. 9831534, 2017, doi: 10.1155/2017/9831534.
- [91] M. Dussoyer, A. Michopoulou, and P. Rousselle, "Decellularized Scaffolds for Skin Repair and Regeneration," *Applied Sciences*, vol. 10, no. 10, doi: 10.3390/app10103435.
- [92] M. Rabbani, N. Zakian, and N. Alimoradi, "Contribution of Physical Methods in Decellularization of Animal Tissues," (in eng), *J Med Signals Sens*, vol. 11, no. 1, pp. 1-11, Jan-Mar 2021, doi: 10.4103/jmss.JMSS\_2\_20.
- [93] L. J. White *et al.*, "The impact of detergents on the tissue decellularization process: A ToF-SIMS study," (in eng), *Acta Biomater*, vol. 50, pp. 207-219, Mar 1 2017, doi: 10.1016/j.actbio.2016.12.033.



- [94] D. Moffat, K. Ye, and S. Jin, "Decellularization for the retention of tissue niches," (in eng), *J Tissue Eng*, vol. 13, p. 20417314221101151, Jan-Dec 2022, doi: 10.1177/20417314221101151.
- [95] A. D. McInnes, M. A. J. Moser, and X. Chen, "Preparation and Use of Decellularized Extracellular Matrix for Tissue Engineering," (in eng), *J Funct Biomater*, vol. 13, no. 4, Nov 14 2022, doi: 10.3390/jfb13040240.
- [96] G. Singh *et al.*, "Impact of various detergent-based immersion and perfusion decellularization strategies on the novel caprine pancreas derived extracellular matrix scaffold," (in eng), *Front Bioeng Biotechnol*, vol. 11, p. 1253804, 2023, doi: 10.3389/fbioe.2023.1253804.
- [97] X. Zhang, X. Chen, H. Hong, R. Hu, J. Liu, and C. Liu, "Decellularized extracellular matrix scaffolds: Recent trends and emerging strategies in tissue engineering," (in eng), *Bioact Mater*, vol. 10, pp. 15-31, Apr 2022, doi: 10.1016/j.bioactmat.2021.09.014.
- [98] C. Mora-Navarro *et al.*, "Monitoring decellularization via absorbance spectroscopy during the derivation of extracellular matrix scaffolds," (in eng), *Biomed Mater*, vol. 17, no. 1, Nov 26 2021, doi: 10.1088/1748-605X/ac361f.
- [99] Z. Sargazi, S. Zavareh, M. Jafarabadi, and M. Salehnia, "An efficient protocol for decellularization of the human endometrial fragments for clinical usage," (in eng), *Prog Biomater*, vol. 10, no. 2, pp. 119-130, Jun 2021, doi: 10.1007/s40204-021-00156-5.
- [100] A. Baiocchi *et al.*, "Extracellular Matrix Molecular Remodeling in Human Liver Fibrosis Evolution," (in eng), *PLoS One*, vol. 11, no. 3, p. e0151736, 2016, doi: 10.1371/journal.pone.0151736.
- [101] Q. Dai, W. Jiang, F. Huang, F. Song, J. Zhang, and H. Zhao, "Recent Advances in Liver Engineering With Decellularized Scaffold," (in eng), *Front Bioeng Biotechnol*, vol. 10, p. 831477, 2022, doi: 10.3389/fbioe.2022.831477.
- [102] K. Dzobo, K. Motaung, and A. Adesida, "Recent Trends in Decellularized Extracellular Matrix Bioinks for 3D Printing: An Updated Review," (in eng), *Int J Mol Sci*, vol. 20, no. 18, Sep 18 2019, doi: 10.3390/ijms20184628.
- [103] L. T. Saldin, M. C. Cramer, S. S. Velankar, L. J. White, and S. F. Badylak, "Extracellular matrix hydrogels from decellularized tissues: Structure and function," (in eng), *Acta Biomater*, vol. 49, pp. 1-15, Feb 2017, doi: 10.1016/j.actbio.2016.11.068.
- [104] V. Magno and C. Werner, "Tissue-Derived Decellularized Materials for Biomedical Applications," in *Handbook of the Extracellular Matrix : Biologically-Derived Materials*, F. R. A. Maia, J. M. Oliveira, and R. L. Reis Eds. Cham: Springer International Publishing, 2023, pp. 1-33.
- [105] Z. Yang *et al.*, "Stem Cell-Laden Hydrogel-Based 3D Bioprinting for Bone and Cartilage Tissue Engineering," (in eng), *Front Bioeng Biotechnol*, vol. 10, p. 865770, 2022, doi: 10.3389/fbioe.2022.865770.
- [106] J. Nicolas, S. Magli, L. Rabbachin, S. Sampaolesi, F. Nicotra, and L. Russo, "3D Extracellular Matrix Mimics: Fundamental Concepts and Role of Materials Chemistry to Influence Stem Cell Fate," *Biomacromolecules*, vol. 21, no. 6, pp. 1968-1994, 2020/06/08 2020, doi: 10.1021/acs.biomac.0c00045.
- [107] X. Ma *et al.*, "Rapid 3D bioprinting of decellularized extracellular matrix with regionally varied mechanical properties and biomimetic microarchitecture," (in eng), *Biomaterials*, vol. 185, pp. 310-321, Dec 2018, doi: 10.1016/j.biomaterials.2018.09.026.
- [108] L. J. Millet and M. U. Gillette, "Over a century of neuron culture: from the hanging drop to microfluidic devices," (in eng), *Yale J Biol Med*, vol. 85, no. 4, pp. 501-21, Dec 2012.
- [109] M. Kapaczyńska *et al.*, "2D and 3D cell cultures - a comparison of different types of cancer cell cultures," (in eng), *Arch Med Sci*, vol. 14, no. 4, pp. 910-919, Jun 2018, doi: 10.5114/aoms.2016.63743.
- [110] M. Shulman and Y. Nahmias, "Long-term culture and coculture of primary rat and human hepatocytes," (in eng), *Methods Mol Biol*, vol. 945, pp. 287-302, 2013, doi: 10.1007/978-1-62703-125-7\_17.
- [111] J. Vajda, M. Milojević, U. Maver, and B. Vihar, "Microvascular Tissue Engineering-A Review," (in eng), *Biomedicines*, vol. 9, no. 6, May 21 2021, doi: 10.3390/biomedicines9060589.
- [112] X. Meng *et al.*, "Rebuilding the Vascular Network: In vivo and in vitro Approaches," (in eng),

- Front Cell Dev Biol*, vol. 9, p. 639299, 2021, doi: 10.3389/fcell.2021.639299.
- [113] M. D. Sarker, S. Naghieh, N. K. Sharma, and X. Chen, "3D biofabrication of vascular networks for tissue regeneration: A report on recent advances," (in eng), *J Pharm Anal*, vol. 8, no. 5, pp. 277-296, Oct 2018, doi: 10.1016/j.jpha.2018.08.005.
- [114] H. Bae *et al.*, "Building vascular networks," (in eng), *Sci Transl Med*, vol. 4, no. 160, p. 160ps 23, Nov 14 2012, doi: 10.1126/scitranslmed.3003688.
- [115] A. Torre-Muruzabal, L. Daelemans, G. Van Assche, K. De Clerck, and H. Rahier, "Creation of a nanovascular network by electrospun sacrificial nanofibers for self-healing applications and its effect on the flexural properties of the bulk material," *Polymer Testing*, vol. 54, pp. 78-83, 2016/09/01/ 2016, doi: <https://doi.org/10.1016/j.polymertesting.2016.06.026>.
- [116] I. S. Kinstlinger *et al.*, "Generation of model tissues with dendritic vascular networks via sacrificial laser-sintered carbohydrate templates," (in eng), *Nat Biomed Eng*, vol. 4, no. 9, pp. 916-932, Sep 2020, doi: 10.1038/s41551-020-0566-1.
- [117] C. K. Arakawa, B. A. Badeau, Y. Zheng, and C. A. DeForest, "Multicellular Vascularized Engineered Tissues through User-Programmable Biomaterial Photodegradation," (in eng), *Adv Mater*, vol. 29, no. 37, Oct 2017, doi: 10.1002/adma.201703156.
- [118] V. T. Duong *et al.*, "Cell Attachment on Inside-Outside Surface and Cell Encapsulation in Wall of Microscopic Tubular Scaffolds for Vascular Tissue-Like Formation," (in eng), *Annu Int Conf IEEE Eng Med Biol Soc*, vol. 2018, pp. 4198-4201, Jul 2018, doi: 10.1109/embc.2018.8513248.
- [119] V. Duong and K. Koo, "Over-five-millimeter diameter alginate-collagen endothelialized tubular scaffold formation," *Basel, Switzerland: MicroTAS*, 2019.
- [120] V.-T. Duong, J.-P. Kim, K.-S. Kim, H.-H. Ko, C.-H. Hwang, and K.-I. Koo, "Three-dimensional bio-printing technique: trend and potential for high volume implantable tissue generation," *의공학회지*, vol. 39, no. 5, pp. 188-207, 2018.
- [121] K. I. Koo, A. Lenshof, L. T. Huong, and T. Laurell, "Acoustic Cell Patterning in Hydrogel for Three-Dimensional Cell Network Formation," (in eng), *Micromachines (Basel)*, vol. 12, no. 1, Dec 22 2020, doi: 10.3390/mi12010003.
- [122] H. Sekine and T. Okano, "Capillary Networks for Bio-Artificial Three-Dimensional Tissues Fabricated Using Cell Sheet Based Tissue Engineering," (in eng), *Int J Mol Sci*, vol. 22, no. 1, Dec 23 2020, doi: 10.3390/ijms22010092.
- [123] S. Bertlein *et al.*, "Development of Endothelial Cell Networks in 3D Tissues by Combination of Melt Electrospinning Writing with Cell-Accumulation Technology," (in eng), *Small*, vol. 14, no. 2, Jan 2018, doi: 10.1002/smll.201701521.
- [124] Z. Wang, S. M. Mithieux, and A. S. Weiss, "Fabrication Techniques for Vascular and Vascularized Tissue Engineering," (in eng), *Adv Healthc Mater*, vol. 8, no. 19, p. e1900742, Oct 2019, doi: 10.1002/adhm.201900742.
- [125] V. van Duinen, D. Zhu, C. Ramakers, A. J. van Zonneveld, P. Vulto, and T. Hankemeier, "Perfused 3D angiogenic sprouting in a high-throughput in vitro platform," (in eng), *Angiogenesis*, vol. 22, no. 1, pp. 157-165, Feb 2019, doi: 10.1007/s10456-018-9647-0.
- [126] C. Del Amo, C. Borau, R. Gutiérrez, J. Asín, and J. M. García-Aznar, "Quantification of angiogenic sprouting under different growth factors in a microfluidic platform," (in eng), *J Biomech*, vol. 49, no. 8, pp. 1340-1346, May 24 2016, doi: 10.1016/j.jbiomech.2015.10.026.
- [127] W. A. Farahat *et al.*, "Ensemble analysis of angiogenic growth in three-dimensional microfluidic cell cultures," (in eng), *PLoS One*, vol. 7, no. 5, p. e37333, 2012, doi: 10.1371/journal.pone.0037333.
- [128] V. T. Duong, T. T. Dang, C. H. Hwang, S. H. Back, and K. I. Koo, "Coaxial printing of double-layered and free-standing blood vessel analogues without ultraviolet illumination for high-volume vascularised tissue," (in eng), *Biofabrication*, vol. 12, no. 4, p. 045033, Sep 24 2020, doi: 10.1088/1758-5090/abafc6.
- [129] G. Gao, J. Y. Park, B. S. Kim, J. Jang, and D. W. Cho, "Coaxial Cell Printing of Freestanding, Perfusable, and Functional In Vitro Vascular Models for Recapitulation of Native Vascular Endothelium Pathophysiology," (in eng), *Adv Healthc Mater*, vol. 7, no. 23, p. e1801102, Dec 20

- 18, doi: 10.1002/adhm.201801102.
- [130] V. Duong, T. Nguyen, and L. Phan, "Multi-lumen tubular calcium-alginate cell-laden scaffold formation for 3D bioprinting," *Taiwan: Presented at the MicroTAS, Kaohsiung, Taiwan*, 2018.
- [131] D. H. Nguyen *et al.*, "Biomimetic model to reconstitute angiogenic sprouting morphogenesis in vitro," (in eng), *Proc Natl Acad Sci U S A*, vol. 110, no. 17, pp. 6712-7, Apr 23 2013, doi: 10.1073/pnas.1221526110.
- [132] M. L. Iruela-Arispe and G. E. Davis, "Cellular and molecular mechanisms of vascular lumen formation," (in eng), *Dev Cell*, vol. 16, no. 2, pp. 222-31, Feb 2009, doi: 10.1016/j.devcel.2009.01.013.
- [133] K. Sugihara *et al.*, "A new perfusion culture method with a self-organized capillary network," (in eng), *PLoS One*, vol. 15, no. 10, p. e0240552, 2020, doi: 10.1371/journal.pone.0240552.
- [134] V. T. Duong *et al.*, "Twelve-day medium pumping into tubular cell-laden scaffold using a lab-made PDMS connector," (in eng), *Eur Cell Mater*, vol. 38, pp. 1-13, Jul 23 2019, doi: 10.2220/3/eCM.v038a01.
- [135] A. B. Fisher, S. Chien, A. I. Barakat, and R. M. Nerem, "Endothelial cellular response to altered shear stress," (in eng), *Am J Physiol Lung Cell Mol Physiol*, vol. 281, no. 3, pp. L529-33, Sep 2001, doi: 10.1152/ajplung.2001.281.3.L529.
- [136] B. Sarker *et al.*, "Evaluation of fibroblasts adhesion and proliferation on alginate-gelatin cross linked hydrogel," (in eng), *PLoS One*, vol. 9, no. 9, p. e107952, 2014, doi: 10.1371/journal.pone.0107952.
- [137] B. Sarker *et al.*, "Fabrication of alginate-gelatin crosslinked hydrogel microcapsules and evaluation of the microstructure and physico-chemical properties," (in eng), *J Mater Chem B*, vol. 2, no. 11, pp. 1470-1482, Mar 21 2014, doi: 10.1039/c3tb21509a.
- [138] T. Jiang *et al.*, "Bioprintable Alginate/Gelatin Hydrogel 3D In Vitro Model Systems Induce Cell Spheroid Formation," (in eng), *J Vis Exp*, no. 137, Jul 2 2018, doi: 10.3791/57826.
- [139] J. Rouwkema, B. Koopman, C. Blitterswijk, W. Dhert, and J. Malda, "Supply of nutrients to cells in engineered tissues," (in eng), *Biotechnol Genet Eng Rev*, vol. 26, pp. 163-78, 2010, doi: 10.5661/bger-26-163.
- [140] A. Krogh, "The supply of oxygen to the tissues and the regulation of the capillary circulation," (in eng), *J Physiol*, vol. 52, no. 6, pp. 457-74, May 20 1919, doi: 10.1113/jphysiol.1919.sp001844.
- [141] T. L. Place, F. E. Domann, and A. J. Case, "Limitations of oxygen delivery to cells in culture: An underappreciated problem in basic and translational research," (in eng), *Free Radic Biol Med*, vol. 113, pp. 311-322, Dec 2017, doi: 10.1016/j.freeradbiomed.2017.10.003.
- [142] M. Abkarian and A. Viallat, "Dynamics of vesicles in a wall-bounded shear flow," (in eng), *Biophys J*, vol. 89, no. 2, pp. 1055-66, Aug 2005, doi: 10.1529/biophysj.104.056036.
- [143] C. Zhu, T. Yago, J. Lou, V. I. Zarnitsyna, and R. P. McEver, "Mechanisms for flow-enhanced cell adhesion," (in eng), *Ann Biomed Eng*, vol. 36, no. 4, pp. 604-21, Apr 2008, doi: 10.1007/s10439-008-9464-5.
- [144] S. Park, Y. K. Joo, and Y. Chen, "Dynamic adhesion characterization of cancer cells under blood flow-mimetic conditions: effects of cell shape and orientation on drag force," *Microfluidics and Nanofluidics*, vol. 22, pp. 1-9, 2018.
- [145] E. Roux, P. Bougaran, P. Dufourcq, and T. Couffignal, "Fluid Shear Stress Sensing by the Endothelial Layer," (in eng), *Front Physiol*, vol. 11, p. 861, 2020, doi: 10.3389/fphys.2020.00861.
- [146] J. C. del Alamo, G. N. Norwich, Y. S. Li, J. C. Lasheras, and S. Chien, "Anisotropic rheology and directional mechanotransduction in vascular endothelial cells," (in eng), *Proc Natl Acad Sci U S A*, vol. 105, no. 40, pp. 15411-6, Oct 7 2008, doi: 10.1073/pnas.0804573105.
- [147] A. Krüger-Genge, A. Blocki, R. P. Franke, and F. Jung, "Vascular Endothelial Cell Biology: An Update," (in eng), *Int J Mol Sci*, vol. 20, no. 18, Sep 7 2019, doi: 10.3390/ijms20184411.
- [148] D. A. Chistiakov, A. N. Orekhov, and Y. V. Bobryshev, "Effects of shear stress on endothelial cells: go with the flow," (in eng), *Acta Physiol (Oxf)*, vol. 219, no. 2, pp. 382-408, Feb 2017, doi: 10.1111/apha.12725.
- [149] A. M. Malek and S. Izumo, "Mechanism of endothelial cell shape change and cytoskeletal remodeling in response to fluid shear stress," (in eng), *J Cell Sci*, vol. 109 ( Pt 4), pp. 713-26, A

- pr 1996, doi: 10.1242/jcs.109.4.713.
- [150] B. J. Ballermann, A. Dardik, E. Eng, and A. Liu, "Shear stress and the endothelium," (in eng), *Kidney Int Suppl*, vol. 67, pp. S100-8, Sep 1998, doi: 10.1046/j.1523-1755.1998.06720.x.
- [151] K. Tsuji-Tamura and M. Ogawa, "Morphology regulation in vascular endothelial cells," (in eng), *Inflamm Regen*, vol. 38, p. 25, 2018, doi: 10.1186/s41232-018-0083-8.
- [152] C. Bai, L. Hou, M. Zhang, Y. Pu, W. Guan, and Y. Ma, "Characterization of vascular endothelial progenitor cells from chicken bone marrow," (in eng), *BMC Vet Res*, vol. 8, p. 54, May 14 2012, doi: 10.1186/1746-6148-8-54.
- [153] D. A. Fletcher and R. D. Mullins, "Cell mechanics and the cytoskeleton," (in eng), *Nature*, vol. 463, no. 7280, pp. 485-92, Jan 28 2010, doi: 10.1038/nature08908.
- [154] M. Inglebert *et al.*, "The effect of shear stress reduction on endothelial cells: A microfluidic study of the actin cytoskeleton," (in eng), *Biomicrofluidics*, vol. 14, no. 2, p. 024115, Mar 2020, doi: 10.1063/1.5143391.
- [155] E. A. Osborn, A. Rabodzey, C. F. Dewey, Jr., and J. H. Hartwig, "Endothelial actin cytoskeleton remodeling during mechanostimulation with fluid shear stress," (in eng), *Am J Physiol Cell Physiol*, vol. 290, no. 2, pp. C444-52, Feb 2006, doi: 10.1152/ajpcell.00218.2005.
- [156] A. Pasini *et al.*, "Perfusion Flow Enhances Viability and Migratory Phenotype in 3D-Cultured Breast Cancer Cells," (in eng), *Ann Biomed Eng*, vol. 49, no. 9, pp. 2103-2113, Sep 2021, doi: 10.1007/s10439-021-02727-w.
- [157] M. Cavey and T. Lecuit, "Molecular bases of cell-cell junctions stability and dynamics," (in eng), *Cold Spring Harb Perspect Biol*, vol. 1, no. 5, p. a002998, Nov 2009, doi: 10.1101/cshperspect.a002998.
- [158] R. S. Ashton, A. Banerjee, S. Punyani, D. V. Schaffer, and R. S. Kane, "Scaffolds based on degradable alginate hydrogels and poly(lactide-co-glycolide) microspheres for stem cell culture," (in eng), *Biomaterials*, vol. 28, no. 36, pp. 5518-25, Dec 2007, doi: 10.1016/j.biomaterials.2007.08.038.
- [159] L. Melly, S. Boccardo, F. Eckstein, A. Banfi, and A. Marsano, "Cell and gene therapy approaches for cardiac vascularization," (in eng), *Cells*, vol. 1, no. 4, pp. 961-75, Nov 5 2012, doi: 10.3390/cells1040961.
- [160] Y. Shin *et al.*, "In vitro 3D collective sprouting angiogenesis under orchestrated ANG-1 and VEGF gradients," (in eng), *Lab Chip*, vol. 11, no. 13, pp. 2175-81, Jul 7 2011, doi: 10.1039/c1lc20039a.
- [161] T. L. Chu, G. Tripathi, M. Park, S.-H. Bae, and B.-T. Lee, "In-vitro and in-vivo biocompatibility of dECM-alginate as a promising candidate in cell delivery for kidney regeneration," *International Journal of Biological Macromolecules*, vol. 211, pp. 616-625, 2022/06/30/ 2022, doi: <https://doi.org/10.1016/j.ijbiomac.2022.05.085>.
- [162] J. Lee, J. Hong, W. Kim, and G. H. Kim, "Bone-derived dECM/alginate bioink for fabricating a 3D cell-laden mesh structure for bone tissue engineering," *Carbohydrate Polymers*, vol. 250, p. 116914, 2020/12/15/ 2020, doi: <https://doi.org/10.1016/j.carbpol.2020.116914>.
- [163] C.-C. Huang, "Characteristics and Preparation of Designed Alginate-Based Composite Scaffold Membranes with Decellularized Fibrous Micro-Scaffold Structures from Porcine Skin," *Polymers*, vol. 13, no. 20, p. 3464, 2021. [Online]. Available: <https://www.mdpi.com/2073-4360/13/20/3464>.
- [164] M. A. Tutty, D. Movia, and A. Prina-Mello, "Three-dimensional (3D) liver cell models - a tool for bridging the gap between animal studies and clinical trials when screening liver accumulation and toxicity of nanobiomaterials," *Drug Delivery and Translational Research*, vol. 12, no. 9, pp. 2048-2074, 2022/09/01 2022, doi: 10.1007/s13346-022-01147-0.
- [165] J. Wang, D. Huang, H. Yu, Y. Cheng, H. Ren, and Y. Zhao, "Developing tissue engineering strategies for liver regeneration," *Engineered Regeneration*, vol. 3, no. 1, pp. 80-91, 2022/03/01/ 2022, doi: <https://doi.org/10.1016/j.engreg.2022.02.003>.
- [166] S. Kammerer, "Three-Dimensional Liver Culture Systems to Maintain Primary Hepatic Properties for Toxicological Analysis In Vitro," (in eng), *Int J Mol Sci*, vol. 22, no. 19, Sep 23 2021, doi: 10.3390/ijms221910214.
- [167] S. P. Harrison, S. F. Baumgarten, R. Verma, O. Lunov, A. Dejneka, and G. J. Sullivan, "Liver



- Organoids: Recent Developments, Limitations and Potential," (in English), *Frontiers in Medicine*, Review vol. 8, 2021-May-05 2021, doi: 10.3389/fmed.2021.574047.
- [168] H. L. Jiang *et al.*, "Roles of spheroid formation of hepatocytes in liver tissue engineering," (in eng), *Int J Stem Cells*, vol. 3, no. 2, pp. 69-73, May 2010, doi: 10.15283/ijsc.2010.3.2.69.
- [169] W.-M. Liu *et al.*, "Establishment of Functional Liver Spheroids From Human Hepatocyte-Derived Liver Progenitor-Like Cells for Cell Therapy," (in English), *Frontiers in Bioengineering and Biotechnology*, Original Research vol. 9, 2021-November-08 2021, doi: 10.3389/fbioe.2021.738081.
- [170] T. S. Karande, J. L. Ong, and C. M. Agrawal, "Diffusion in musculoskeletal tissue engineering scaffolds: design issues related to porosity, permeability, architecture, and nutrient mixing," (in eng), *Ann Biomed Eng*, vol. 32, no. 12, pp. 1728-43, Dec 2004, doi: 10.1007/s10439-004-7825-2.
- [171] T. Rademakers, J. M. Horvath, C. A. van Blitterswijk, and V. L. S. LaPointe, "Oxygen and nutrient delivery in tissue engineering: Approaches to graft vascularization," (in eng), *J Tissue Eng Regen Med*, vol. 13, no. 10, pp. 1815-1829, Oct 2019, doi: 10.1002/term.2932.
- [172] J. M. C. Puguán, X. Yu, and H. Kim, "Diffusion characteristics of different molecular weight solutes in Ca-alginate gel beads," *Colloids and Surfaces A: Physicochemical and Engineering Aspects*, vol. 469, pp. 158-165, 2015/03/20/ 2015, doi: <https://doi.org/10.1016/j.colsurfa.2015.01.027>.
- [173] L. Goers, P. Freemont, and K. M. Polizzi, "Co-culture systems and technologies: taking synthetic biology to the next level," (in eng), *J R Soc Interface*, vol. 11, no. 96, Jul 6 2014, doi: 10.1098/rsif.2014.0065.
- [174] P. Kuppusamy, D. Kim, I. Soundharrajan, I. Hwang, and K. C. Choi, "Adipose and Muscle Cell Co-Culture System: A Novel In Vitro Tool to Mimic the In Vivo Cellular Environment," (in eng), *Biology (Basel)*, vol. 10, no. 1, Dec 24 2020, doi: 10.3390/biology10010006.
- [175] H. Lee *et al.*, "Development of Liver Decellularized Extracellular Matrix Bioink for Three-Dimensional Cell Printing-Based Liver Tissue Engineering," *Biomacromolecules*, vol. 18, no. 4, pp. 1229-1237, 2017/04/10 2017, doi: 10.1021/acs.biomac.6b01908.
- [176] F. Meng, A. Assiri, D. Dhar, and D. Broering, "Whole liver engineering: A promising approach to develop functional liver surrogates," *Liver International*, vol. 37, no. 12, pp. 1759-1772, 2017, doi: <https://doi.org/10.1111/liv.13444>.
- [177] D. R. Sahoo and T. Biswal, "Alginate and its application to tissue engineering," *SN Applied Sciences*, vol. 3, no. 1, p. 30, 2021/01/08 2021, doi: 10.1007/s42452-020-04096-w.
- [178] T. T. Tsai *et al.*, "The contemporary safety and effectiveness of lower extremity bypass surgery and peripheral endovascular interventions in the treatment of symptomatic peripheral arterial disease," *Circulation*, vol. 132, no. 21, pp. 1999-2011, 2015.
- [179] J. S. Hiramoto, M. Teraa, G. J. de Borst, and M. S. Conte, "Interventions for lower extremity peripheral artery disease," *Nature Reviews Cardiology*, vol. 15, no. 6, pp. 332-350, 2018.
- [180] B. A. Hacken *et al.*, "A novel scoring instrument to assess donor site morbidity after anterior cruciate ligament reconstruction with a patellar tendon autograft at 2-year follow-up using contemporary graft-harvesting techniques," *Orthopaedic Journal of Sports Medicine*, vol. 8, no. 6, p. 2325967120925482, 2020.
- [181] L. Xue and H. P. Greisler, "Biomaterials in the development and future of vascular grafts," *Journal of vascular surgery*, vol. 37, no. 2, pp. 472-480, 2003.
- [182] M. B. Elliott *et al.*, "Regenerative and durable small-diameter graft as an arterial conduit," *Proceedings of the National Academy of Sciences*, vol. 116, no. 26, pp. 12710-12719, 2019.
- [183] T. Gourlay and S. Gunaydin, *Minimized cardiopulmonary bypass techniques and technologies*. Elsevier, 2012.
- [184] M. Carrabba and P. Madeddu, "Current strategies for the manufacture of small size tissue engineering vascular grafts," *Frontiers in bioengineering and biotechnology*, vol. 6, p. 41, 2018.
- [185] I. Skovrind, E. B. Harvald, H. Juul Belling, C. D. Jørgensen, J. S. Lindholt, and D. C. Andersen, "Concise review: patency of small-diameter tissue-engineered vascular grafts: a meta-analysis of preclinical trials," *Stem cells translational medicine*, vol. 8, no. 7, pp. 671-680, 2019.
- [186] R. Y. Kannan, H. J. Salacinski, P. E. Butler, G. Hamilton, and A. M. Seifalian, "Current status

- of prosthetic bypass grafts: a review," *Journal of Biomedical Materials Research Part B: Applied Biomaterials: An Official Journal of The Society for Biomaterials, The Japanese Society for Biomaterials, and The Australian Society for Biomaterials and the Korean Society for Biomaterials*, vol. 74, no. 1, pp. 570-581, 2005.
- [187] W. G. Goodman *et al.*, "Coronary-artery calcification in young adults with end-stage renal disease who are undergoing dialysis," *New England Journal of Medicine*, vol. 342, no. 20, pp. 1478-1483, 2000.
- [188] D. Chong, J. Constantinou, M. Davis, and G. Hamilton, "Calcification of a synthetic renovascular graft in a child," *EJVES Short Reports*, vol. 33, pp. 13-15, 2016.
- [189] N. L'heureux, S. Pâquet, R. Labbé, L. Germain, and F. A. Auger, "A completely biological tissue-engineered human blood vessel," *The FASEB Journal*, vol. 12, no. 1, pp. 47-56, 1998.
- [190] N. L'Heureux *et al.*, "Human tissue-engineered blood vessels for adult arterial revascularization," *Nature medicine*, vol. 12, no. 3, pp. 361-365, 2006.
- [191] M. Costa *et al.*, "Cell sheet engineering using the stromal vascular fraction of adipose tissue as a vascularization strategy," *Acta Biomaterialia*, vol. 55, pp. 131-143, 2017.
- [192] S. Meghezi, D. G. Seifu, N. Bono, L. Unsworth, K. Mequanint, and D. Mantovani, "Engineering 3D cellularized collagen gels for vascular tissue regeneration," *JoVE (Journal of Visualized Experiments)*, no. 100, p. e52812, 2015.
- [193] A. Nasr, "The radial artery and its variations: anatomical study and clinical implications," *Folia Morphologica*, vol. 71, no. 4, pp. 252-262, 2012.
- [194] K. C. Chung, *Operative techniques: hand and wrist surgery*. Elsevier Health Sciences, 2021.
- [195] S. Beniwal, K. Bhargava, and S. K. Kausik, "Size of distal radial and distal ulnar arteries in adults of southern Rajasthan and their implications for percutaneous coronary interventions," *Indian heart journal*, vol. 66, no. 5, pp. 506-509, 2014.
- [196] M. Fathi, E. Hatamipour, H. R. Fathi, and A. Abbasi, "The anatomy of superficial inferior epigastric artery flap," *Acta Cirúrgica Brasileira*, vol. 23, pp. 429-434, 2008.
- [197] K. A. Gold *et al.*, "3D bioprinted multicellular vascular models," *Advanced healthcare materials*, vol. 10, no. 21, p. 2101141, 2021.
- [198] A. G. Tabriz, M. A. Hermida, N. R. Leslie, and W. Shu, "Three-dimensional bioprinting of complex cell laden alginate hydrogel structures," *Biofabrication*, vol. 7, no. 4, p. 045012, 2015.
- [199] Q. Gao *et al.*, "3D bioprinting of vessel-like structures with multilevel fluidic channels," *ACS biomaterials science & engineering*, vol. 3, no. 3, pp. 399-408, 2017.
- [200] H. Onoe *et al.*, "Metre-long cell-laden microfibres exhibit tissue morphologies and functions," *Nature materials*, vol. 12, no. 6, pp. 584-590, 2013.
- [201] C. T. Nguyen, V. T. Duong, C. H. Hwang, and K. I. Koo, "Angiogenesis in Free-Standing Two-Vasculature-Embedded Scaffold Extruded by Two-Core Laminar Flow Device," (in eng), *Int J Bioprint*, vol. 8, no. 3, p. 557, 2022, doi: 10.18063/ijb.v8i3.557.
- [202] R. Edri *et al.*, "Personalized hydrogels for engineering diverse fully autologous tissue implants," *Advanced materials*, vol. 31, no. 1, p. 1803895, 2019.
- [203] Q. Pi *et al.*, "Digitally tunable microfluidic bioprinting of multilayered cannular tissues," *Advanced Materials*, vol. 30, no. 43, p. 1706913, 2018.
- [204] G. Gao *et al.*, "Tissue engineered bio-blood-vessels constructed using a tissue-specific bioink and 3D coaxial cell printing technique: a novel therapy for ischemic disease," *Advanced functional materials*, vol. 27, no. 33, p. 1700798, 2017.
- [205] Q. Liang *et al.*, "Coaxial scale-up printing of diameter-tunable biohybrid hydrogel microtubes with high strength, perfusability, and endothelialization," *Advanced Functional Materials*, vol. 30, no. 43, p. 2001485, 2020.
- [206] M. Wang *et al.*, "Molecularly cleavable bioinks facilitate high-performance digital light processing-based bioprinting of functional volumetric soft tissues," *Nature communications*, vol. 13, no. 1, p. 3317, 2022.
- [207] B. Rehm, A. Haghshenas, A. S. Paknejad, and J. Schubert, "Situational problems in MPD," in *Managed Pressure Drilling*: Elsevier, 2008, pp. 39-80.
- [208] P. Kundu, I. Cohen, and D. Dowling, "Fluid Mechanics 6th ed. ISBN: 9780124059351," ed: Academic Press, Elsevier, San Diego, 2016.

- [209] H. Fujita and T. Kato, *On the Navier-Stokes initial value problem. I* (no. 121). Department of Mathematics, Stanford University, 1963.
- [210] H. Devarbhavi, S. K. Asrani, J. P. Arab, Y. A. Nartey, E. Pose, and P. S. Kamath, "Global burden of Liver Disease: 2023 Update," *Journal of Hepatology*, 2023/03/27/ 2023, doi: <https://doi.org/10.1016/j.jhep.2023.03.017>.
- [211] Y. Li, L. Lu, and X. Cai, "Liver Regeneration and Cell Transplantation for End-Stage Liver Disease," (in eng), *Biomolecules*, vol. 11, no. 12, Dec 20 2021, doi: 10.3390/biom11121907.
- [212] Y. Yajima, C. N. Lee, M. Yamada, R. Utoh, and M. Seki, "Development of a perfusable 3D liver cell cultivation system via bundling-up assembly of cell-laden microfibers," (in eng), *J Biosci Bioeng*, vol. 126, no. 1, pp. 111-118, Jul 2018, doi: 10.1016/j.jbiosc.2018.01.022.
- [213] Y. Kurashina, R. Sato, and H. Onoe, "Microfiber-shaped building-block tissues with endothelial networks for constructing macroscopic tissue assembly," (in eng), *APL Bioeng*, vol. 3, no. 4, p. 046101, Dec 2019, doi: 10.1063/1.5109966.
- [214] V. T. Duong *et al.*, "Double-layered blood vessels over 3 mm in diameter extruded by the inverse-gravity technique," *Biofabrication*, vol. 15, no. 4, p. 045022, 2023/09/22 2023, doi: 10.1088/1758-5090/acf61f.



# Appendices

## Appendix A: Credits & Copyright Permissions

Notes on Copyright Licenses for Reproduction of Text and Figures in this Dissertation

### ***Part 1:***

For reproducing those figures that appeared in the following publication with credit to other sources, permission has also been sought from the respective sources.

### ***Part 2:***

The text excerpts and the figures presented in Part Two are reproduced with permission from the following article:

Nguyen CT, Duong VT, Hwang CH, Koo KI. Angiogenesis in Free-Standing Two-Vasculature-Embedded Scaffold Extruded by Two-Core Laminar Flow Device. *Int J Bioprint*. 2022 May 13;8(3):557. doi: 10.18063/ijb.v8i3.557.

CT Nguyen, VP Le, TH Le, MS Kim, JM Seo, KI Koo. Bioinspired Liver dECM Scaffold using sacrificial Calcium Alginate for artificial Liver. *International Conference on Biofabrication 2023*.

VT Duong, CT Nguyen, HL Phan, VP Le, TT Dang, CL Choi, JM Seo, CN Cha, SH Back, KI Koo . Double-layered blood vessels over 3 mm in diameter extruded by the inverse-gravity technique. *Biofabrication*, vol. 15, no. 4, p. 045022. doi: 10.1088/1758-5090/acf61f.